Using Sensors to Investigate the Effectiveness of Portable Air Filtration for Reducing Particle Exposures: Implications for Community Congregate Settings

Ching-Hsuan Huang

A dissertation

submitted in partial fulfillment of the

requirements for the degree of

Doctor of Philosophy

University of Washington

2024

Reading Committee:

Edmund Seto, Chair

Elena Austin

Martin Cohen

Program Authorized to Offer Degree:

Department of Environmental and Occupational Health Sciences

University of Washington

Abstract

Using Sensors to Investigate the Effectiveness of Portable Air Filtration for Reducing Particle Exposures: Implications for Community Congregate Settings

Ching-Hsuan Huang

Chair of the Supervisory Committee:

Edmund Seto

Department of Environmental and Occupational Health Sciences

This study addresses critical aspects of indoor air quality management with a focus on community congregate settings through a combination of laboratory and field studies. We aimed to 1) Develop a standardized laboratory protocol for characterizing and calibrating the performance of low-cost optical particle sensors, 2) Evaluate the real-world effectiveness of portable HEPA air cleaners (HEPA PACs) in reducing indoor particle levels in community congregate settings, while assessing usage patterns and factors influencing their efficacy, and 3) Understand the impact of filter dust loading on HEPA PAC's long-term performance concerning wood smoke particles.

For Aim 1, we developed a standardized laboratory experimental protocol to assess the performance of a low-cost optical particle sensors against a lab-grade aerodynamic particle sizer in a controlled environment. This involved utilizing standardized polydisperse testing aerosols

and developing improved calibration algorithms based on particle sizes, physical characteristics, number concentration, and mass indices. The sensor-to-sensor reproducibility was also evaluated.

For Aim 2, we assessed the real-world effectiveness of HEPA PACs in reducing particle concentrations in community congregate living settings. We deployed multiple HEPA PACs in three homeless shelters in King County, Washington, and utilized low-cost optical particle sensors to measure indoor and outdoor optical particle number concentration (OPNC). Additionally, we tracked HEPA PAC usage with power data loggers and modeled its relationship to indoor/outdoor ratios of total OPNC. Post-hoc surveys were implemented to identify the challenges in HEPA PAC utilization.

For Aim 3, we conducted a laboratory study to assess how filter dust loading affects HEPA PAC's long-term performance. We pre-loaded HEPA PAC filter combinations of pre-filter, charcoal filter, and HEPA filter with varying amounts of ISO 12103-1 A2 fine test dust, simulating 1 to 11 months of continuous use at max fan speed in typical US homes. Fresh woodsmoke was used to test filter performance. We examined the relationship between filter loading and airflow rate, pressure drop, power consumption, and clean air delivery rate (CADR).

Results revealed discrepancies in particle size distribution between low-cost particle sensor original equipment manufacturer's (OEM) calibration and reference aerodynamic particle sizer measurements. Calibration models demonstrated improved accuracies for number and mass concentrations, with limitations at lower concentrations and larger size bins. Additionally,

evidence was found of HEPA PACs effectively reducing indoor particle concentrations, with usage patterns significantly influencing efficacy. Keeping HEPA PACs on was the main challenge to operate them in multi-zone congregate living settings. Laboratory investigations supported the use of HEPA PACs under max fan speed for up to 7 months without a significant decrease in CADR in typical US residential environment.

This study advances indoor air quality management through laboratory experimentations and field evaluations. Our findings refine low-cost optical particle sensor calibration, underscore the efficacy of HEPA portable air cleaners (PACs) in community settings, and highlight the importance of filter maintenance for sustained performance. Through evidence-based findings, this research contributes to ongoing efforts to improve public health outcomes and indoor air quality.

ACKNOWLEDGEMENT

I would like to express my deepest gratitude to my dissertation committee chair, Dr. Edmund Seto, and to my committee members, Dr. Elena Austin, Dr. Martin Cohen, and Dr. John Kramlich, for their invaluable guidance and support throughout my Ph.D. journey. Their expertise and insights have been instrumental in shaping my personal and academic growth.

I am grateful to the past and present members of the Seto lab, Jeffry Shirai, Lilian Liu, and Dr. Ningrui Liu, for their assistance, collaboration, and camaraderie. Their contributions have been crucial to my work, and their support has made my research endeavors more enriching and fulfilling. I am also thankful to Dr. Igor Novosselov, Dr. Shirlee Tan, and the HEART Team members of Public Health – Seattle and King County. Their willingness to offer opportunities to work with them and integrate their expertise into my dissertation work has been invaluable.

Most importantly, I would like to express my deepest appreciation to my family, especially my parents, for their unconditional support and encouragement. Their unwavering belief in my potential has enabled me to pursue my studies abroad and achieve my academic and personal goals. They have always been there to provide guidance, wisdom, and love, even from afar. Their enduring faith in my abilities has been a constant source of motivation and strength. I am profoundly grateful for their presence in my life and for everything they have done to make this achievement possible.

Table of Contents

INTRODUCTION

Fine particulate matter ($PM_{2.5}$) exposure is associated with various adverse health outcomes, including cardiovascular and respiratory morbidity and mortality [1]. While ambient air quality standards have been established and enforced to mitigate outdoor air pollution in the US, indoor air quality remains a persistent concern [2]. Individuals in the US spend a significant portion of their time indoors [3], emphasizing the importance of addressing indoor air pollution. The recent WHO global air quality guidelines recommend that indoor air quality levels meet the same standards as ambient air quality [4]. This indicates the necessity of proactive efforts in indoor air quality management, which is especially critical for regions where seasonal pollution events, such as wildfire activity and residential wood burning contribute to elevated levels of indoor particulate matter [5-7].

The emergence of low-cost particle sensors presents both opportunities and challenges in monitoring indoor air quality. These sensors offer the potential for high temporal and spatial resolution data collection, facilitating a better characterization of indoor air quality dynamics and human exposure. However, concerns regarding the accuracy and reliability of data collected by these sensors have been raised. Despite these challenges, there is widespread usage of low-cost sensors for ambient air quality monitoring for both citizen science and research purposes [8-11], indicating growing interest in leveraging sensor technology for environmental monitoring applications.

The context of controlling infectious diseases, particularly in the wake of the COVID-19 pandemic, further complicates indoor air quality management. Guidance, such as increasing

ventilation and outdoor air exchange, may be effective for controlling infectious disease transmission, but can lead to infiltration of particles of outdoor origin and exacerbate indoor air quality. In light of this, public health agencies recommend the use of portable high-efficiency particulate air (HEPA) air cleaners as a mitigation strategy during high pollution periods, such as wildfire smoke events, when increasing building air exchange rate via ventilation is not desired [12, 13].

The HEPA air cleaning devices have demonstrated efficacy in reducing indoor particle concentrations in residential settings, and their initial performance have been well-studied [14-16]. However, their effectiveness in multi-zone indoor environments, such as congregate living settings, remains understudied. Congregate living settings pose unique challenges compared to residential settings due to higher occupant density, increased activity levels, and diverse sources of particulate matter, which could potentially impact the overall performance of HEPA air cleaners. Furthermore, the long-term performance of HEPA air cleaners, particularly under conditions of prolonged exposure to elevated particulate matter levels that can lead to significant dust buildup on filters, requires further investigation. This is crucial because filter loading affects maintenance efforts, cost, sustainability, and HEPA air cleaners' filtration efficacy. The cost associated with filter replacement and maintenance could be substantial especially for congregate settings that require the use of multiple HEPA air cleaners to achieve optimal air cleaning performance. Disposal of used filters is also a concern, as it could contribute to environmental waste. Additionally, the overall filtration efficacy of HEPA air cleaners could potentially be impacted if filters become clogged.

In this study, we addressed these knowledge gaps through a combination of laboratory and field investigation. We aimed to 1) Develop a standardized laboratory protocol for characterizing and calibrating the performance of low-cost optical particle sensors, 2) Evaluate the real-world effectiveness of HEPA air cleaners in reducing indoor particulate levels in community congregate settings, while assessing usage patterns and factors influencing their efficacy, and 3) Understand the impact of filter dust loading on HEPA air cleaner performance concerning wood smoke particles.

By achieving these aims, we seek to advance understanding of indoor air pollution mitigation strategies, particularly within congregate living settings and regions facing seasonal air quality challenges. Results from Aim 1 will help us establish a standardized protocol for characterizing low-cost particle sensors, thereby enhancing our ability to accurately monitor indoor and outdoor particle concentrations for understanding human exposure patterns. Results from Aim 2 will help us understand the real-world effectiveness of HEPA air cleaners in reducing indoor particle levels in community congregate settings. By examining usage patterns and factors influencing their efficacy, we can tailor intervention strategies to better meet the needs of these communities, thereby improving indoor air quality and public health outcomes. Results from Aim 3 will help us understand the impact of filter dust loading on HEPA air cleaner performance, concerning wood smoke particles. This knowledge will inform recommendations for optimizing long-term performance and maintenance of these devices, ensuring sustained efficacy in mitigating indoor air pollution in vulnerable communities and regions with seasonal air quality challenges.

CHAPTER 1. ASSESSING THE VALUE OF COMPLEX REFRACTIVE INDEX AND PARTICLE DENSITY FOR CALIBRATION OF LOW-COST PARTICLE MATTER SENSOR FOR SIZE-RESOLVED PARTICLE COUNT AND $PM_{2.5}$ MEASUREMENTS

 The authors of the manuscript are:

Ching-Hsuan Huang [1], Jiayang He [2], Elena Austin [1], Edmund Seto [1], Igor Novosselov [2, *]

[1] Department of Environmental and Occupational Health Sciences, School of Public Health, University of Washington, Seattle, Washington, United States of America

[2] Department of Mechanical Engineering, College of Engineering, University of Washington, Seattle, Washington, United States of America

* Corresponding author

DOI: https://doi.org/10.1371/journal.pone.0259745

1.1 ABSTRACT

Low-cost optical scattering particulate matter (PM) sensors report total or size-specific particle counts and mass concentrations. The PM concentration and size are estimated by the original equipment manufacturer (OEM) proprietary algorithms, which have inherent limitations since particle scattering depends on particles' properties such as size, shape, and complex index of refraction (CRI) as well as environmental parameters such as temperature and relative humidity (RH). As low-cost PM sensors are not able to resolve individual particles, there is a need to characterize and calibrate sensors' performance under a controlled environment. Here, we present improved calibration algorithms for Plantower PMS A003 sensor for mass indices and size-resolved number concentration. An aerosol chamber experimental protocol was used to evaluate sensor-to-sensor data reproducibility. The calibration was performed using four polydisperse test aerosols. The particle size distribution OEM calibration for PMS A003 sensor did not agree with the reference single particle sizer measurements. For the number concentration calibration, the linear model without adjusting for the aerosol properties and environmental conditions yields an absolute error (NMAE) of ~ 4.0% compared to the reference instrument. The calibration models adjusted for particle CRI and density account for non-linearity in the OEM's mass concentrations estimates with NMAE within 5.0%. The calibration algorithms developed in this study can be used in indoor air quality monitoring, occupational/industrial exposure assessments, or near-source monitoring scenarios where field calibration might be challenging.

1.2 INTRODUCTION

The direct measurement of time- and size-resolved particle matter (PM) concentrations is essential to health-related applications, such as exposure assessments and air quality (AQ) studies, but are challenging to implement at fine spatial and temporal scales. Human exposure to PM is associated with multiple adverse health effects, including cardiovascular disease, cardiopulmonary disease, and lung cancer [17-23]. Estimates show that approximately 3% of cardiopulmonary and 5% of lung cancer deaths are attributed to exposures to $PM_{2.5}$ (particles less than 2.5 μm in diameter) globally [24]. Particle deposition in the human respiratory tract and the resultant adverse health effects depend on the particles' size distribution [25, 26]. PM concentration varies significantly in space and time across community settings [27, 28]. Hence, time- and size-resolved PM measurements are more informative than traditional total PM weight measurements for assessing adverse health effects. As part of the Clean Air Act, the National Ambient Air Quality Standard (NAAQS) set by the U.S. Environmental Protection Agency (EPA) has adopted and established monitoring requirements for six criteria air pollutants, including $PM_{2.5}$ and PM_{10} [29, 30]. However, the sparse spatial distribution of government monitoring sites makes fine spatial scale exposure assessment challenging [24]. Traditional PM measurement instruments are large and expensive, thus have limited use in high spatial and temporal resolution mapping applications; these applications instead demand compact, low-cost sensors with reliable performance.

Low-cost PM sensors find increasing use in various applications, including monitoring AQ in the outdoor [9, 31-33] and indoor environment [34-36] by academic researchers and citizen scientists. The low-cost sensor networks have the potential to provide high spatial and temporal and resolution, identifying pollution sources and hotspots, which in turn can lead to the

development of intervention strategies for exposure assessment and intervention strategies for susceptible individuals. Time-resolved exposure data from wearable monitors can be used to assess individual exposure in near real-time [37].

As low-cost sensors find applications in pollution monitoring, and there is a need to characterize and calibrate their performance under various conditions, calibration in controlled environments with standardized test aerosols can provide the basis for such assessments. Various studies have evaluated the performance of low-cost PM sensors in laboratory and field settings [38-45]; these reports show that low-cost sensors yield usable data when calibrated against research-grade reference instruments, although some drawbacks have been reported. One common concern is that calibrations for number concentrations have not been reported, and the mass concentration of the low-cost PM sensors is based on numerous assumptions. Second, there is a lack of information on low-cost sensors' ability to assess particle size distributions, which is critical for assessing health and environmental impacts. Third, calibrations based on short-term field colocations with reference instruments are often limited by the range of particle properties, concentrations, and environmental conditions and thus cannot be generalized to other studies. This is a concern because with improving air quality in the developed nations, the typical $PM_{2.5}$ levels are relatively low (<20 $\mu g/m^3$); however, PM concentration during wildfires [46] and in occupational settings [47, 48] often exceeds regulatory limits for short periods. In developing countries with less strict regulations, the PM level associated with, e.g., traffic emissions [49], agricultural waste burning [50], indoor cooking [51] is significantly higher. In these settings, field colocations with reference instruments required for calibration studies can be challenging. Thus, evaluating low-cost PM sensors' performance under high and low loading

conditions is necessary if the sensors were to be used in epidemiological studies and PM surveillance networks.

Low-cost optical PM sensors rely on elastic light scattering to measure time- and size-resolved PM concentrations; they are widely used in aerosol research, particularly when measuring particles in the 0.5 μm to 10 μm range. Aerosol photometers that measure the bulk light scatter of multiple particles simultaneously have limited success in measuring mass concentration [30]. Typical low-cost (<$100) particle monitors often yield unreliable number concentrations data [52], but PM mass estimation error can be as high as 1000% [53]. Also, low-cost sensor measurements may suffer from sensor-to-sensor variability due to a lack of quality control and differences between individual components [45, 52]. Sensor geometry can be optimized to reduce the effect of particle CRI. Researchers have addressed CRI sensitivity by designing optical particle sizers (OPSs) that measure scattered light at multiple different angles simultaneously [54] or by employing dual-wavelength techniques [55]. However, these solutions involve complex and expensive components not suitable for compact, low-cost devices. Optimizing the detector angle relative to the excitation beam can reduce dependency on CRI [56]; however, this approach has not been translated to high volume production.

Some commercially available low-cost sensors provide output in total particle counts or particle mass concentrations, and some provide size-specific counts or mass concentrations. These quantities are not measured directly as an individual particle's scattering signature (as in the single particle counters) but are estimated by the OEM proprietary algorithms. These algorithms have inherent limitations because particle scattering depends on the particles' composition, size, shape, and CRI [57]. A common workaround is to collect PM on a filter after or in parallel with

the OPS measurements. The filters are analyzed to determine their average particle optical properties; these data are then used to correct the optical measurements after the fact.

Environmental conditions can affect sensor output, e.g., a non-linear response has been reported with increasing RH [58-62]. High humidity (RH > 75%) creates challenges for particle instruments; e.g., significant variations were observed between different commercially available instruments, such as Nova PM sensor [58] and personal DataRAM [60]. In addition, the RH measurement approach could also affect the sensor output [58, 59], e.g., the RH measurement based on reference monitoring site rather than inside the sensor enclosure may be different due to the microenvironment and transient effects. The selection of reference instruments with different measuring principles may also influence the calibration of low-cost sensors. For example, the calibration of the Plantower PM sensor in Jayaratne et al., 2018 was based on the tapered element oscillating microbalance (TEOM), while Zusman et al., 2020 calibrated the same sensor against the beta attenuation monitor (BAM) and federal reference method (FRM) measurements [44, 59]. The integrated mass measurements cannot account for temporal particle size and concentration variation during the calibration experiment. The instruments that directly measure aerosol size and concentration can be a better fit for sensor calibration [45, 63]. The calibration against aerodynamic particle sizer (APS) or single optical particle counter instruments can potentially provide a more robust calibration for low-cost optical particle sensors. Correlating particle diameter measured low-cost sensor to aerodynamic diameter measured by an APS is relevant since the aerodynamic diameter determines particle deposition in the respiratory tract.

This study presents calibration for PMS A003 (Beijing Plantower Co., Ltd, China; referred to as PMS hereafter) sensors as a function of particle sizes and concentration, as well as the $PM_{2.5}$ and

PM_1 indices. The calibration is based on four polydisperse standard testing aerosols, including the Arizona Test Dust (ATD), two types of ceramic particles, and NaCl particles. The PMS data from six sensors were calibrated against the APS for particle size range 0.5–10 μm and number concentration in the range of 0–1000 #/cc. A standardized laboratory experimental protocol was developed to control the PM concentration, environmental conditions and to assess sensor-to-sensor reproducibility.

1.3 MATERIALS AND METHODS

1.3.1 Plantower PMS A003 and Sensor Test Platform

The low-cost sensor PMS A003 was evaluated. The sensor's photodiode is positioned perpendicular to the excitation beam and measures the ensemble scattering of particles in the optical volume. The scattering light intensity is then converted to a voltage signal to estimate PM number density and mass concentration using a proprietary calibration algorithm. The PMS provides estimated particle counts in six size bins with the optical diameter in 0.3–10 μm (#/0.1L) range and mass concentration ($\mu g/m^3$) for PM_1, $PM_{2.5}$, and PM_{10}. The mass concentrations are reported for two settings: "factory" and "atmospheric" conditions. The factory condition applies a correction factor (CF) of unity to the concentration measured, whereas the "atmospheric" condition is designed for use in the ambient environment.

Six PMS units were installed on a custom printed circuit board (PCB), which also included a Bosch BME680 temperature and relative humidity (RH) sensor (**Figure 1**). All sensors were connected to an Arduino Nano microcontroller through a data selector (multiplexer NXP 74HC4051 breakout board, Sparkfun, Boulder, CO). The controller collects data from the six

PMS sensors and an RH and temperature sensor simultaneously with the data acquisition rate of 1 Hz. The data reported in "factory" mode were used in the analysis.

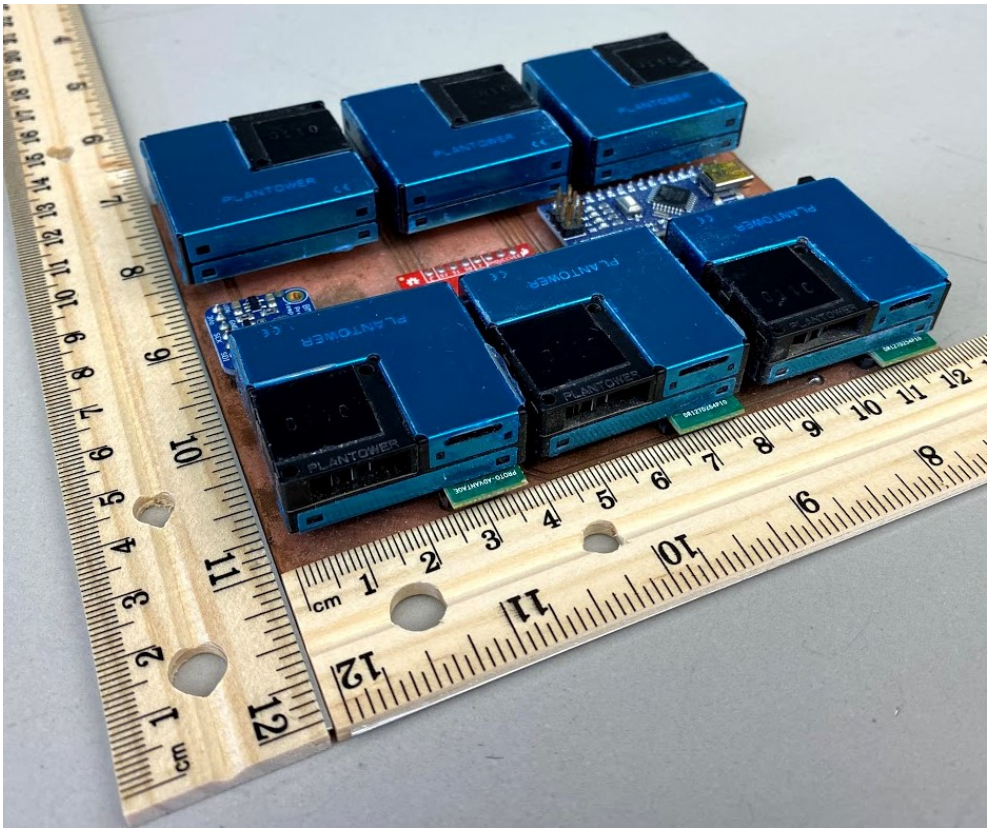

Figure 1. Photograph test platform, consisting of six PMS units mounted on the PCB, a temperature and humidity sensor, a multiplexer, and an Arduino microcontroller.

The reference instrument used in this study is the TSI Aerodynamic Particle Sizer (APS) 3321 spectrometer. APS measures both the aerodynamic size and optical size of a particle. Using the time-of-flight principle, the APS measures size-resolved particle counts with aerodynamic particle diameter (AD) of 0.523 to 20 μm in 52 size bins. The lower detection limit for optical size is 0.37 μm. The APS's optical sensor detects particles with AD<0.523 μm, but they cannot be resolved based on their aerodynamic size. Thus these particles are assigned to a single bin

<0.523 μm. The aerodynamic size determined the particle's aerodynamic behavior, such as settling velocity or penetration into the respiratory tract. Thus, we evaluate the correlation between the PMS number concentrations and the APS aerodynamic size bin number concentrations. The instrument estimates mass concentration by assuming spherical particles and particle density input. APS reports particle concentrations with a 5-second resolution. In the experiments, the sampling inlet was placed near the PMS sensors. Per APS specifications, the maximum recommended particle concentration is 1000 #/cm^3 at 0.5 μm with < 5% coincidence. Therefore, the total number concentration of the aerosols in the test chamber was maintained below 1000 #/cc (10^5 #/0.1L).

1.3.2 Aerosol Chamber Tests

We tested four polydisperse aerosols: Arizona Test Dust (ATD) (Powder Technology Incorporated, Arden Hills, MN), polydisperse W210, and W410 ceramic particles (3M™, St. Paul, MN), and sodium chloride (NaCl) particles. NaCl particles were generated by nebulizing the aqueous solution of 10% wt [64]. The challenge aerosols' properties and typical size distributions are summarized in **Table 1** and **Figure S3**., respectively. The experiments were conducted in a custom-built aerosol chamber (0.56 m × 0.52 m × 0.42 m) (**Figure 2**). A full description of the chamber can be found in ref [65]. The PMS sensor platform was placed in the well-mixed aerosol test chamber, elevated to the same height as the APS inlet. The APS sampled particle-laden air through static-dissipative tubing to eliminate electrostatic losses in the tubing. Particles were generated using a medical nebulizer (MADA Up-Mist Medication Nebulizer) [66]. During the experiments, the RH was controlled by nebulizing deionized water using a separate nebulizer or introducing dry filtered air; tests were conducted in the range of RH =

17%– 80%. Two mixing fans inside the chamber provided well-mixed conditions through the experiments; particle concentration was continuously monitored.

Table 1. Characteristics of the standard testing aerosols used in the study [52].

Aerosol	ATD	W210	W410	NaCl
Composition	SiO_2, Al_2O_3, Fe_2O_3, Na_2O [a]	Alkali aluminosilicate ceramic	Alkali aluminosilicate ceramic	Sodium Chloride
Assumed density (g/cm^3)	2.5 – 2.7 [b]	2.4	2.4	1.03
CRI	1.63	1.53	1.53	1.54

[a] Four major components were listed.

[b] For analysis purposes, 2.6 g/cm^3 was used.

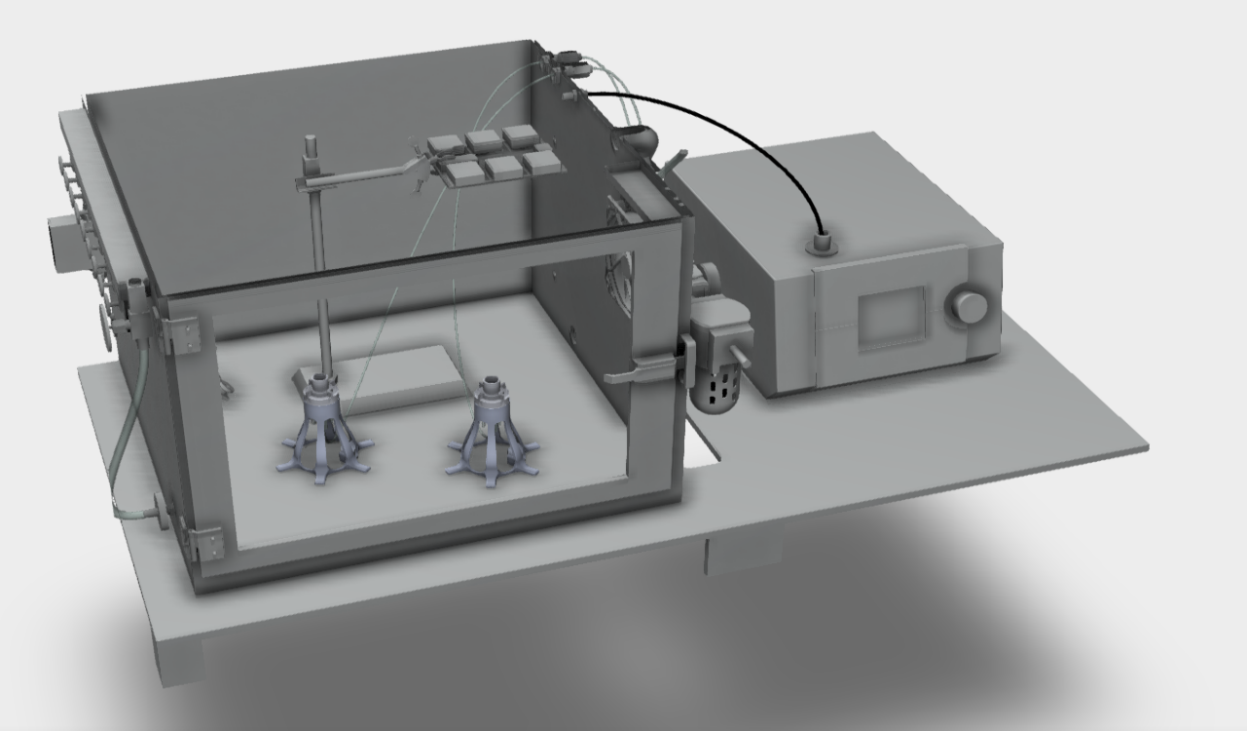

Figure 2. A 3D view of the experimental setup.

We controlled the aerosol generation rate by adjusting the compressed air flow rate to the nebulizer. The aerosol generation was stopped when the total number concentration (based on the APS count) reached 1000 #/cm^3. Then, the particle concentration was allowed to decay as the chamber was evacuated at a rate of 9.8 L/min; the make-up air entering the test was aspirated through a HEPA filter. The sensor array data and the APS data were acquired via two universal serial buses (USB) cables in real-time until the total number concentration from the APS reached 15 #/cm^3.

1.3.3 Data Analysis and Modeling

The collected data with concentrations > 1000 #/ cm^3 were removed. The number concentration reported by the APS was aggregated as summarized in **Table 2** to match the cumulative number concentrations of the PMS. The 1-second PMS measurement and 5-second APS measurement were aggregated to obtain 1-minute averaged data for calibration. The smallest size bin of the APS (< 0.523 μm) was used as a reference for calibrating PMS size bin > 0.3 μm.

Table 2. The PMS manufacturer's specified size bins and mass indices with the corresponding reference APS aerodynamic size bins for calibration.

PMS indices	Reference APS indices
Number concentration	
> 0.3 μm	counts aggregated from all size bins (< 0.523 μm and 0.542 – 19.81 μm)
> 0.5 μm	counts aggregated from size bins 0.542 – 19.81 μm
> 1 μm	counts aggregated from size bins 1.037 – 19.81 μm
> 2.5 μm	counts aggregated from size bins 2.642 – 19.81 μm
> 5 μm	counts aggregated from size bins 5.048 – 19.81 μm
> 10 μm	counts aggregated from size bins 10.37 – 19.81 μm
Mass concentration	
PM_1	mass aggregated from size bin < 0.523 μm – 0.965 μm
$PM_{2.5}$	mass aggregated from size bin < 0.523 μm – 2.458 μm

PM_{10}	mass aggregated from size bin < 0.523 μm – 9.647 μm

Figure 3 shows the data from all six PMS sensors during the typical experimental run. In all experiments, the time-series of the uncalibrated concentration measurements from the six PMS sensors were consistent for all size bins (Pearson correlation coefficient (r) > 0.98) (**Figures S4–S12**). The data consistency between the six sensors allows us to develop generalized models by fusing the readings from all sensors and then correlating the data against the APS measurement with matching time stamps for each size bin. The calibrations models of the following form were fit for number concentration data from the APS and PMS:

$$APS_t = \beta_0 + \beta_1 PMS_t + \varepsilon_t \quad \text{Eq. (1)}$$

where APS_t is the number concentration for each aggregated APS size bin at timestamp t; PMS_t is the linear term of the PMS measurement (the number concentration of each PMS size bin) at timestamp t; RH_t is the RH measurement of the Bosch BME680 sensor at timestamp t; β_0 and β_1 are regression coefficients; ε_t is the residual. In addition to Eq. (1), other forms of linear models adjusted for relative humidity, particle density, and CRI were evaluated (**Table S1**). For calibration of mass concentration, models including quadratic terms of the PMS measurement were evaluated (**Table S1**). Since the test temperature variations were within ±2°C, the temperature was not included as a variable in the models. Based on a priori assumption that the PMS particle count and mass indices should be zero when the APS count is zero, the intercept (β_0) of the models was set to zero. The number of terms included in the optimal calibration model for each size bin was determined based on the Bayesian Information Criterion (BIC). The models with lower BIC were chosen as the optimal models. After identifying the optimal models

using BIC and estimating model coefficients, the model was then applied to the pre-calibrated 1-minute PMS measurement to produce the post-calibrated concentrations for model evaluation. Calibration performance was assessed using the normalized mean absolute error (NMAE), which was calculated using the following equation [67]:

$$\text{NMAE}\ (\%) = \frac{\text{Mean}\left(\left|C_{PMS_{post-cal}} - C_{APS}\right|\right)}{\text{Mean}\ (C_{APS})} \quad \text{Eq. (2)}$$

where $C_{PMS\_post\text{-}cal}$ is the post-calibrated 1-minute averaged PMS concentration and C_{APS} is the 1-minute averaged APS concentration. The linear models were fitted using the lm function in R. All the analyses were conducted using R version 3.6.3.

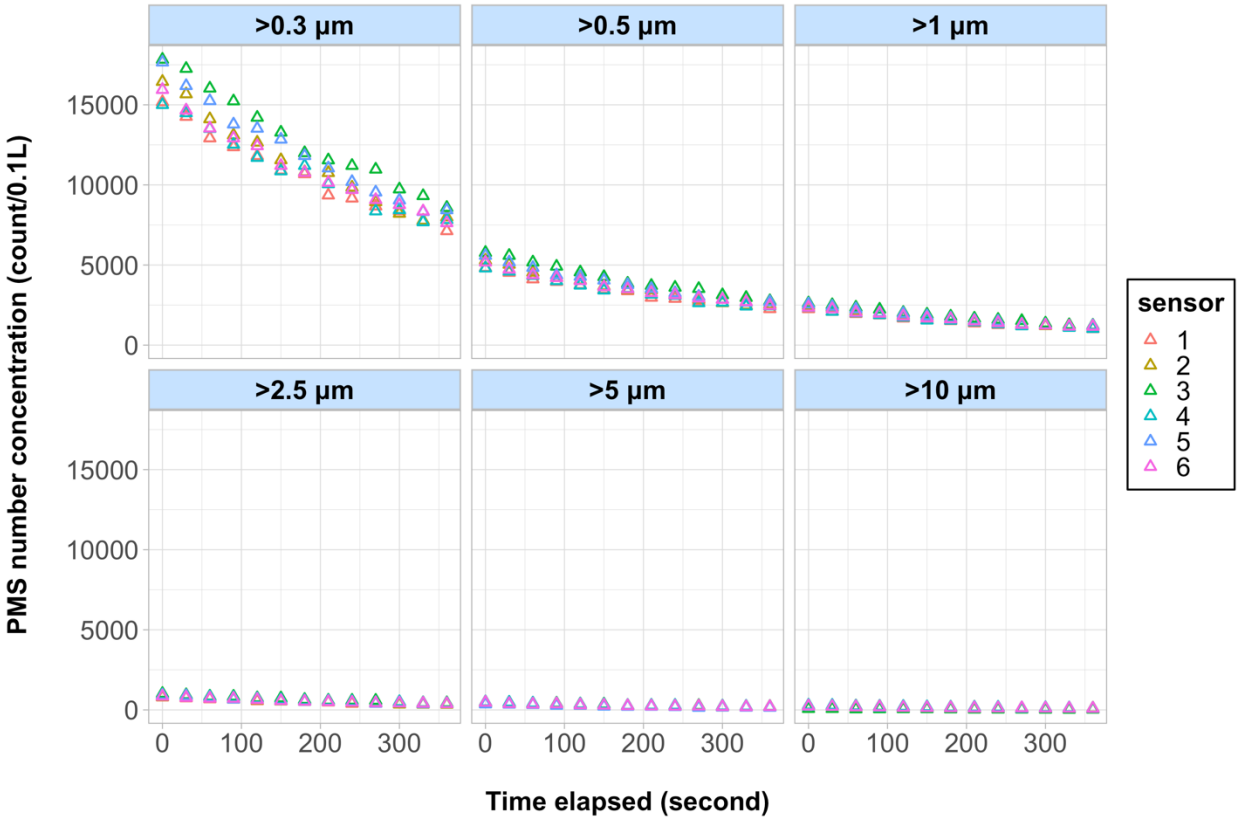

Figure 3. Time-series plots of the uncalibrated, 1-second number concentration measurement from the six PMS sensors are presented. The experiments were conducted under 30% relative humidity with W210 aerosols.

1.4 RESULTS AND DISCUSSION

1.4.1 Test Conditions

During the experiments, the average temperature in the chamber was 24.8°C (range: 23.2 to 26.6°C), the RH was varied in the range of 17.5–79.4%, all experiments were performed at atmospheric pressure conditions. The one-minute APS total number concentration averaged 237.9 #/cm^3 (range: 8.5 to 985.9 #/cm^3). The one-minute $PM_{2.5}$ measurement from the APS and PMS before calibration (6 sensors pooled together) averaged 106.0 µg/m^3 (range: 1.9 to 641.3 µg/m^3) and 51.5 µg/m^3 (range: 0 to 218.8 µg/m^3), respectively.

1.4.2 Particle Size Distribution

The particle size distribution of each test aerosol by the APS is shown in **Figure S3**. The NaCl particles (from the nebulized liquid solution) were the smallest among the test aerosols, with nearly all particles < 3 μm. The W410 mixture had slightly larger particles than W210 and had the same CRI as W210 [68]. **Figure 4** shows the typical particle size distributions reported by the PMS and the APS; the APS bins were aggregated to match the PMS. For all aerosols and all tested concentrations, the PMS appeared to underestimate particle counts for the size bin 0.5–1 μm and 1–2.5 μm. For larger size bins (2.5–5 μm and 5–10 μm), the PMS overestimate the particle counts. The particle count varies significantly in the lowest size bin (PMS: dp = 0.3–0.5 μm; APS: dp <0.523 μm). Both the APS and PMS use the optical channel. Since APS is a single particle instrument, its detection limit is based on the excitation wavelength, photodetector sensitivity, and particle optical properties; it is reported to be 0.37 μm. The PMS does not count every single particle; it relies on the internal calibration of the bulk scattering signal. The PMS OEM calibration significantly overestimates the counts in the 0.3–0.5 μm size range. For PMS, we measured the lower detection limit for the number concentration for the NaCl particles. In NaCl particle experiments, the initial (non-zero) response in the most sensitive PMS bin (dp > 0.3 μm) was observed at ~ 83 #/0.1 L as measured by APS. The PMS sensors seemed to follow the overall trends in the size distribution of the particles greater than 0.5 μm; however, the number concentration and particle sizing do not agree with the single-particle counter. Thus, calibration is needed if PMS is to be used for PM number concentration measurement.

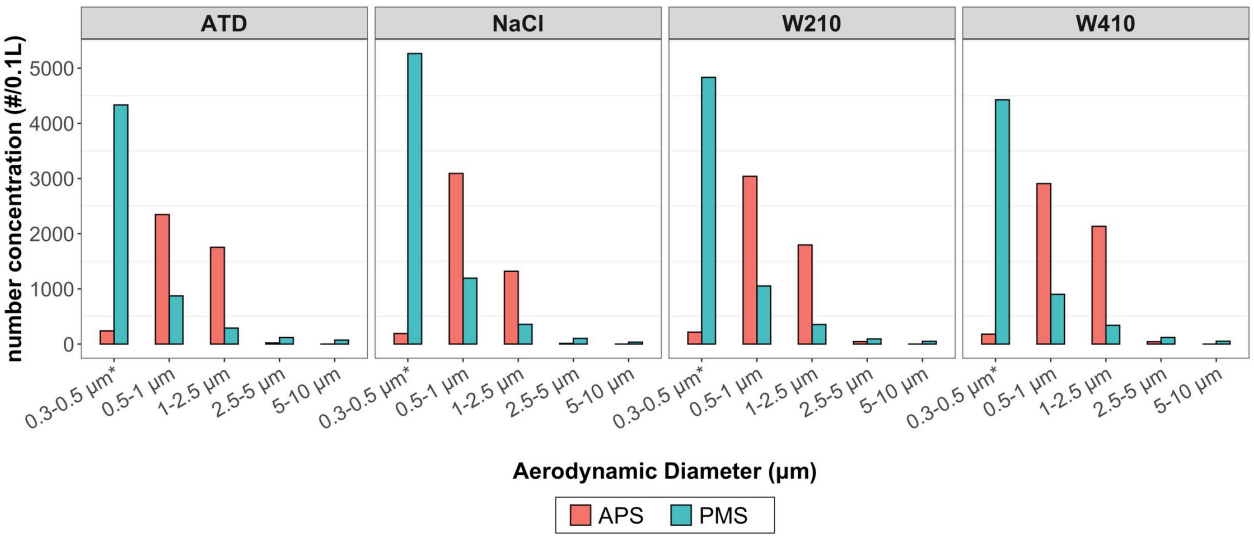

Figure 4. A comparison of the size distribution measured by the APS and PMS using OEM calibration: Data from one of the six PMS for ATD, NaCl, W210, and W410 particles taken 15 minutes after the aerosols were introduced into the chamber. The data from APS bins are aggregated to match the size bins reported by PMS. For PMS bin 0.3–0.5 µm, APS bin < 0.523 µm was used for comparison.

1.4.3 Model Fit

Despite the apparent shift in size distribution shown by **Figure 4**, a matrix of Pearson correlations between the PMS number concentrations (before calibration) and the APS reference number concentrations for different size ranges suggests that the matching size bins between the two instruments are well-correlated (**Figure S1**). Notably, the PMS number concentration data correlated well with the APS for size bin up to 2.5 µm ($r > 0.97$). For measurement of size bin larger than 2.5 µm, the PMS exhibited moderate correlation with the APS ($r < 0.78$). The worst correlation was observed for particles > 5 µm.

A similar Pearson correlation matrix comparing the mass concentrations measured by the PMS (before calibration) and the APS for different particle size ranges suggests a good correlation

between matching sizes (**Figure S2**). The PM_1, $PM_{2.5}$, and PM_{10} measurements by the PMS all exhibited high correlations with their corresponding sizes measured by the APS ($r > 0.90$). Because of the close correlations between corresponding APS and PMS size-specific measurements (**Figure S1** and **S2**), the sizes listed in **Table 2** were chosen to develop calibration models for both PM number concentration and PM mass concentration. For example, APS size bin > 0.5 μm number concentrations was chosen as the reference (independent variable) for calibrating the PMS size bin > 0.5 μm number concentrations (dependent variable). Based on the same rationale, the corresponding APS mass concentration measurement was chosen as the reference for calibrating the PMS mass concentration index. The densities for each testing aerosol are shown in **Table 1**; these were used to determine the APS mass concentration measurement for calibration.

After fitting a set of alternative calibration model forms to the APS and PMS number concentration data, the results show excellent R^2 and low NMAE for >0.3 μm, >0.5 μm, and >1 μm size bins when the full range of concentrations from 0–1000 #/cm^3 was used for fitting (**Table 3** and **Table S2**). However, the model performance was worse for larger size bins, i.e., >2.5 μm, >5 μm, and >10 μm size bins. Based on the previous findings on the impacts of relative humidity on optical particle sensor output and particle optical properties, the models adjusted for CRI and RH were considered in addition to the linear model, see **Table 3**. For most size ranges, the relatively simple linear model without the CRI dependent term performed nearly as well as the models with the additional parameters. The BIC suggests that the models (shown in bold in **Table S2**) with the adjustment for CRI and RH have similar NMAE. The table also includes the models based on the lower concentration data (data points with APS total number

concentration <100 #/cm^3). The models based on the low PM concentration do not perform as well as the full range concentration models.

Table 3. Summary of the calibration models for number concentration, R^2, BIC, and the NMAE of the calibration models.

Indices	Equation	Regression [a]	R^2	BIC	NMAE
Full concentration range (APS total number concentration 0 – 1000 #/ cm^3) (n = 4,134)					
>0.3 µm	Linear	y = 5.93 x	0.99	78723	2.20%
	Linear + CRI + RH	y = 6.00 x – 1090 CRI + 28.23 RH	0.99	78567	2.06%
>0.5 µm	Linear	y = 14.17 x	0.98	79716	2.92%
	Linear + CRI + RH	y = 14.40 x - 1434 CRI + 40.68 RH	0.98	79518	2.78%
>1 µm	Linear	y = 14.85 x	0.96	76002	2.88%
	Linear + CRI + RH	y = 14.98 x - 784.93 CRI + 26.40 RH	0.97	75884	2.89%
>2.5 µm	Linear	y = 2.20 x	0.66	62906	3.87%
	Linear + CRI + RH	y = 2.42 x - 156.71 CRI + 3.38 RH	0.68	62695	3.95%
>5 µm	Linear	y = 0.11 x	0.31	38958	2.71%
	Linear + CRI + RH	y = 0.14 x - 2.41 CRI - 0.06 RH	0.33	38848	2.83%
>10 µm	Linear	y = 0.11 x	0.70	8117	3.66%
	Linear + CRI + RH	y = 0.14 x - 2.41 CRI - 0.06 RH	0.71	8000	3.68%
Lower concentration range (APS total number concentration < 100 #/ cm^3) (n = 1,838)					
>0.3 µm	Linear	y = 4.84 x	0.97	30263	7.96%
	Linear + CRI + RH	y = 4.94 x - 358.12 CRI + 13.68 RH	0.97	30235	7.94%
>0.5 µm	Linear	y = 14.17 x	0.93	30285	10.39%
	Linear + CRI + RH	y = 10.83 x - 385.61 CRI + 18.91 RH	0.94	30234	10.23%
>1 µm	Linear	y = 14.85 x	0.92	26963	8.50%
	Linear + CRI + RH	y = 11.10 x - 105.04 CRI + 10.59 RH	0.93	26713	7.57%
>2.5 µm	Linear	y = 2.20 x	0.60	14298	7.73%
	Linear + CRI + RH	y = 0.45 x - 8.38 CRI + 0.48 RH	0.66	14018	7.22%
>5 µm	Linear	y = 0.11 x	0.35	-2612	11.52%
	Linear + CRI + RH	y = 0.003 x + 0.007 CRI + 0.002 RH	0.44	-2869	11.91%
>10 µm	Linear	y = 0.11 x	0.19	-5846	15.16%
	Linear + CRI + RH	y = 0.002 x + 0.003 CRI + 0.0003 RH	0.22	-5920	17.91%

[a] y: APS measurement; x: PMS measurement.

Definition of abbreviations: n = number of data points;

The OEM calibration for PM mass concentration showed significantly better agreement with the reference instrument than the OEM number density calibration. An additional quadratic term was included for fitting mass concentration data, as shown in **Table 4** and **Table S3**. Similar to the number concentration models, restricting the mass concentration model to only lower concentrations (data points with APS total number concentration <100 #/cm^3) resulted in worse performance vs. model based on the entire concentration range. The optimal models (shown in bold in **Table S3**) included quadratic terms of PMS measurement, terms related to particle properties, and environmental conditions (CRI, density, and in some cases, RH) resulted in NMAE < 3.4% for the entire concentration range. Compared to the relatively simple linear models without these added parameters (CRI, density, and RH terms), the improvements in NMAE for models adjusted for these parameters tended to be larger than those observed for the number concentration models. The inclusion of quadratic term of PMS measurement in these optimal models also highlighted the non-linearity in the OEM's mass concentrations estimates (**Table 4** and **Table S3**). CRI adjustment did not produce a significantly better fit for mass concentration calibration. In addition, the R^2 values of the PM_{10} models (ranged between 0.85–0.88) are lower than the R^2 values of the $PM_{2.5}$ models (ranged between 0.94–0.96), which potentially indicated that the sensor performance dropped for particle size within the range of 2.5–10 μm. The poorer performance of the PMS for the coarse PM fraction was observed; the relationship between the estimated PMS and APS mass concentration values for the coarse size fraction (i.e., particle sizes from 2.5 to 10 μm) was markedly worse than smaller size fractions (**Figure S3**).

Table 4. Summary of the calibration models for mass concentration [a], R^2, BIC, and the NMAE of the calibration models.

Indices	Equation	Regression [b]	R^2	BIC	NMAE
Full concentration range (APS total number concentration between 0 – 1000 #/ cm^3) (n = 4,134)					
PM_1	Linear	$y = 1.06\ x$	0.96	25852	3.11%
	Polynomial	$y = 0.76\ x + 0.007\ x^2$	0.97	24480	2.41%
	Linear + CRI + density	$y = 1.13\ x + 13.88\ CRI - 10.13\ density$	0.97	24181	2.84%
	Polynomial + CRI + density	$y = 0.83\ x + 0.01x^2 + 14.44\ CRI - 9.58\ density$	0.98	23432	2.33%
$PM_{2.5}$	Linear	$y = 2.29\ x$	0.94	42435	4.53%
	Polynomial	$y = 1.55\ x + 0.006\ x^2$	0.96	41341	3.41%
	Linear + CRI + RH	$y = 2.51\ x - 23.27\ CRI + 0.36\ RH$	0.95	41565	4.07%
	Polynomial + CRI + RH	$y = 1.80\ x + 0.004\ x^2 - 15.55\ CRI + 0.42\ RH$	0.96	41152	3.44%
PM_{10}	Linear	$y = 1.53\ x$	0.85	49963	3.56%
	Polynomial	$y = 0.72\ x - 0.003\ x^2$	0.88	48959	2.61%
	Linear + CRI + RH	$y = 1.69\ x - 39.14\ CRI + 0.56\ RH$	0.87	49544	3.31%
	Polynomial + CRI + RH	$y = 0.73\ x + 0.003\ x^2 - 17.94\ CRI + 0.75\ RH$	0.88	48931	2.61%
Lower concentration range (APS total number concentration < 100 #/ cm^3) (n = 1,838)					
PM_1	Linear	$y = 0.72\ x$	0.90	6211	10.10%
	Polynomial	$y = 0.91\ x - 0.02\ x^2$	0.91	6053	9.23%
	Linear + CRI + density	$y = 0.57\ x + 4.80\ CRI - 2.68\ density$	0.93	5746	8.16%
	Polynomial + CRI + density	$y = 0.80\ x - 0.02\ x^2 + 4.93\ CRI - 2.95\ density$	0.93	5694	8.08%
$PM_{2.5}$	Linear	$y = 1.10\ x$	0.91	11170	9.14%
	Polynomial	$y = 1.34\ x - 0.01\ x^2$	0.91	11087	8.80%
	Linear + CRI + RH	$y = 0.97\ x - 1.87\ CRI + 0.16\ RH$	0.92	10890	8.01%
	Polynomial + CRI + RH	$y = 1.14\ x - 0.006\ x^2 - 2.43\ CRI + 0.17\ RH$	0.92	10885	7.97%
PM_{10}	Linear	$y = 0.63\ x$	0.89	11878	9.30%
	Polynomial	$y = 0.86\ x - 0.01\ x^2$	0.90	11686	8.53%
	Linear + CRI + RH	$y = 0.54\ x - 2.15\ CRI + 0.20\ RH$	0.91	11627	8.01%
	Polynomial + CRI + RH	$y = 0.78\ x - 0.004\ x^2 - 3.57\ CRI + 0.21\ RH$	0.91	11461	7.75%

[a] The APS mass concentration measurement was obtained with the assumed density for testing aerosols in Table 1.

[b] y: APS measurement; x: PMS measurement

Definition of abbreviations: n = number of datapoints

Figure 5 shows a comparison between the pre-calibrated and post-calibrated PMS and APS particle number concentrations for full and lower concentration ranges. The pre-calibrated (OEM) number concentration vs. APS exhibits a linear trend over the entire range for all aerosols; however, the PMS underestimates the number of particles. The calibration significantly improves the agreement demonstrating the importance of calibration and the accuracy gains from applying calibrations. The simple linear relationship shows excellent agreement over the entire range of particle concentration and properties, the fitting parameter are shown in **Table 3**.

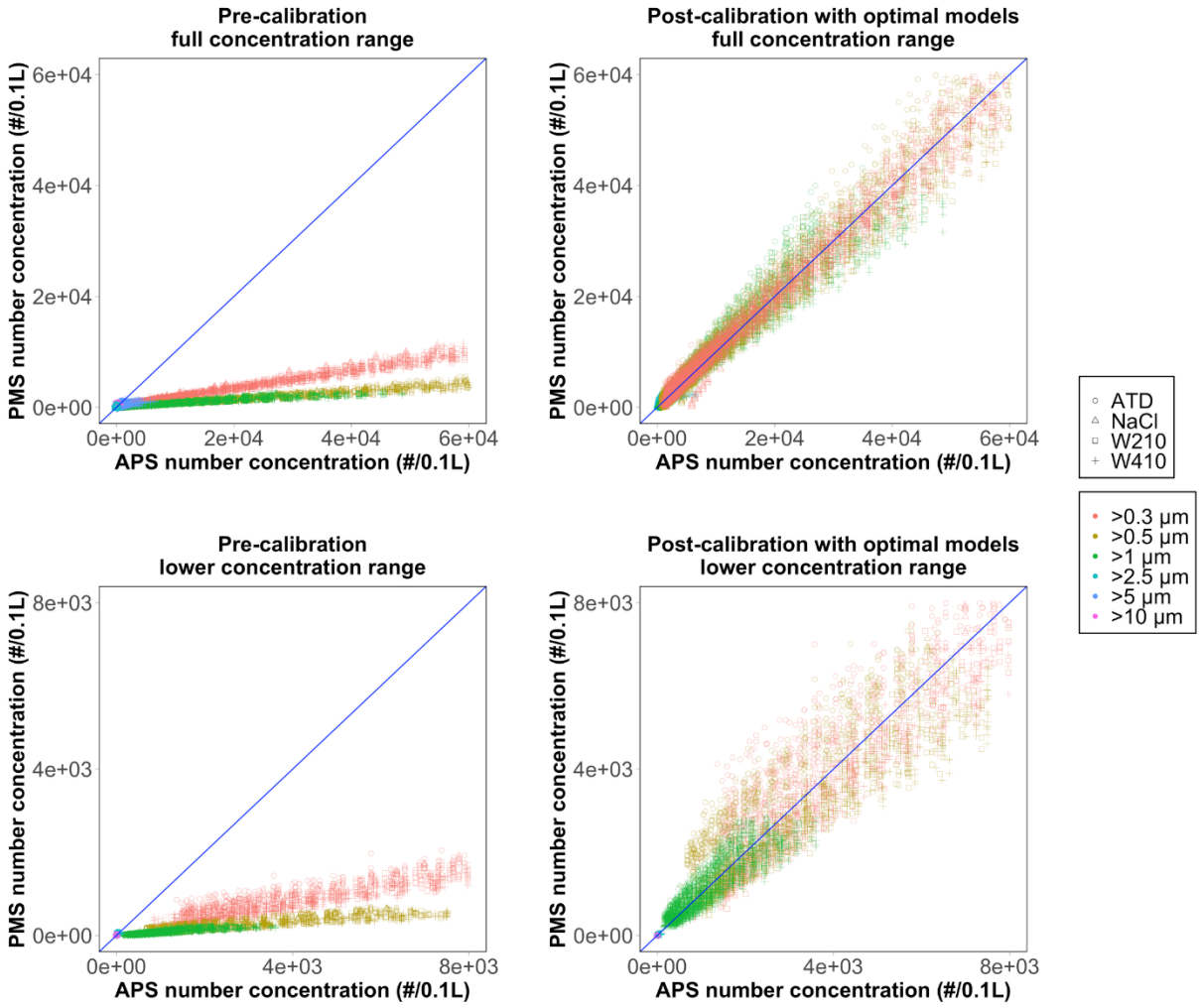

Figure 5. A comparison of the pre-calibrated and post-calibrated number concentrations by full and lower concentration range. The blue line represents the 1:1 relationship between the PMS and APS concentration.

For mass concentration (**Figure 6**), the PMS does not increase linearly compared to APS estimates, especially at higher concentrations. We do not have a satisfactory explanation for the non-linear trend when using the OEM calibration. Also, we observed a notable discrepancy in the PMS and APS relationship between ATD and other test aerosols, which may be related to a wide range of particle CRI in ATD; see **Table 1**. The graphical comparison is consistent with our results from **Table 4** that shows lower NMAE for the models with a quadratic term. Overall, the

mass concentration models adjusted for particle and environmental specific properties such as CRI, density, RH, as well as adjustment for non-linearity, seem to be necessary.

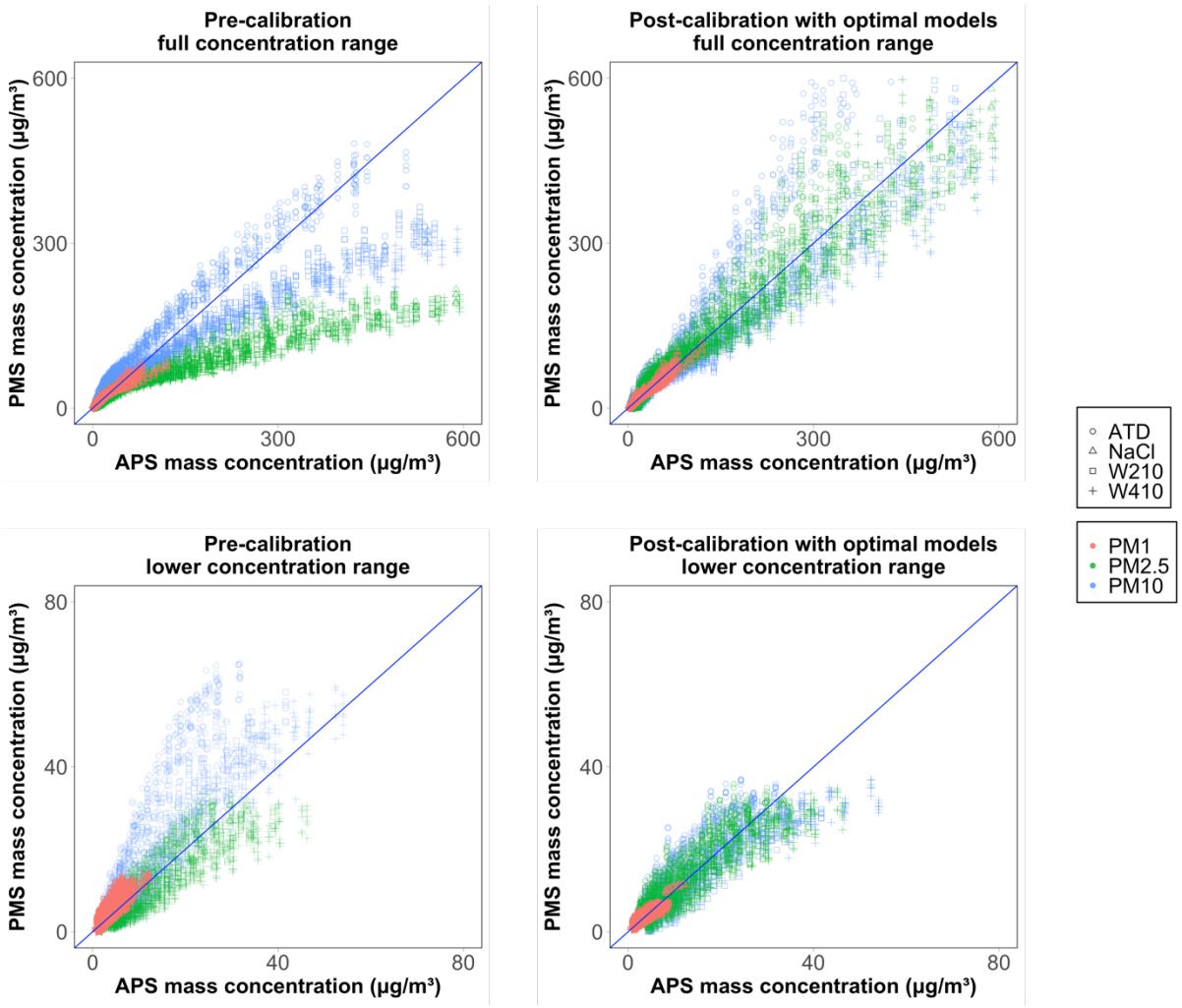

Figure 6. A comparison of the pre-calibrated and post-calibrated mass concentrations by full and lower concentration range. The blue line represents the 1:1 relationship between the PMS and APS concentration.

1.5 CONCLUSIONS

This study evaluated the PMS sensors and reported the calibration algorithm for both number concentration and mass concentration. We found that the PMS's number concentrations can be

corrected using a simple linear model, and mass concentrations can be better corrected using a polynomial model. Although the BIC indicated models adjusted for particle properties and environmental conditions are statistically superior, those models did not significantly improve NMAE. When restricting the fit to the lower concentration, the model's accuracy decreases for both number and mass concentration, and the larger size bins tended to have higher errors. We used particles in a relatively narrow range of CRIs (1.53–1.64) and densities (1.03–2.7 g/cm^3), and our RH was restricted within 17–80%. If the particle properties and environmental conditions of interest are significantly different from tested scenarios, one may need to consider these effects. Despite these limitations, these results are relevant when size-resolved number concentration is desired, especially for using these sensors in high concentration environments, including indoor air quality monitoring, occupational/industrial exposure assessments, or near-source monitoring scenarios. Since the test aerosols used in this study are applicable for several occupational health scenarios, a better exposure assessment could be achieved. In monitoring near-source and indoor air quality, where field calibration might be challenging, the more general algorithms applicable for a broader concentration range and known particle properties could substitute for the labor-intensive gravimetric measurements. The low-cost monitors also enable the development of distributed sensor networks with a much higher special resolution than those currently available from government air quality monitoring sites.

1.6 SUPPLEMENTARY MATERIALS

Table S1. Forms of linear model fitted for number concentration and mass concentration for calibration.

Indices	Form of linear model	Equation
Number concentration	Linear	$\mathrm{APS}_t = \beta_0 + \beta_1\,\mathrm{PMS}_t + \varepsilon_t$
	Linear + CRI	$\mathrm{APS}_t = \beta_0 + \beta_1\,\mathrm{PMS}_t + \beta_2\mathrm{CRI} + \varepsilon_t$
	Linear + RH	$\mathrm{APS}_t = \beta_0 + \beta_1\,\mathrm{PMS}_t + \beta_2\mathrm{RH} + \varepsilon_t$
	Linear + Density	$\mathrm{APS}_t = \beta_0 + \beta_1\,\mathrm{PMS}_t + \beta_2\mathrm{Density} + \varepsilon_t$
	Linear + CRI + Density	$\mathrm{APS}_t = \beta_0 + \beta_1\,\mathrm{PMS}_t + \beta_2\mathrm{CRI} + \beta_3\mathrm{Density} + \varepsilon_t$
	Linear + CRI + RH	$\mathrm{APS}_t = \beta_0 + \beta_1\,\mathrm{PMS}_t + \beta_2\mathrm{CRI} + \beta_3\mathrm{RH} + \varepsilon_t$
Mass concentration	Linear	$\mathrm{APS}_t = \beta_0 + \beta_1\,\mathrm{PMS}_t + \varepsilon_t$
	Linear + CRI	$\mathrm{APS}_t = \beta_0 + \beta_1\,\mathrm{PMS}_t + \beta_2\mathrm{CRI} + \varepsilon_t$
	Linear + RH	$\mathrm{APS}_t = \beta_0 + \beta_1\,\mathrm{PMS}_t + \beta_2\mathrm{RH} + \varepsilon_t$
	Linear + Density	$\mathrm{APS}_t = \beta_0 + \beta_1\,\mathrm{PMS}_t + \beta_2\mathrm{Density} + \varepsilon_t$
	Linear + CRI + Density	$\mathrm{APS}_t = \beta_0 + \beta_1\,\mathrm{PMS}_t + \beta_2\mathrm{CRI} + \beta_3\mathrm{Density} + \varepsilon_t$
	Linear + CRI + RH	$\mathrm{APS}_t = \beta_0 + \beta_1\,\mathrm{PMS}_t + \beta_2\mathrm{CRI} + \beta_3\mathrm{RH} + \varepsilon_t$
	Polynomial	$\mathrm{APS}_t = \beta_0 + \beta_1\,\mathrm{PMS}_t + \beta_2\,\mathrm{PMS}^2{}_t + \varepsilon_t$
	Polynomial + CRI	$\mathrm{APS}_t = \beta_0 + \beta_1\,\mathrm{PMS}_t + \beta_2\,\mathrm{PMS}^2{}_t + \beta_3\mathrm{CRI} + \varepsilon_t$
	Polynomial + RH	$\mathrm{APS}_t = \beta_0 + \beta_1\,\mathrm{PMS}_t + \beta_2\,\mathrm{PMS}^2{}_t + \beta_3\mathrm{RH} + \varepsilon_t$
	Polynomial + Density	$\mathrm{APS}_t = \beta_0 + \beta_1\,\mathrm{PMS}_t + \beta_2\,\mathrm{PMS}^2{}_t + \beta_3\mathrm{Density} + \varepsilon_t$
	Polynomial + CRI + Density	$\mathrm{APS}_t = \beta_0 + \beta_1\,\mathrm{PMS}_t + \beta_2\,\mathrm{PMS}^2{}_t + \beta_3\mathrm{CRI} + \beta_4\mathrm{Density} + \varepsilon_t$
	Polynomial + CRI + RH	$\mathrm{APS}_t = \beta_0 + \beta_1\,\mathrm{PMS}_t + \beta_2\,\mathrm{PMS}^2{}_t + \beta_3\mathrm{CRI} + \beta_4\mathrm{RH} + \varepsilon_t$

Table S2. Summary of the R^2, Bayesian information criterion (BIC), and the normalized mean absolute error (NMAE) of the calibration models for number concentration.

Indices	Equation	Regression [a]	R^2	BIC	NMAE
Full concentration range (APS total number concentration between 0 – 1000 #/ cm^3) (n = 4,134)					
>0.3 µm	Linear	y = 5.93 x	0.99	78723	2.20%
	Linear + CRI	y = 6.02 x - 516.26 CRI	0.99	78603	2.07%
	Linear + RH	y = 5.99 x - 13.72 RH	0.99	78684	2.12%
	Linear + density	y = 6.00 x - 244.83 density	0.99	78659	2.09%
	Linear + CRI + density	**y = 6.06 x - 7924 CRI + 4709 density**	**0.99**	**78134**	**2.02%**
	Linear + CRI + RH	y = 6.00 x - 1090 CRI + 28.23 RH	0.99	78567	2.06%
>0.5 µm	Linear	y = 14.17 x	0.98	79716	2.92%
	Linear + CRI	y = 14.52 x - 605.95 CRI	0.98	79584	2.83%
	Linear + RH	y = 14.39 x - 14.59 RH	0.98	79682	2.85%
	Linear + density	y = 14.46 x - 322.64 density	0.98	79618	2.83%
	Linear + CRI + density	**y = 14.59 x - 5054 CRI + 2828 density**	**0.98**	**79462**	**2.81%**
	Linear + CRI + RH	y = 14.40 x - 1434 CRI + 40.68 RH	0.98	79518	2.78%
>1 µm	Linear	y = 14.85 x	0.96	76002	2.88%
	Linear + CRI	y = 15.15 x - 243.6 CRI	0.97	75950	2.91%
	Linear + RH	y = 14.99 x - 4.28 RH	0.96	76000	2.89%
	Linear + density	y = 15.08 x - 121.37 density	0.96	75973	2.90%
	Linear + CRI + density	**y = 15.23 x - 3476 CRI + 2064 density**	**0.97**	**75789**	**2.87%**
	Linear + CRI + RH	y = 14.98 x - 784.93 CRI + 26.40 RH	0.97	75884	2.89%
>2.5 µm	Linear	y = 2.2 x	0.66	62906	3.87%
	Linear + CRI	y = 2.48 x - 86.58 CRI	0.68	62717	3.95%
	Linear + RH	y = 2.43 x - 2.79 RH	0.67	62808	3.84%
	Linear + density	y = 2.46 x - 52.33 density	0.67	62737	3.93%
	Linear + CRI + density	y = 2.48 x - 343.19 CRI + 164.55 density	0.68	62699	3.93%
	Linear + CRI + RH	**y = 2.42 x - 156.71 CRI + 3.38 RH**	**0.68**	**62695**	**3.95%**
>5 µm	Linear	y = 0.11 x	0.31	38958	2.71%
	Linear + CRI	y = 0.14 x - 3.72 CRI	0.33	38843	2.83%
	Linear + RH	y = 0.14 x - 0.16 RH	0.32	38849	2.78%
	Linear + density	y = 0.14 x - 2.27 density	0.32	38853	2.82%
	Linear + CRI + density	**y = 0.13 x - 12.76 CRI + 5.81 density**	**0.33**	**38841**	**2.82%**

	Linear + CRI + RH	y = 0.14 x - 2.41 CRI - 0.06 RH	0.33	38848	2.83%
>10 µm	Linear	y = 0.11 x	0.70	8117	3.66%
	Linear + CRI	y = 0.14 x - 3.72 CRI	0.71	7997	3.69%
	Linear + RH	y = 0.14 x - 0.16 RH	0.71	7998	3.65%
	Linear + density	y = 0.14 x - 2.27 density	0.71	8022	3.66%
	Linear + CRI + density	**y = 0.13 x - 12.76 CRI + 5.81 density**	**0.72**	**7918**	**3.67%**
	Linear + CRI + RH	y = 0.14 x - 2.41 CRI - 0.06 RH	0.71	8000	3.68%
Lower concentration range (APS total number concentration < 100 #/ cm^3) (n = 1,838)					
>0.3 µm	Linear	y = 4.84 x	0.97	30263	7.96%
	Linear + CRI	y = 4.95 x - 86.88 CRI	0.97	30263	8.02%
	Linear + RH	y = 4.80 x - 1.08 RH	0.97	30270	7.94%
	Linear + density	y = 4.92 x - 43.29 Density	0.97	30265	8.01%
	Linear + CRI + density	y = 4.98 x - 723.33 CRI + 396.15 Density	0.97	30259	7.98%
	Linear + CRI + RH	**y = 4.94 x - 358.12 CRI + 13.68 RH**	**0.97**	**30235**	**7.94%**
>0.5 µm	Linear	y = 10.84 x	0.93	30285	10.39%
	Linear + CRI	y = 10.89 x - 9.97 CRI	0.93	30293	10.41%
	Linear + RH	y = 10.38 x + 5.12 RH	0.93	30276	10.21%
	Linear + density	y = 10.89 x - 5.98 Density	0.93	30293	10.41%
	Linear + CRI + density	y = 10.89 x - 15.80 CRI + 3.63 density	0.93	30300	10.41%
	Linear + CRI + RH	**y = 10.83 x - 385.61 CRI + 18.91 RH**	**0.94**	**30234**	**10.23%**
>1 µm	Linear	y = 12.50 x	0.92	26963	8.50%
	Linear + CRI	y = 11.21 x + 105.13 CRI	0.93	26844	7.99%
	Linear + RH	y = 10.88 x + 6.37 RH	0.93	26734	7.68%
	Linear + density	y = 11.17 x + 69.72 density	0.93	26828	7.97%
	Linear + CRI + density	y = 11.33 x - 361.34 CRI + 294.27 density	0.93	26812	7.94%
	Linear + CRI + RH	**y = 11.10 x - 105.04 CRI + 10.59 RH**	**0.93**	**26713**	**7.57%**
>2.5 µm	Linear	y = 0.51 x	0.60	14298	7.73%
	Linear + CRI	y = 0.46 x + 1.20 CRI	0.60	14284	7.72%
	Linear + RH	y = 0.41 x + 0.13 RH	0.62	14192	7.76%
	Linear + density	y = 0.46 x + 0.80 density	0.60	14282	7.72%
	Linear + CRI + density	y = 0.46 x - 4.61 CRI + 3.71 density	0.60	14286	7.68%
	Linear + CRI + RH	**y = 0.45 x - 8.38 CRI + 0.48 RH**	**0.66**	**14018**	**7.22%**
>5 µm	Linear	y = 0.01 x	0.35	-2612	11.52%

	Linear + CRI	y = 0.003 x + 0.04 CRI	0.43	-2845	12.04%
	Linear + RH	**y = 0.004 x + 0.002 RH**	**0.44**	**-2876**	**11.89%**
	Linear + density	y = 0.003 x + 0.03 density	0.43	-2856	12.01%
	Linear + CRI + density	y - 0.003 x - 0.06 CRI + 0.06 density	0.44	-2855	11.95%
	Linear + CRI + RH	y = 0.003 x + 0.007 CRI + 0.002 RH	0.44	-2869	11.91%
>10 µm	Linear	y = 0.004 x	0.19	-5846	15.16%
	Linear + CRI	y = 0.002 x + 0.009 CRI	0.22	-5922	17.97%
	Linear + RH	**y = 0.002 x + 0.0004 RH**	**0.22**	**-5926**	**17.74%**
	Linear + density	y = 0.002 x + 0.006 density	0.22	-5922	17.95%
	Linear + CRI + density	y = 0.002 x + 0.004 CRI + 0.003 density	0.22	-5915	17.97%
	Linear + CRI + RH	y = 0.002 x + 0.003 CRI + 0.0003 RH	0.22	-5920	17.91%

[a] y: APS measurement; x: PMS measurement. The models emboldened for each size bin were the optimal model selected according to the BIC.

Definition of abbreviations: n = number of datapoints; CRI = complex index of refraction; RH = relative humidity; BIC = Bayesian information criteria; NMAE = normalized mean absolute error.

Table S3. Summary of the R^2, Bayesian information criterion (BIC), and the normalized mean absolute error (NMAE) of the calibration models for mass concentration.

Indices	Equation	Regression [a]	R^2	BIC [b]	NMAE
Full concentration range (APS total number concentration between 0 – 1000 #/ cm^3) (n = 4,134)					
PM_1	Linear	$y = 1.06\ x$	0.96	25852	3.11%
	Polynomial	$y = 0.76\ x + 0.007\ x^2$	0.97	24480	2.41%
	Linear + CRI	$y = 1.16\ x - 2.12\ CRI$	0.97	25137	2.99%
	Polynomial + CRI	$y = 0.82\ x + 0.006\ x^2 - 0.58\ CRI$	0.97	24446	2.48%
	Linear + RH	$y = 1.15\ x - 0.08\ RH$	0.97	25333	3.03%
	Polynomial + RH	$y = 0.79\ x + 0.01\ x^2 - 0.02\ RH$	0.97	24471	2.46%
	Linear + density	$y = 1.16\ x - 1.51\ density$	0.97	24906	3.00%
	Polynomial + density	$y = 0.87\ x + 0.01\ x\ x^2 - 0.65\ density$	0.97	24351	2.54%
	Linear + CRI + density	$y = 1.13\ x + 13.88\ CRI - 10.13\ density$	0.97	24181	2.84%
	Polynomial + CRI + density	**$y = 0.83\ x + 0.01\ x^2 + 14.44\ CRI - 9.58\ density$**	**0.98**	**23432**	**2.33%**
	Linear + CRI + RH	$y = 1.15\ x - 2.14\ CRI + 0.001\ RH$	0.97	25143	2.99%
	Polynomial + CRI + RH	$y = 0.82\ x + 0.006\ x^2 - 0.78\ CRI + 0.01\ RH$	0.97	24451	2.47%
$PM_{2.5}$	Linear	$y = 2.29\ x$	0.94	42435	4.53%
	Polynomial	$y = 1.55\ x + 0.006\ x^2$	0.96	41341	3.41%
	Linear + CRI	$y = 2.54\ x - 16.04\ CRI$	0.95	41613	4.07%
	Polynomial + CRI	$y = 1.86\ x + 0.004\ x^2 - 7.36\ CRI$	0.96	41227	3.47%
	Linear + RH	$y = 2.50\ x - 0.53\ RH$	0.95	41983	4.12%
	Polynomial + RH	$y = 1.64\ x + 0.005\ x^2 - 0.1\ RH$	0.96	41337	3.41%
	Linear + density	$y = 2.53\ x - 10.36\ density$	0.95	41568	4.05%
	Polynomial + density	$y = 1.88\ x + 0.004\ x^2 - 5.11\ density$	0.96	41199	3.48%
	Linear + CRI + density	$y = 2.52\ x + 13.55\ CRI - 18.82\ density$	0.95	41565	4.04%
	Polynomial + CRI + density	$y = 1.85\ x + 0.004\ x^2 + 22.74\ CRI - 19.13\ density$	0.96	41172	3.44%
	Linear + CRI + RH	$y = 2.51\ x - 23.27\ CRI + 0.36\ RH$	0.95	41565	4.07%
	Polynomial + CRI + RH	**$y = 1.80\ x + 0.004\ x^2 - 15.55\ CRI + 0.42\ RH$**	**0.96**	**41152**	**3.44%**
PM_{10}	Linear	$y = 1.53\ x$	0.85	49963	3.56%
	Polynomial	$y = 0.72\ x - 0.003\ x^2$	0.88	48959	2.61%
	Linear + CRI	$y = 1.72\ x - 27.80\ CRI$	0.86	49555	3.31%
	Polynomial + CRI	$y = 0.78\ x + 0.003\ x^2 - 3.13\ CRI$	0.88	48963	2.63%

	Linear + RH	$y = 1.69\ x - 0.96\ RH$	0.86	49716	3.33%
	Polynomial + RH	$y = 0.66\ x - 0.003\ x^2 + 0.13\ RH$	0.88	48963	2.62%
	Linear + density	$y = 1.71\ x - 17.91\ density$	0.86	49541	3.32%
	Polynomial + density	$y = 0.80\ x - 0.003\ x^2 - 2.9\ density$	0.88	48958	2.65%
	Linear + CRI + density	$y = 1.71\ x + 12.33\ CRI - 25.67\ density$	0.86	49548	3.32%
	Polynomial + CRI + density	$y = 0.75\ x + 0.003\ x^2 + 55.58\ CRI - 37.27\ density$	0.88	48934	2.62%
	Linear + CRI + RH	$y = 1.69\ x - 39.14\ CRI + 0.56\ RH$	0.87	49544	3.31%
	Polynomial + CRI + RH	**$y = 0.73\ x + 0.003\ x^2 - 17.94\ CRI + 0.75\ RH$**	**0.88**	**48931**	**2.61%**
Lower concentration (APS total number concentration < 100 #/ cm^3) (n = 1,838)					
	Linear	$y = 0.72\ x$	0.90	6211	10.10%
	Polynomial	$y = 0.91\ x - 0.02\ x^2$	0.91	6053	9.23%
	Linear + CRI	$y = 0.6\ x + 0.50\ CRI$	0.91	6020	8.82%
	Polynomial + CRI	$y = 0.71\ x - 0.01\ x^2 + 0.36\ CRI$	0.91	6017	8.82%
	Linear + RH	$y = 0.60\ x + 0.02\ RH$	0.92	5979	8.75%
PM_1	Polynomial + RH	$y = 0.70\ x - 0.001\ x^2 + 0.02\ RH$	0.92	5971	8.68%
	Linear + density	$y = 0.62\ x + 0.26\ density$	0.91	6077	9.04%
	Polynomial + density	$y = 0.82\ x - 0.02\ x^2 + 0.1\ density$	0.91	6052	9.06%
	Linear + CRI + density	$y = 0.57\ x + 4.80\ CRI - 2.68\ density$	0.93	5746	8.16%
	Polynomial + CRI + density	**$y = 0.80\ x - 0.02\ x^2 + 4.93\ CRI - 2.95\ density$**	**0.93**	**5694**	**8.08%**
	Linear + CRI + RH	$y = 0.60\ x + 0.08\ CRI + 0.02\ RH$	0.92	5989	8.73%
	Polynomial + CRI + RH	$y = 0.72\ x - 0.01\ x^2 - 0.1\ CRI + 0.02\ RH$	0.92	5987	8.69%
	Linear	$y = 1.10\ x$	0.91	11170	9.14%
	Polynomial	$y = 1.34\ x - 0.01\ x^2$	0.91	11087	8.80%
	Linear + CRI	$y = 0.98\ x + 1.37\ CRI$	0.92	11061	8.48%
	Polynomial + CRI	$y = 1.09\ x - 0.004\ x^2 + 1.06\ CRI$	0.92	11064	8.49%
	Linear + RH	$y = 0.94\ x + 0.09\ RH$	0.92	10932	8.11%
$PM_{2.5}$	Polynomial + RH	$y = 0.92\ x + 0.001\ x^2 + 0.09\ RH$	0.92	10939	8.11%
	Linear + density	$y = 0.99\ x + 0.80\ density$	0.91	11076	8.55%
	Polynomial + density	$y = 1.14\ x - 0.01\ x^2 + 0.54\ density$	0.92	11074	8.58%
	Linear + CRI + density	$y = 0.97\ x + 6.51\ CRI - 3.23\ density$	0.92	11043	8.40%
	Polynomial + CRI + density	$y = 1.09\ x - 0.004\ x^2 + 6.28\ CRI - 3.31\ density$	0.92	11045	8.42%
	Linear + CRI + RH	$y = 0.97\ x - 1.87\ CRI + 0.16\ RH$	0.92	10890	8.01%

Polynomial + CRI + RH	**$y = 1.14\ x - 0.006\ x^2 - 2.43\ CRI + 0.17\ RH$**	**0.92**	**10885**	**7.97%**
PM_{10}	Linear	$y = 0.63\ x$	0.89	11878	9.30%
	Polynomial	$y = 0.86\ x - 0.01\ x^2$	0.90	11686	8.53%
	Linear + CRI	$y = 0.55\ x + 1.92\ CRI$	0.90	11716	8.45%
	Polynomial + CRI	$y = 0.75\ x - 0.004\ x^2 + 0.88\ CRI$	0.90	11675	8.34%
	Linear + RH	$y = 0.52\ x + 0.12\ RH$	0.91	11566	8.10%
	Polynomial + RH	$y = 0.62\ x - 0.002\ x^2 + 0.1\ RH$	0.91	11556	7.99%
	Linear + density	$y = 0.55\ x + 1.12\ density$	0.90	11741	8.54%
	Polynomial + density	$y = 0.78\ x - 0.004\ x^2 + 0.38\ density$	0.90	11685	8.41%
	Linear + CRI + density	$y = 0.54\ x - 11.26\ CRI - 5.92\ density$	0.90	11662	8.26%
	Polynomial + CRI + density	$y = 0.72\ x - 0.003\ x^2 + 9.58\ CRI - 5.45\ density$	0.90	11631	8.16%
	Linear + CRI + RH	$y = 0.54\ x - 2.15\ CRI + 0.20\ RH$	0.91	11627	8.01%
	Polynomial + CRI + RH	**$y = 0.78\ x - 0.004\ x^2 - 3.57\ CRI + 0.21\ RH$**	**0.91**	**11461**	**7.75%**

[a] y: APS measurement; x: PMS measurement. The models emboldened for each size bin were the optimal model selected according to the BIC.

Definition of abbreviations: n = number of datapoints; CRI = complex index of refraction; RH = relative humidity; BIC = Bayesian information criteria; NMAE = normalized mean absolute error.

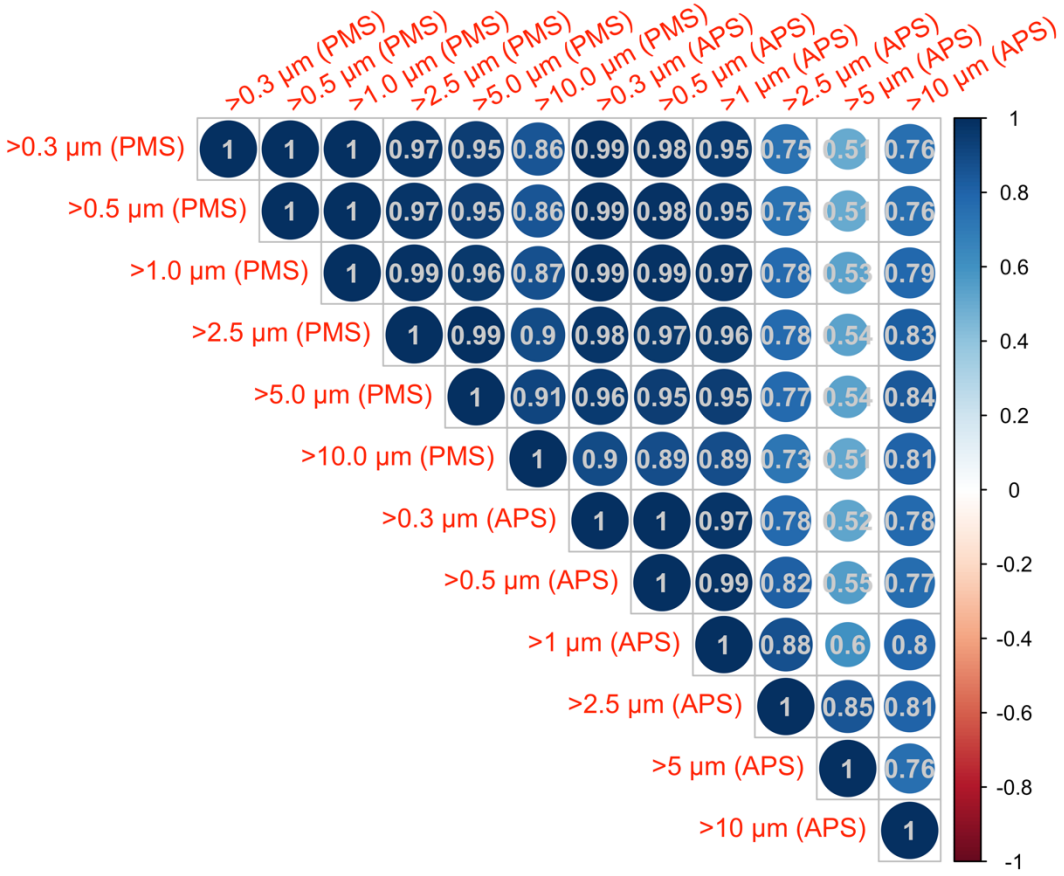

Figure S1. Pearson correlation between the uncalibrated PMS number concentration (6 sensors pooled together) and APS number concentration for different size ranges.

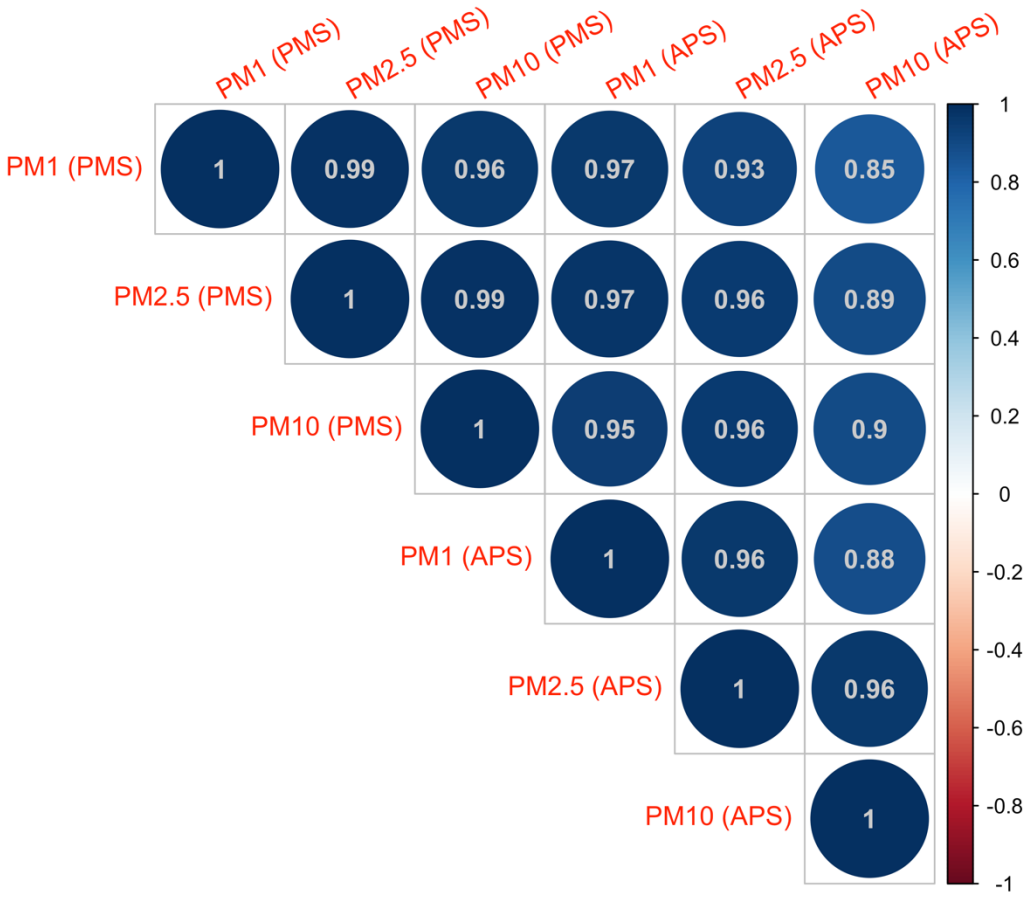

Figure S2. Pearson correlation between the uncalibrated PMS mass concentration (6 sensors pooled together) and APS mass concentration for different size ranges.

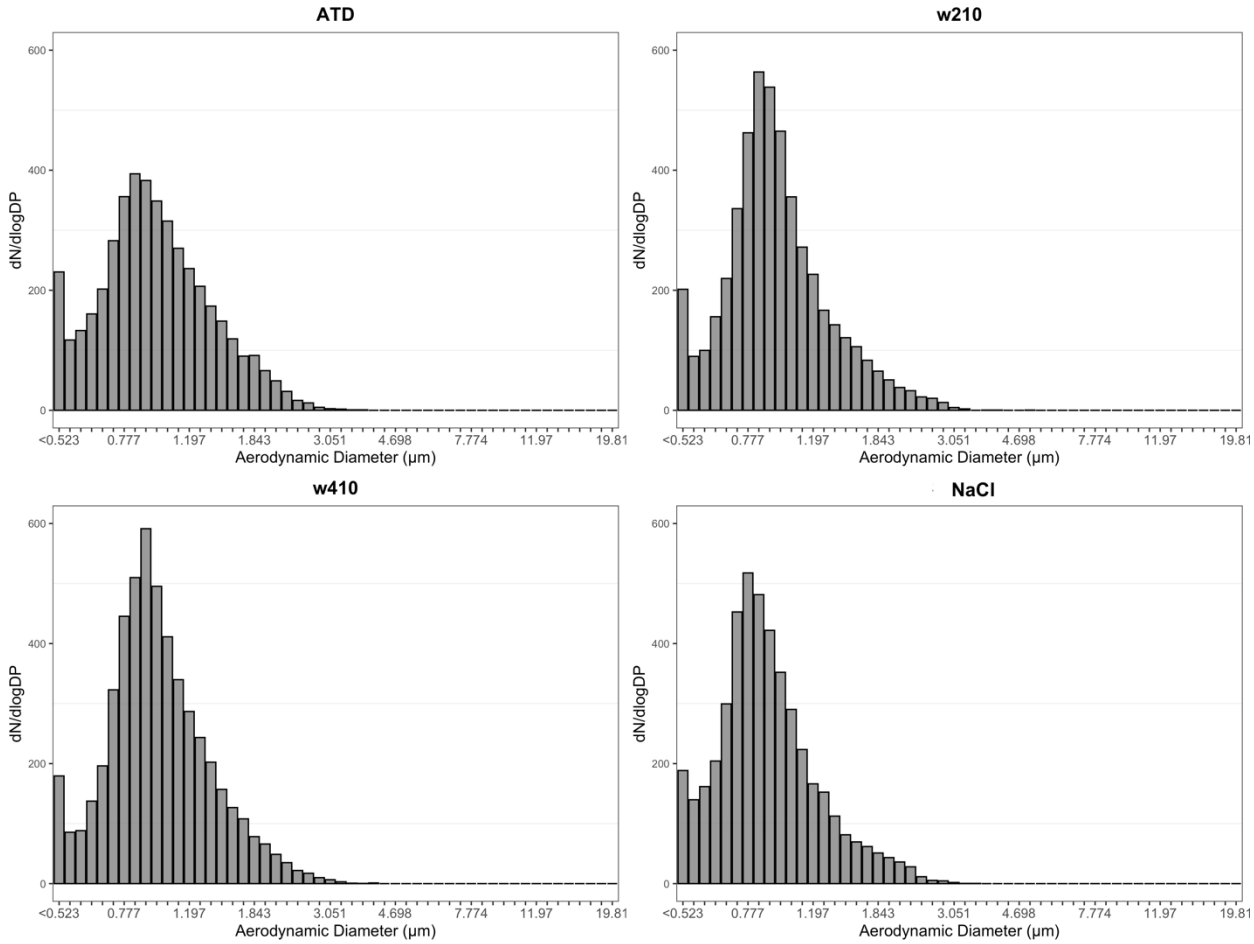

Figure S3. The normalized particle size distribution of the Arizona Test Dust (ATD), NaCl, W210, and W410 measured by the APS. The median diameter of the ATD, saline, W210 and W410 aerosol are 0.94 µm, 0.86 µm, 0.92 µm and 0.96 µm, respectively.

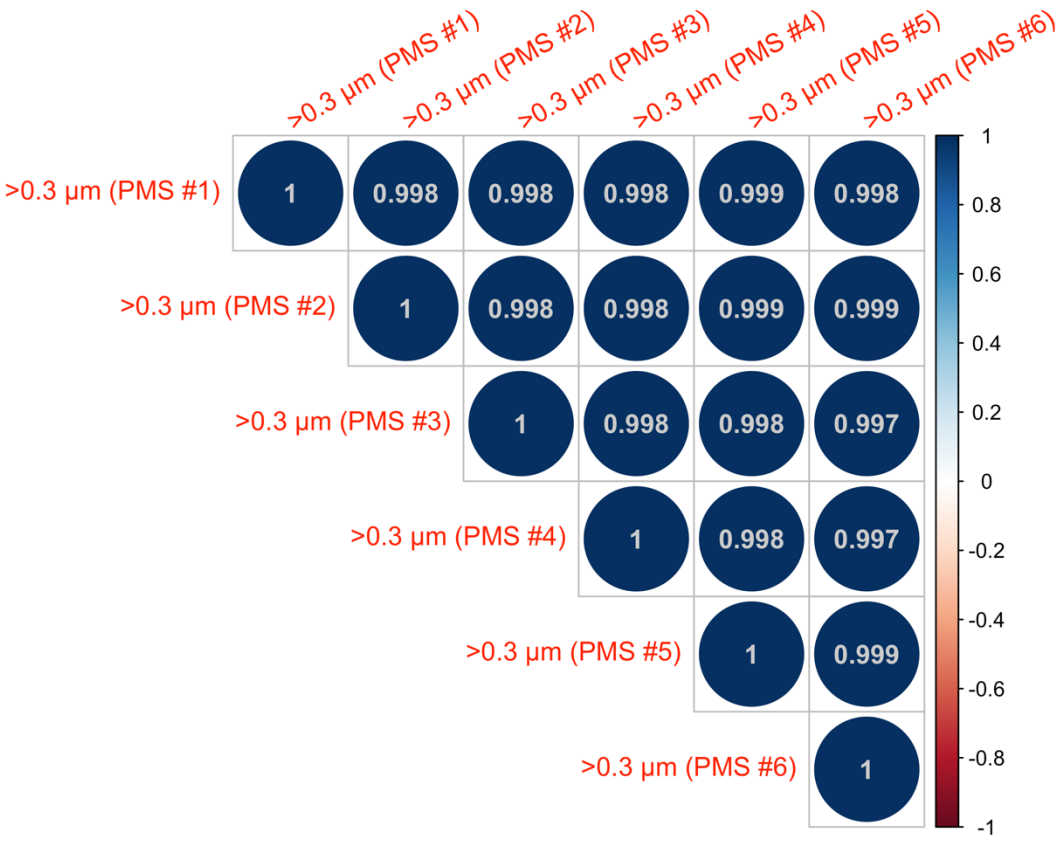

Figure S4. Pearson correlation between pairs of PMS for number concentration (for size range > 0.3 µm).

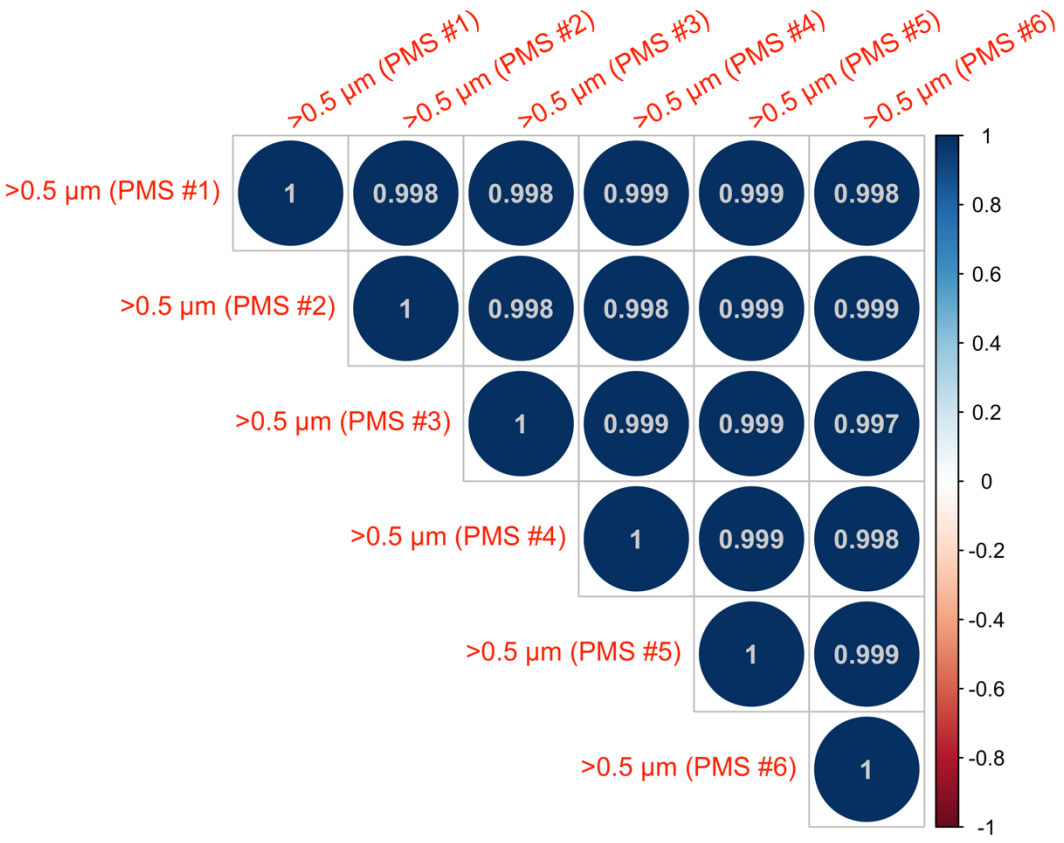

Figure S5. Pearson correlation between pairs of PMS for number concentration (for size range > 0.5 µm).

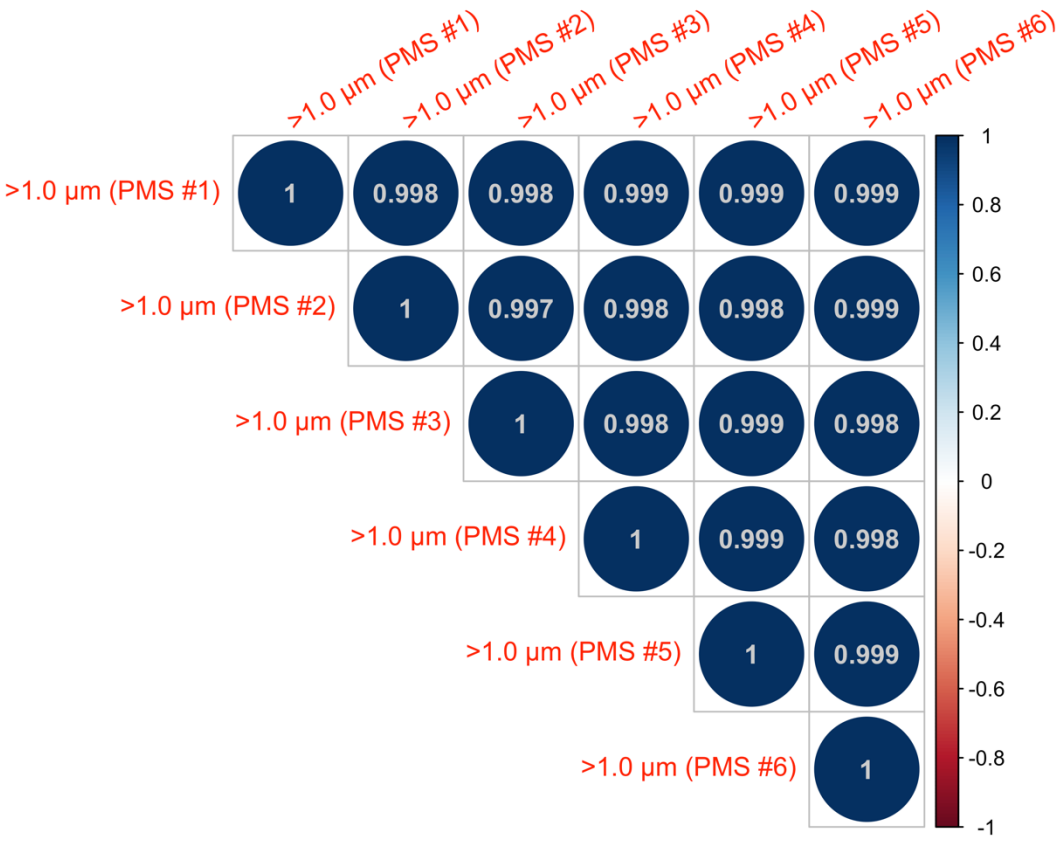

Figure S6. Pearson correlation between pairs of PMS for number concentration (for size range > 1 µm).

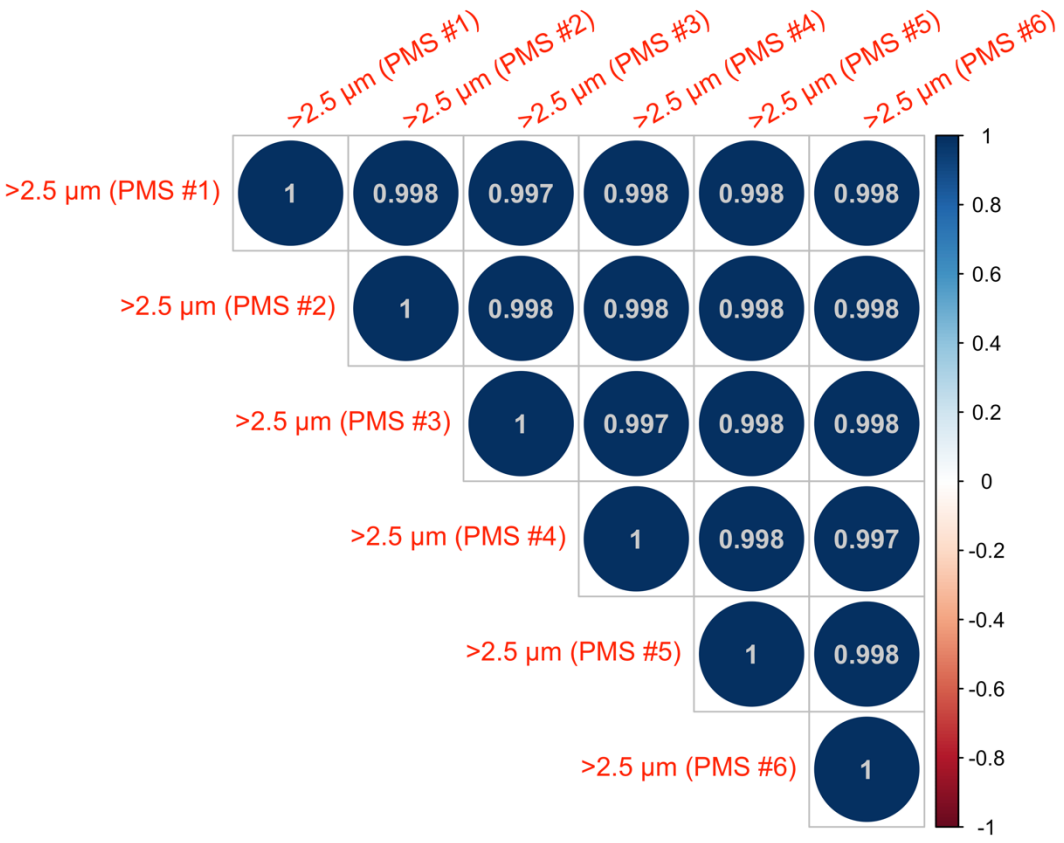

Figure S7. Pearson correlation between pairs of PMS for number concentration (for size range > 2.5 µm).

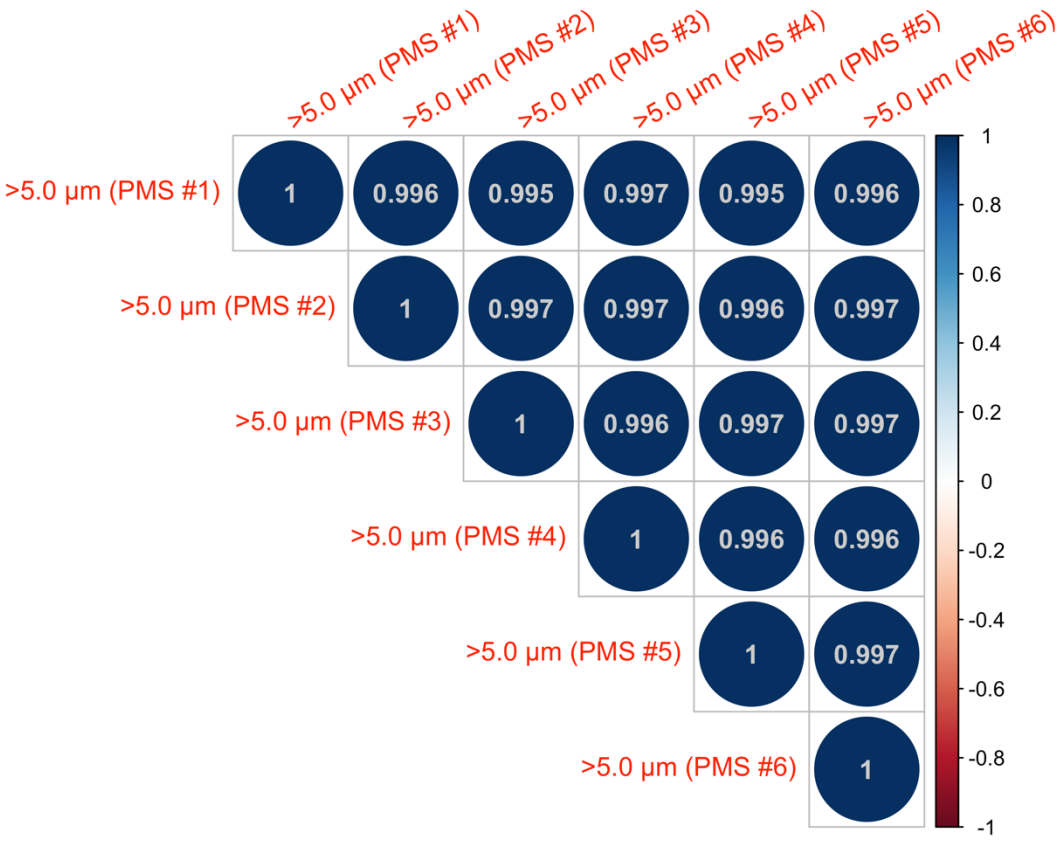

Figure S8. Pearson correlation between pairs of PMS for number concentration (for size range > 5 µm).

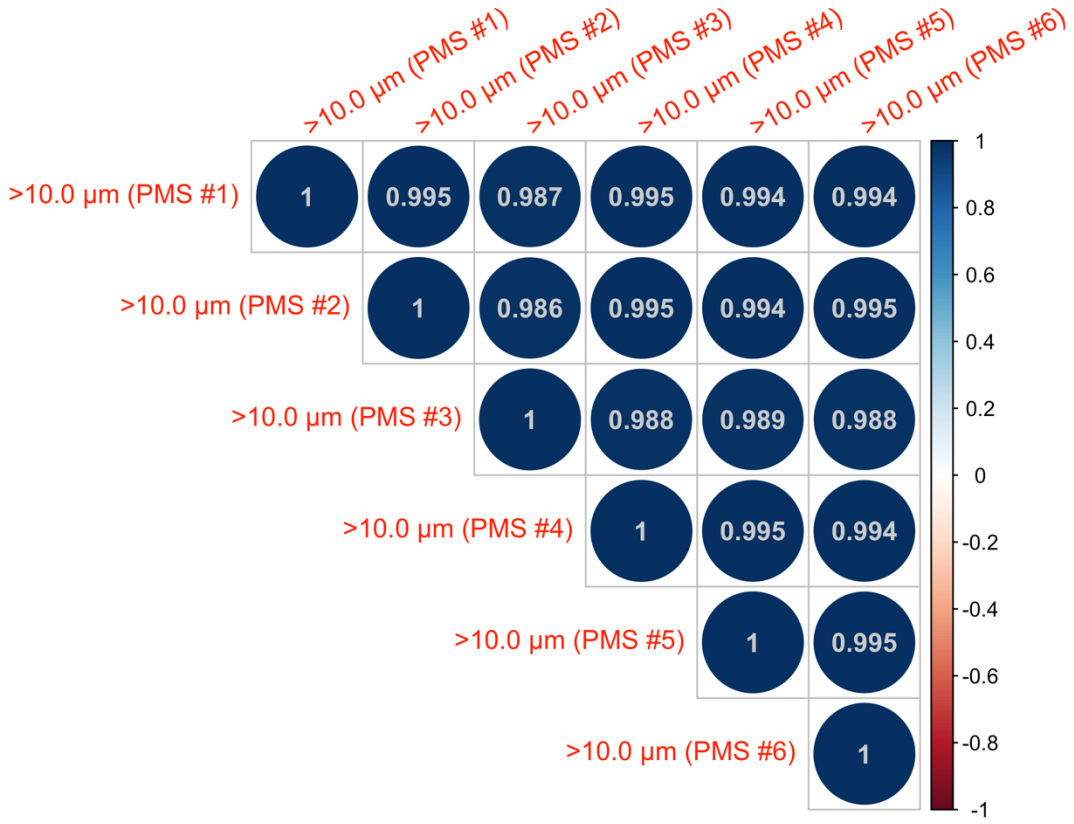

Figure S9. Pearson correlation between pairs of PMS for number concentration (for size range > 10 µm).

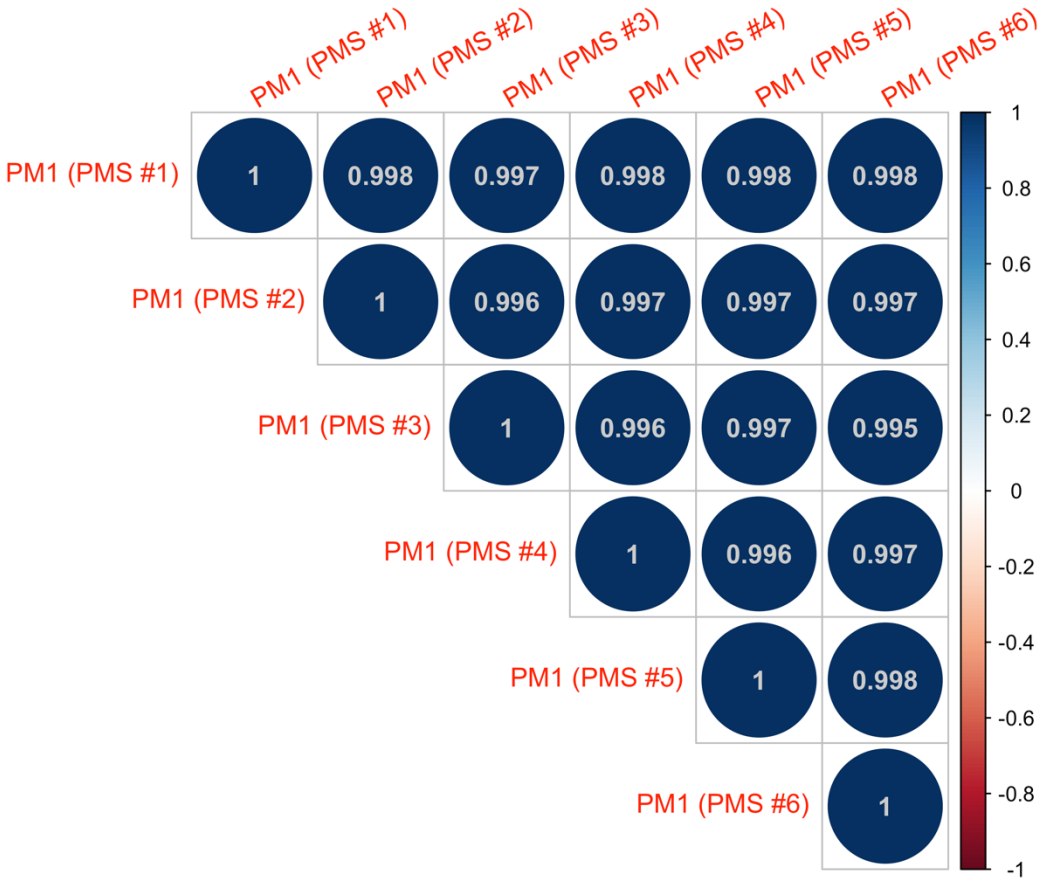

Figure S10. Pearson correlation between pairs of PMS for mass concentration (for PM_1).

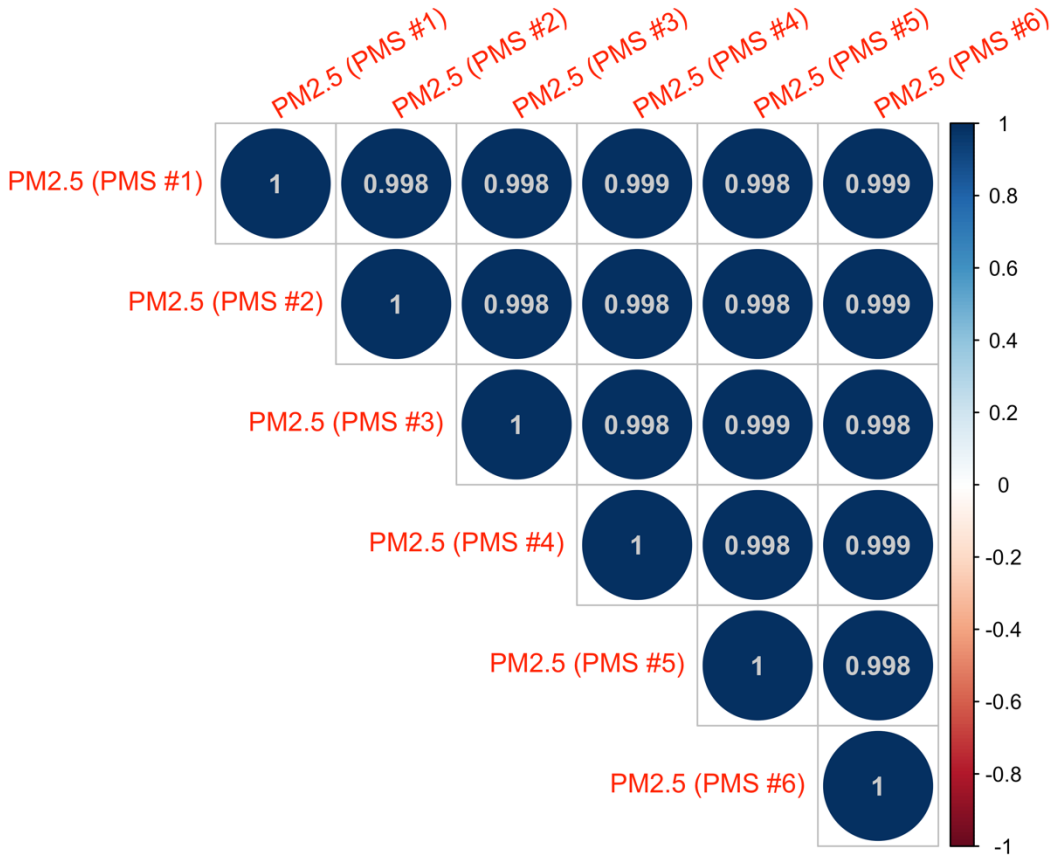

Figure S11. Pearson correlation between pairs of PMS for mass concentration (for $PM_{2.5}$).

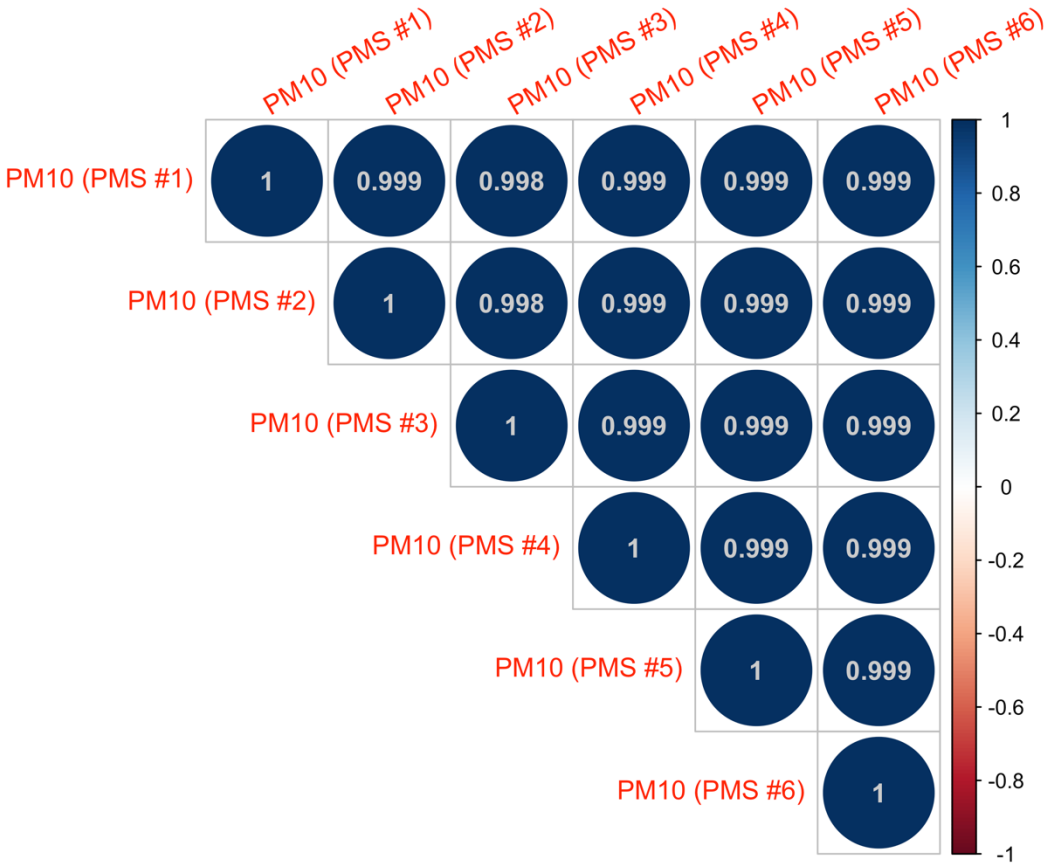

Figure S12. Pearson correlation between pairs of PMS for mass concentration (for PM_{10}).

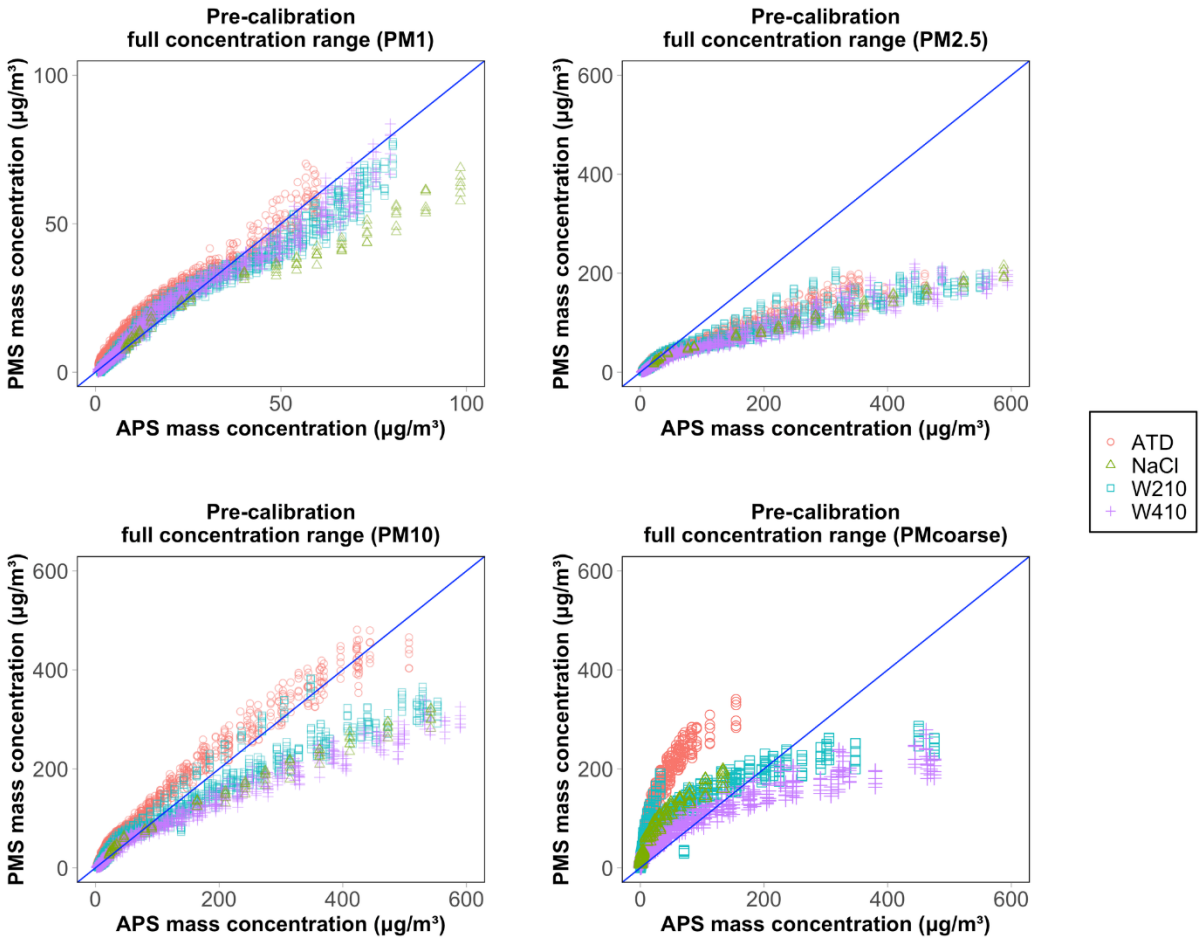

Figure S13. A comparison of the pre-calibrated PM_1, $PM_{2.5}$, PM_{10}, and PMcoarse size fraction (i.e., particle sizes from 2.5 to 10 µm).

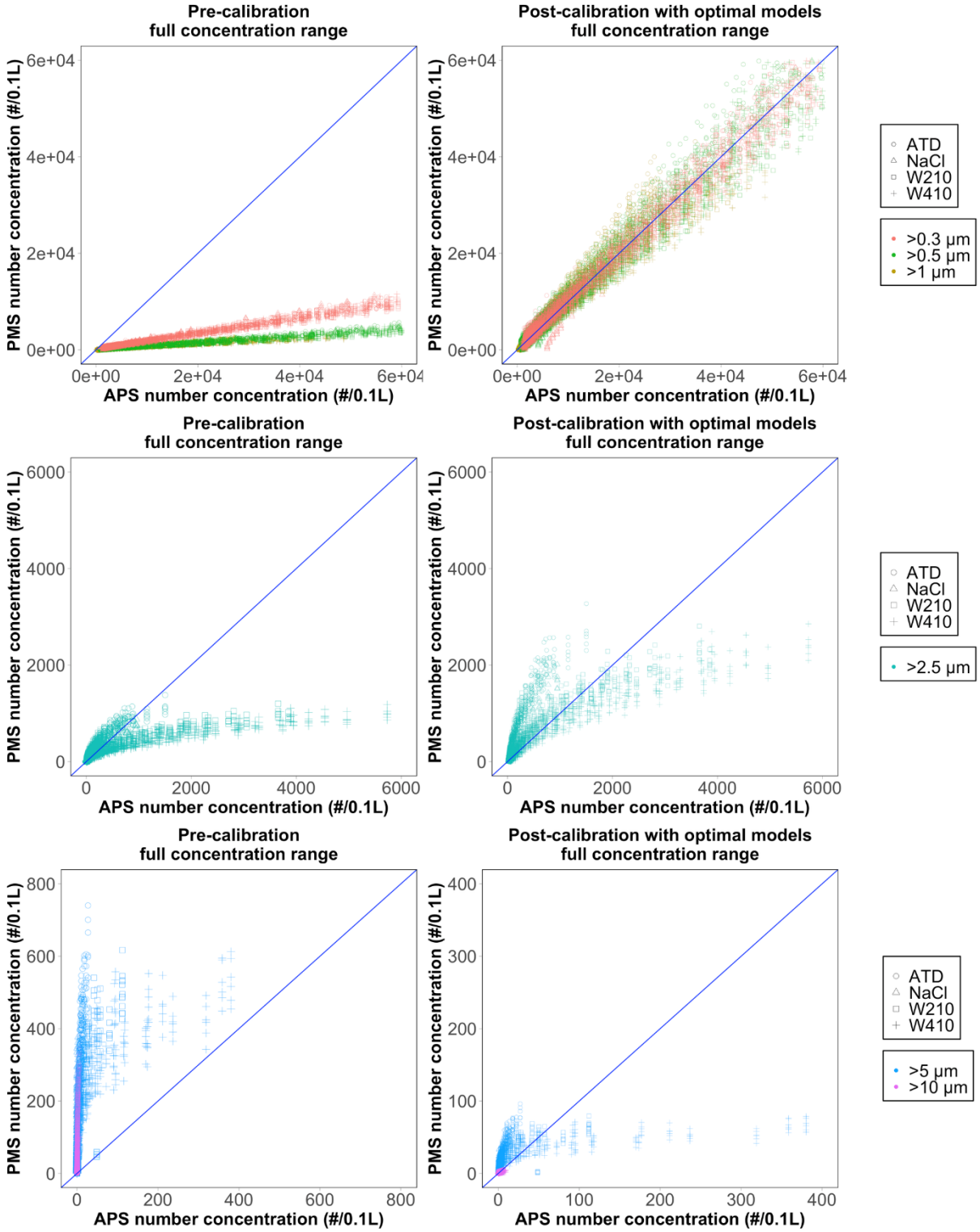

Figure S14. A comparison of the pre-calibrated and post-calibrated number concentrations by different size bins.

Author contributions: Conceptualization, C-H.H., J.H., E.A., E.S., and I.N.; Data curation: C-H.H.; Formal analysis: C-H.H.; Funding acquisition: I.N.; Methodology: C-H.H., J.H., E.A., E.S., and I.N.; Project administration: J.H., I.N.; Resources: J.H., E.S., and I.N.; Software: C-H.H., Supervision: E.A., E.S., and I.N.; Validation: J.H., E.A., E.S., and I.N.; Visualization; C-H. H., Writing – original draft: C-H. H.; Writing – reviewing & editing: J.H., E.A., E.S., and I.N.

Funding: This work was partially supported by the National Institute of Environmental Health Sciences [grant numbers 1R21ES024715 and 1R33ES024715]; and the National Institute of Biomedical Imaging and Bioengineering [grant number U01 EB021923].

Acknowledgments: The authors wish to express special thanks to William Lin and Koustubh Muluk, the students at the University of Washington, for helping to run the aerosol chamber tests in this study.

Competing interests: The authors have declared that no competing interests exist.

CHAPTER 2. ASSESSING THE EFFECTIVENESS OF PORTABLE HEPA AIR CLEANERS FOR REDUCING PARTICULATE MATTER EXPOSURE IN KING COUNTY, WASHINGTON HOMELESS SHELTERS: IMPLICATIONS FOR COMMUNITY CONGREGATE SETTINGS

 The authors of the manuscript are:

Ching-Hsuan Huang [a,*], Thu Bui [b], Daniel Hwang [b], Jeffry Shirai [a], Elena Austin [a], Martin Cohen [a], Timothy Gould [c], Timothy Larson [a, c], Igor Novosselov [d], Shirlee Tan [b], Julie Fox [e], Edmund Seto [a]

[a] Department of Environmental and Occupational Health Sciences, School of Public Health, University of Washington, Seattle, Washington, United States 98195

[b] Public Health – Seattle and King County, Seattle, Washington, United States 98104

[c] Department of Civil and Environmental Engineering, College of Engineering, University of Washington, Seattle, Washington, United States 98195

[d] Department of Mechanical Engineering, College of Engineering, University of Washington, Seattle, Washington, United States 98195

[e] Washington State Department of Health, Tumwater, Washington, United States 98501

* Corresponding author

DOI: http://dx.doi.org/10.1016/j.scitotenv.2023.164402

2.1 ABSTRACT

Over four thousand portable air cleaners (PACs) with high-efficiency particulate air (HEPA) filters were distributed by Public Health - Seattle & King County to homeless shelters during the COVID-19 pandemic. This study aimed to evaluate the real-world effectiveness of these HEPA PACs in reducing indoor particles and understand the factors that affect their use in homeless shelters. Four rooms across three homeless shelters with varying geographic locations and operating conditions were enrolled in this study. At each shelter, multiple PACs were deployed based on the room volume and PAC's clean air delivery rate rating. The energy consumption of these PACs was measured using energy data loggers at 1-min intervals to allow tracking of their use and fan speed for three two-week sampling rounds, separated by single-week gaps, between February and April 2022. Total optical particle number concentration (OPNC) was measured at 2-min intervals at multiple indoor locations and an outdoor ambient location. The empirical indoor and outdoor total OPNC were compared for each site. Additionally, linear mixed-effects regression models (LMERs) were used to assess the relationship between PAC use time and indoor/outdoor total OPNC ratios (I/O_{OPNC}). Based on the LMER models, a ten percent increase in the hourly, daily, and total time PACs were used significantly reduced I/O_{OPNC} by 0.034 [95% CI: 0.028, 0.040; $p< 0.001$], 0.051 [95% CI: 0.020, 0.078; $p< 0.001$], and 0.252 [95% CI: 0.150, 0.328; $p< 0.001$], respectively, indicating that keeping PACs on resulted in significantly lower I/O_{OPNC}. The survey suggested that keeping PACs on and running was the main challenge when operating them in shelters. These findings suggested that HEPA PACs were an effective short-term strategy to reduce indoor particle levels in community congregate living settings during non-wildfire seasons and the need for formulating practical guidance for using them in such an environment.

Keywords: Congregate living setting, homeless shelter, particulate matter (PM), portable air cleaner (PAC), indoor/outdoor ratio (I/O), COVID-19

2.2 INTRODUCTION

Individuals experiencing homelessness account for a significant proportion of the US population, estimated at approximately 568,000 people each night in 2019, with the majority (63%) of homeless persons housed in shelters [69]. Research has documented infectious disease outbreaks in homeless shelters, including airborne droplet transmission of M. tuberculosis in shelters operated in multiple U.S cities. Findings from these previous studies included inspections of air handling and air flows and resulted in recommendations for the use of improved filtration, improved fresh air supplies, maintenance of existing ventilation units, and the need for written respiratory protection plans and separation of suspected infected individuals from the general population. With the COVID- 19 pandemic, there has been renewed concern over the potential for airborne transmission of infectious droplets and particles in homeless shelters. Homeless people are more vulnerable to severe COVID-19 due to a higher burden of comorbidities, with estimates that they may be two to three times as likely to die of the disease than the general population [70, 71]. These concerns have been partially supported by case reports of SARS-CoV-2 transmission in homeless shelters in different US metropolitan areas, including in King County, Washington [72-75].

In King County, Washington, the single night count of individuals experiencing homelessness was estimated to be 13,368 in 2022, with 43% of the population sheltered [76]. A case report

from King County documented outbreaks in April 2020 at three homeless shelters, with 10.5% test positivity among the 181 residents and higher numbers of positives in the ensuing weeks afterward, including infections in both shelter occupants and staff members [75]. In shelter settings, where masks and vaccinations are not consistently adopted, reducing airborne particles may be one of the most effective interventions that can be deployed in congregate shelter settings to reduce SARS-CoV-2 transmission [77, 78].

Controlling infectious airborne droplets and particles in congregate living settings or homeless shelters is further complicated by the summer wildfire smoke season, which results in conflicting guidance on ventilation for indoor air. Generally, increasing ventilation and outdoor air exchange, and improving filtration may be considered for infection control. But, for managing wildfire smoke, it is recommended that outdoor air exchange be minimized to reduce the infiltration of outdoor smoke into the indoor environment. Managing the potential overlapping risks of SARS-CoV-2 transmission and wildfire smoke-related respiratory health effects may be especially challenging as there may be increased demand for and occupancy of homeless shelters (thus greater density of people) during wildfire smoke episodes [79]. Although generally less severe, a similar situation can occur in the winter during wood burning, which settles in the central low-lying areas of Seattle and King County, sometimes leading to poor air quality during winter inversion events. This could be a problem for congregate and emergency shelters that are set up during extreme weather events.

Portable air cleaners (PACs) equipped with a high-efficiency particulate air (HEPA) filter have been shown to be effective in reducing particle concentrations in several studies conducted in

residential settings, and for wildfire smoke specifically. Multiple agencies, including the Centers for Disease Control (CDC) and the Environmental Protection Agency (EPA), have recommended using HEPA PACs to supplement HVAC systems to reduce indoor particle levels [12]. Barn et al. summarized some studies, many of which were based on randomized controlled study designs [80, 81], that support this recommendation. Henderson et al. documented up to 63-88% lowered $PM_{2.5}$ concentrations with HEPA PACs [82], while crossover studies by Barn et al. and Allen et al. found lower infiltration of smoke when PACs were used compared to when they were not [83, 84]. A recent study of HEPA PACs used during the September 2020 Washington State wildfire episode indicated $PM_{2.5}$ reduction effectiveness ranged from 48-78% across seven homes [6], while other studies have investigated the use of PACs in reducing indoor particle concentration in large open spaces such as workplaces [85] and schools [86].

Despite the evidence supporting home HEPA PAC use for reducing particle exposure, there are challenges for PAC performance in multi-zone indoor environments. There remains considerable uncertainty in the performance of HEPA PACs in multi-zone congregate housing settings such as homeless shelters, where there may be competing decisions related to ventilation due to the need to manage both SARS-CoV-2 transmission and wildfire smoke. To date, there have been no studies presenting data on the real-world effectiveness of HEPA PACs for reducing particle exposures in larger multi-zone homeless shelters. Further, no empirical studies have quantified the usage of HEPA PACs in homeless shelters and attempted to correlate performance with site, building, or management decisions. Most studies of PACs are based on optimal usage without considering real-world scenarios, such as user behaviors, compliance, and building characteristics [87].

Since 2020, over 4,000 HEPA portable air cleaners were deployed at homeless shelters in King County, Washington, by Public Health – Seattle & King County (PHSKC) to help control the COVID-19 pandemic and protect the homeless population from acquiring infection. Considering the significant demand, shelters were prioritized for distribution using an equity tool that considered location, population served, and shelter resources. Multiple units were given to shelters for use in the common and sleeping areas. In this study, we aimed to evaluate the real-world effectiveness of these PACs in reducing indoor particles in these community congregate living settings. The objectives of this research were to understand the (1) usage pattern and (2) factors that affect the use of the HEPA PACs deployed at the shelters, and (3) the effectiveness of these PACs in reducing indoor particle levels, relative to the outdoor particle concentrations at each site.

2.3 METHODS

2.3.1 Site selection and collection of site characteristics

Four rooms across three different homeless shelters (denoted as sites 1, 2a, 2b, and 3 hereafter) in King County, Washington with varying geographic locations and building/operating conditions were selected to participate in this study. These three sites were among the sites that were pre-selected by the county for HEPA PACs deployment. For each selected site, information on building openings (including doors and windows), operating schedules, HVAC system, floor plan, room size, and the primary indoor and outdoor particle sources were collected via field survey. Additional site characteristics, including the residential history of clients, were collected via a post-hoc survey. The survey was anonymous and administered to the site operators and

clients aged 18 or older at the end of the study via email and paper. The survey also collected information about residents' perceptions of air quality and pollution sources, and attitudes toward HEPA PACs. The study protocol and recruitment and consent procedures were approved by the University of Washington Human Subjects Division and the Washington State Institutional Review Board and qualified for exemption status.

2.3.2 Deployment of HEPA PACs and usage monitoring

Multiple portable HEPA PACs (C535 3-stage True HEPA Air Purifier and XQ dual 4-stage True HEPA Air Purifier; Winix America) with brand new sets of filters were deployed in the sleeping dorm or main activity area of each shelter based on the room volume and the clean air delivery rate (CADR) rating of the PACs using the ANSI/AHAM (American National Standards Institute/Association of Home Appliance manufacturers) AC-1 method (recommended PAC working room size (with an 8 ft ceiling height) in square feet = 1.55 × CADR rating in cubic feet per minute) [88]. The locations of the PACs were recorded and tracked during the study. The C535 PACs contain three stages of filters, including a pre-filter, an activated carbon filter, and a HEPA filter. The XQ PACs contain two sets of 3-stage filters (a pre-filter, an activated carbon filter, and a HEPA filter) on the front and rear sides of the body. Both models of PAC contain a bipolar ionizer (which can be disabled) and provide five fan speed level settings, including sleep mode, fan speed 1 to 3, Turbo, and an "Auto-mode" feature (i.e., the fan speed level will be adjusted according to the feedback of the built-in air quality sensor). According to the manufacturer, the CADR ratings for dust and smoke of the C535 PAC are 243 m^3/h and 232 m^3/h, respectively, whereas the CADR ratings for dust and smoke of the XQ PAC are 360 m^3/h and 419 m^3/h. The detailed specifications of these two PACs and the measured energy

consumption under different fan speed levels were summarized in **Table A1**. Both PAC models were certified by the California Air Resources Board (CARB) to meet the ANSI/UL 867 (Underwriters Laboratories) standard (i.e., produce an ozone emission concentration of less than 0.050 parts per million) [89]. Before the second and third sampling round, the pre-filter of each PAC was vacuumed with a handheld vacuum cleaner to remove the dust built-up. The bipolar ionizer of each PAC was turned off before each sampling round.

The PACs were deployed and monitored for three two-week sampling rounds at each site, separated by single-week gaps, between February and April 2022. Each of the PACs deployed at each site was assigned a unique ID and plugged into a power data logger (HOBO® Plug Load Logger Model UX120-018; Onset Computer Corp.), which measured time-stamped energy usage at 1-minute intervals for the entire study period to allow tracking of their usage and fan speed. The logged data were downloaded by study staff for each data collection period. During the round 1 and round 2 deployments, the PACs were purposely set to operate on Auto-mode. During the round 3 deployment, the PACs were set to operate on fan speed level 3. However, the clients or shelter staff were allowed to change the fan speed setting however they wished during each deployment. At the beginning of each deployment, if a PAC was found unplugged or turned off, it was plugged back in and turned on according to the fan speeds noted above by the research staff.

2.3.3 Indoor and outdoor particle concentration monitoring

At each site, multiple indoor locations in the selected sleeping dorm or main activity area with PAC were monitored throughout the three sampling rounds using real-time air quality monitors

(PurpleAir PA-II-SD; PurpleAir) placed and secured at the height of 1-2 m above the floor and at least 1 m away from any PAC or HVAC inlet/outlet. The PurpleAir PA-II-SD monitor contains two duplicate optical particle counters (OPC) (Plantower PMS 5003; Beijing Plantower Co. Ltd.), pressure, temperature, and humidity sensor (BME280; Bosch SensorTec). The OPC uses the laser scattering principle to measure the number of particles suspended in the air. The photodiode of the OPC is positioned perpendicular to the excitation beam and measures the ensemble scattering of particles in the optical volume. The measured scattering light intensity is converted to a voltage signal to estimate the number concentration of particles with an optical diameter ranging from 0.3 to 10 microns in six size bins (>0.3, > 0.5, >1.0, >2.5, >5.0, and >10.0 μm) and mass concentrations for PM_1, $PM_{2.5}$, and PM_{10} (See Fig A.6 for the correlations between particle count measurements for the different size bins in our study). In this study, the number concentration reported in size bin >0.3 μm was defined as the total optical particle concentration (OPNC). OPNC was used because previous studies have observed lower limit of detection issues associated with the $PM_{2.5}$ algorithm of the PurpleAir monitor, in which low concentrations are reported as a value of zero, while the OPNC measurements are less susceptible to this limit of detection issue and will still be able to resolve particle count concentrations when the PurpleAir reports zero mass concentration [90, 91]. Because this is an issue with low concentrations, the use of OPNC may be more appropriate for indoor air studies involving HEPA PACs (See **Table A3** for more information on the frequency of zero $PM_{2.5}$ measurements observed in our study).

The OPNC data were timestamped and saved to the internal Secure Digital (SD) memory card at 2-minute intervals. Prior to their use in the study, these monitors were individually calibrated in a chamber experiment with woodsmoke particles against a real-time optical particle sizer (TSI

optical particle sizer model 3330, TSI Inc.). The calibration shows R^2 ranging from 0.97 to 0.99 for these monitors, and the root mean squared error (RMSE) of these calibrated monitors was less than 900 #/cm^3 within the measurement range of 0 – 20000 #/cm^3 (**Table A2** and **Fig A7**). The optical particle sizer was factory-calibrated prior to this study. In addition to the multiple indoor sampling locations at each site, a single PurpleAir PA-II-SD was placed outside at each shelter that monitored the outdoor ambient particle concentrations throughout the study periods. The outdoor locations were selected based on the representativeness of the general ambient air situation at each shelter, access to an electrical outlet, and were secured to minimize the potential for theft.

2.3.4 Statistical analysis

For the analysis, the 2-minute particle monitoring data were first aggregated hourly. The empirical indoor and outdoor total OPNC data were then compared within sites. Based on the Shapiro-Wilk tests, the indoor and outdoor total OPNC data were not normally distributed. Thus, the Wilcoxon signed-rank tests (for paired comparison) were conducted to compare the indoor and outdoor total OPNC levels of each site and for each individual sampling round.

Next, three PAC usage metrics were computed for each site: (1) the percent time the PACs were on different fan speed levels, including sleep mode, fan speed level 1 to level 3, and Turbo; (2) the percent time the PACs were on; and (3) the total energy consumption of all PACs. Linear mixed effects regression (LMER), which incorporated random intercepts for sites to account for between-site correlations, as well as within-site correlations of repeated measurements, was used

to examine the relationship between the indoor/outdoor total particle number concentration ratio (I/O_{OPNC}) and different PAC usage metrics (Eq. (1) – (3)):

$$I/O_{OPNC_{it}} = \beta_0 + \beta_1 T_{PAC-sleep_{it}} + \beta_2 T_{PAC-fan\ 1it} + \beta_3 T_{PAC-fan\ 2_{it}} + \beta_4 T_{PAC-fan\ 3_{it}} + \beta_5 T_{PAC-turbo_{it}} + W_i + \varepsilon_{it} \quad \text{Eq. (1)}$$

$$I/O_{OPNC_{it}} = \beta_0 + \beta_1 T_{PAC-on_{it}} + W_i + \varepsilon_{it} \quad \text{Eq. (2)}$$

$$I/O_{OPNC_{it}} = \beta_0 + \beta_1 P_{it} + W_i + \varepsilon_{it} \quad \text{Eq. (3)}$$

where $I/O_{OPNC_{it}}$ is the indoor/outdoor total optical particle number concentration ratio of site i at time (hour) t; $\beta_0 - \beta_5$ are the coefficients of the LMER models; $T_{PAC-sleep\ mode_{it}}$, $T_{PAC-fan\ 1_{it}}$, $T_{PAC-fan\ 2_{it}}$, $T_{PAC-fan\ 3_{it}}$, $T_{PAC-turbo_{it}}$ in Eq. (1) are the percent time that the PACs were on sleep mode, fan speed 1, 2, 3, and Turbo of site i at time t, respectively, %; $T_{PAC-on_{it}}$ in Eq. (2) is the percent time that the PACs were on of site i at time t, %; P_{it} in Eq. (3) is the total energy consumption of all PACs of site i at time t, Watts; W_i is the random effect factor, and ε_{it} is the residual. The LMER models were also assessed on daily and round levels. The outliers of $I/O_{OPNC_{it}}$ (i.e., measurements that were 1.5 interquartile range below the first quartile or above the third quartile) were removed for the modeling. For all statistical tests, $p \leq 0.05$ indicated statistical significance in this study. All calculations and figures were made using "nlme", "data.table", and "ggplot2" packages in R Version 4.1.1 embedded in Rstudio Version 2021.09.0.

2.4 RESULTS

2.4.1 Site characteristics

Table 1 summarizes the characteristics of the enrolled sites based on the field and post-hoc surveys. All three sites were located on the 1st floor. Site 1 and site 3 were mechanically ventilated 24 hours per day with built-in HVAC systems, whereas site 2 (including two separate rooms 2a and 2b) was naturally ventilated without HVAC systems. Due to the study seasons (winter and spring), site 1 and site 3 used central heating systems to provide warmth to the rooms. Site 2 (including two separate rooms 2a and 2b) used wall radiators for heating. While windows were not available in the monitored area at site 1 and site 3, doors leading to the outdoor area were present and could have been opened during the study periods by shelter clients or staff. Site 1 is in the busy metro center and about 120 meters away from the major highway in the area. This site served approximately 20 clients from 9 am to 8 pm on weekdays, and 10 am to 2 pm on Saturdays. Site 2 (including two separate rooms 2a and 2b) is about 320 meters away from a major highway, whereas site 3 is only 60 meters away from the closest highway. Site 2 (including two separate rooms 2a and 2b) and site 3 offered overnight services, were open 24 hours per day, seven days per week, and served approximately 50 and 100 clients per day, respectively. Onsite cooking took place only at sites 1 and 3, although already cooked meals were provided at sites 2a and 2b.

Table 1. General characteristics of the study sites.

Site ID	Monitored area	Room volume (m^3)	Year first built	Ventilation type	Window opening	Cooking onsite
Site 1	Main activity area	996	1922	Mechanical	NA[a]	Y
Site 2a[b]	Sleeping dorm #1	921	1903	Natural	Possible	N
Site 2b[b]	Sleeping dorm #2	1021	1903	Natural	Possible	N
Site 3	Sleeping dorm	238	1975	Mechanical	NA[a]	Y

[a] No windows present in the monitored area.
[b] Site 2 had two areas monitored.

2.4.2 Measured PAC energy consumption and usage

Fig. 1 illustrates the measured % time of PACs operating under different fan speed levels at each site. The PACs deployed at site 1, site 2a, and site 2b were found operating under the Turbo fan speed during round 1 most of the time (~45%). This could be because the shelter clients or staff adjusted the PAC fan speed settings manually to Turbo rather than keeping them running in Auto mode during the study. This assumption is supported by the time series of the individual PAC energy consumption shown in **Fig. A1-A4. Fig. A1** shows the time series of the 13 PACs deployed at site 1. During sampling round 1, the energy consumption of multiple PACs (e.g., PAC-003, PAC-004, and PAC-006) remained at ~ 60 watts most of the time. This watt level corresponds to the energy consumption of the PAC running at Turbo fan speed (**Table A1**). Because the PACs were set to Auto-mode by the study staff at the beginning of sampling round 1, it is unlikely that the PACs remained at the Turbo fan speed for such extended periods of time due to the decreasing particle concentration in the environment (**Fig. 2** and **Fig. 3**). The PAC

operating fan speed would stay at Turbo for such extended hours only if it were manually adjusted. Similar PAC energy consumption can be observed for round 1 sampling at site 2a (**Fig. A2**), site 2b (**Fig. A3**), and site 3 (**Fig. A4**). Diurnal patterns of PAC usage were also observed.

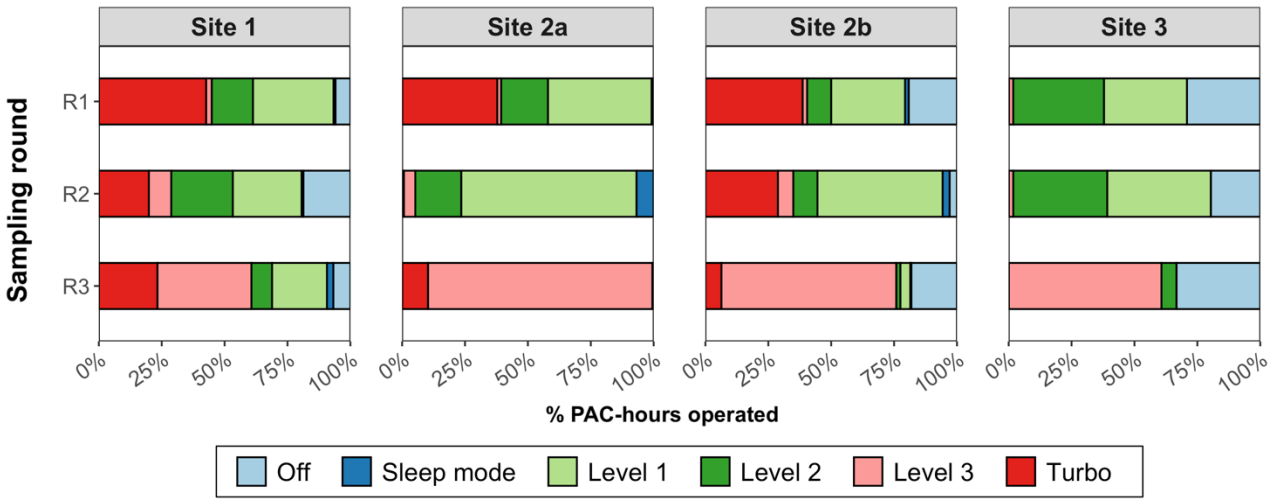

Fig. 1. The measured % time of PACs operated under different fan speed levels. R1: round 1; R2: round 2; R3: round3. The PACs were initially set to operate on Auto-mode during round 1 and round 2, and fan speed level 3 during round 3.

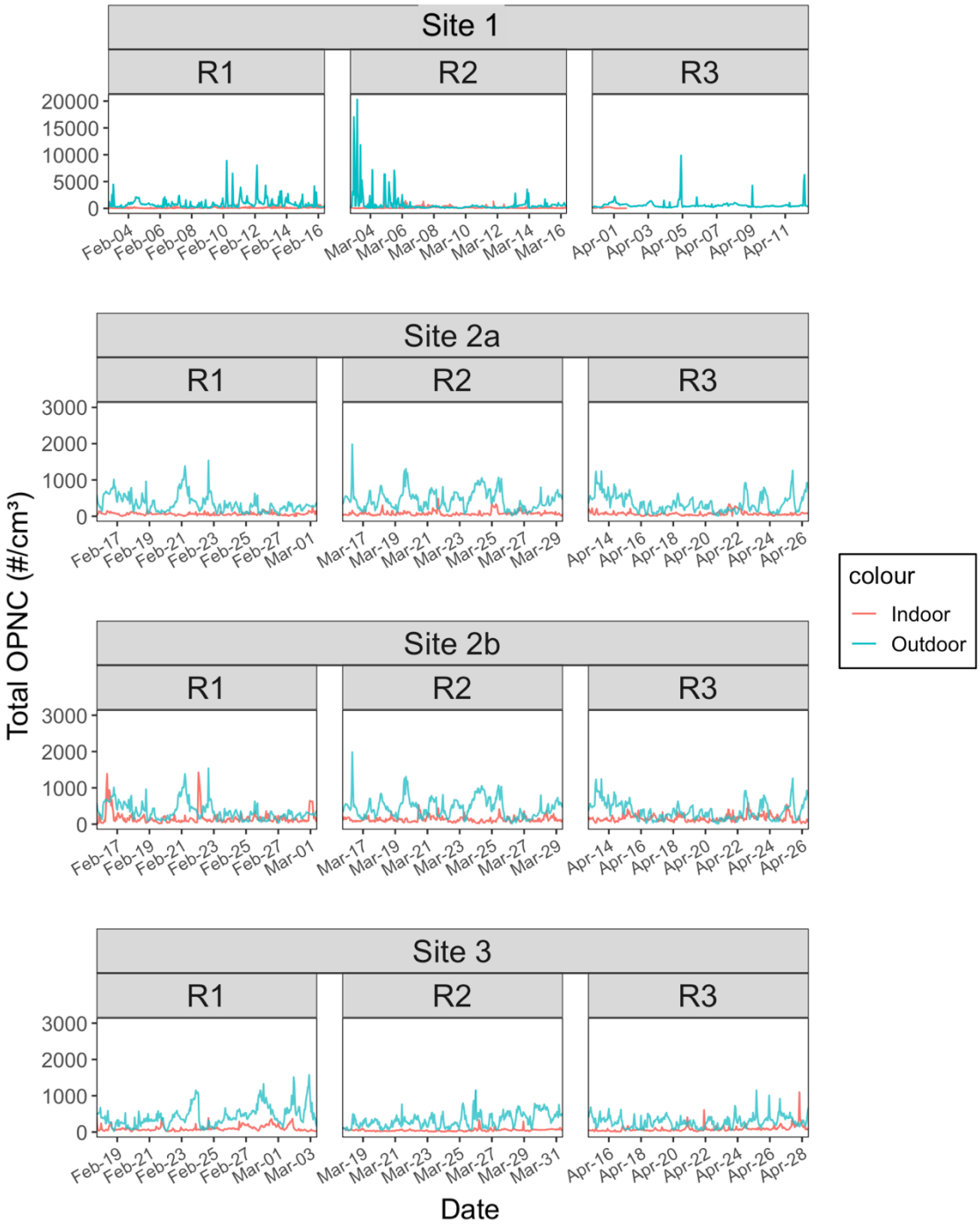

Fig. 2. Time series of the indoor and outdoor total OPNC at three sites. For sites with multiple indoor monitors (site 1, site 2a, and site 2b), the average concentrations were plotted. The y-axis of site 1 was plotted on a different scale.

Fig A.5 shows the heatmap of the normalized hourly total PAC energy consumption at each site. Lower hourly total PAC energy consumption can be seen during the nighttime compared to the daytime, especially during round 2 sampling at Site 2a, and round 1 and round 2 sampling at Site 3. This again highlighted users' preferences for adjusting the PAC operating fan speed. The total minutes of the PAC energy consumption monitored at each site are summarized in **Table A4.** The incompleteness of site 1 and site 3 data was due to the power data loggers being unplugged from the PACs during the monitoring.

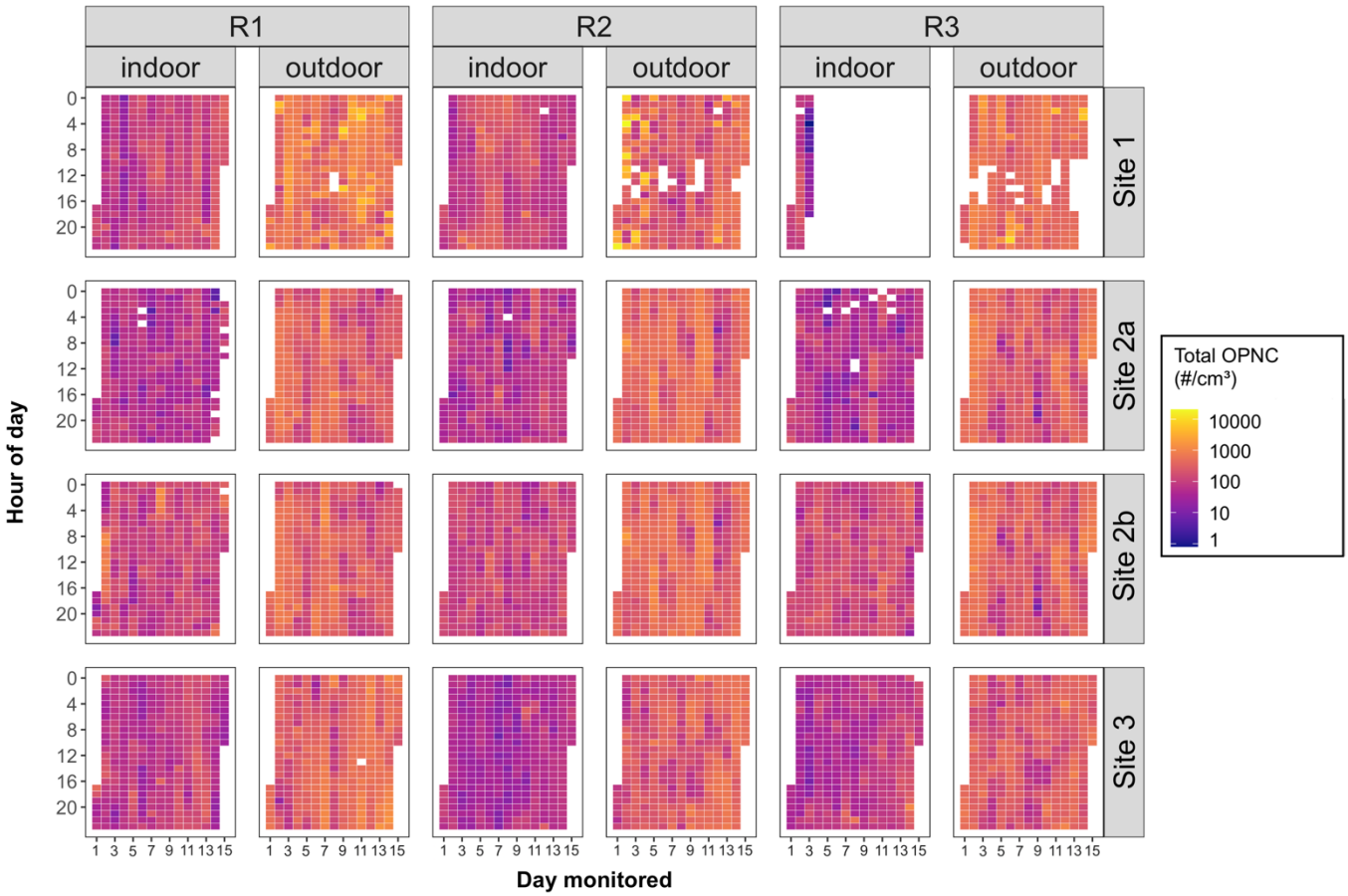

Fig. 3. Heatmap of the indoor and outdoor total OPNC at each site. For sites with multiple indoor monitors (site 1, site 2a, and site 2b), the average concentrations were plotted.

2.4.3 Empirical particle concentrations

Table 2 shows the hourly mean indoor and outdoor total particle concentrations, and temperature and humidity at four sites. Overall, the mean indoor total OPNC concentrations at each site were relatively low during all sampling rounds (< 200 #/cm^3). In contrast, the outdoor total OPNC concentrations were significantly higher than the indoor levels across all three sites and sampling rounds ($p < 0.001$). Pooling all sampling rounds together within each site, the median (interquartile range, IQR) reduction of hourly indoor total OPNC level was 78% (49%), 84% (25%), 65% (58%), and 80% (30%) compared to outdoor levels at site 1, site 2a, site 2b, and site 3, respectively. At site 1, multiple peaks were observed in the outdoor total OPNC levels, with a maximum concentration of 20298 #/cm^3 during round 2 sampling (**Table 2** & **Fig. 2**). Despite the indoor OPNC levels being lower than outdoors most of the time, the hourly indoor levels observed at each site sometimes were comparable to or higher than the outdoor levels (**Fig. 2**, site 2b), indicating the presence of strong indoor particle sources. The heatmap in **Fig. 3** shows the temporal variation in total indoor and outdoor OPNC levels. For site 1, over 90% of the indoor total OPNC observations were missing during round 1 sampling because the indoor monitors were unplugged by people at the site.

Table 2. Summary of the hourly averaged indoor and outdoor total particle concentration at three sites.

Site	Round	Indoor total OPNC (#/cm^3) [a]					Outdoor total OPNC (#/cm^3)					p-value [c]
		Min	Median (IQR)	Mean (SD)	Max	N	Min	Median (IQR)	Mean (SD)	Max	N [b]	
Site 1	R1	0.50	94.43 (114.23)	133.22 (124.36)	750.89	659	91.26	609.39 (684.99)	891.08 (1011.65)	8882.23	327	< 2.2e-16
	R2	6.63	101.28 (115.73)	156.38 (169.90)	1420.44	657	35.16	319.15 (344.75)	780.26 (1982.68)	20298.03	312	< 2.2e-16
	R3	0.70	82.76 (95.01)	89.85 (76.73)	251.60	49	117.55	452.71 (321.34)	639.17 (827.45)	9850.99	276	1.82e-12
Site 2a	R1	0.51	53.22 (64.10)	64.51 (52.35)	346.7	610	31.61	286.26 (274.20)	346.28 (237.02)	1537.67	329	< 2.2e-16
	R2	0.11	61.02 (58.78)	78.18 (80.97)	639.93	652	13.19	427.94 (349.83)	452.46 (270.22)	1983.50	330	< 2.2e-16
	R3	0.27	53.67 (57.67)	70.41 (82.45)	636.80	619	8.05	289.38 (339.51)	357.79 (243.59)	1259.93	330	< 2.2e-16
Site 2b	R1	3.60	101.57 (99.47)	163.91 (264.25)	2768.55	637	31.61	286.26 (274.20)	346.28 (237.02)	1537.67	329	< 2.2e-16
	R2	4.82	102.39 (92.41)	131.16 (109.34)	999.80	659	13.19	427.94 (349.83)	452.46 (270.22)	1983.50	330	< 2.2e-16
	R3	0.42	122.88 (143.37)	161.51 (134.86)	980.24	660	8.05	289.38 (339.51)	357.79 (243.59)	1259.93	330	< 2.2e-16
Site 3	R1	14.40	77.15 (71.87)	99.82 (72.38)	431.55	330	21.40	376.63 (291.69)	433.78 (275.73)	1574.26	329	< 2.2e-16
	R2	6.60	44.89 (31.92)	49.44 (33.16)	337.44	330	44.11	286.86 (278.43)	318.00 (194.83)	1165.74	330	< 2.2e-16
	R3	8.87	64.19 (54.19)	85.12 (86.86)	1098.08	330	43.49	275.72 (208.92)	283.39 (159.06)	1148.29	330	< 2.2e-16

[a] For sites with multiple indoor monitors (site 1, site 2a, and site 2b), the average concentrations across all indoor monitors were presented.

[b] Number of data points.

[c] Comparison between the indoor and outdoor total OPNC based on the Wilcoxon signed-rank tests (for paired comparison).

Fig. 4 and **Table 3** show the hourly indoor/outdoor total OPNC ratios (I/O_{OPNC}) under different sampling rounds at each site. For all sites, the median hourly I/O_{OPNC} during all sampling rounds was lower than 1, indicating that the indoor total OPNC levels were lower than the outdoor ones for 50% of the study period. However, the maximum I/O_{OPNC} at each site was larger than 1 (the data for round 3 of site 1 was excluded from the discussion due to incompleteness), suggesting the presence of indoor particle sources at each site.

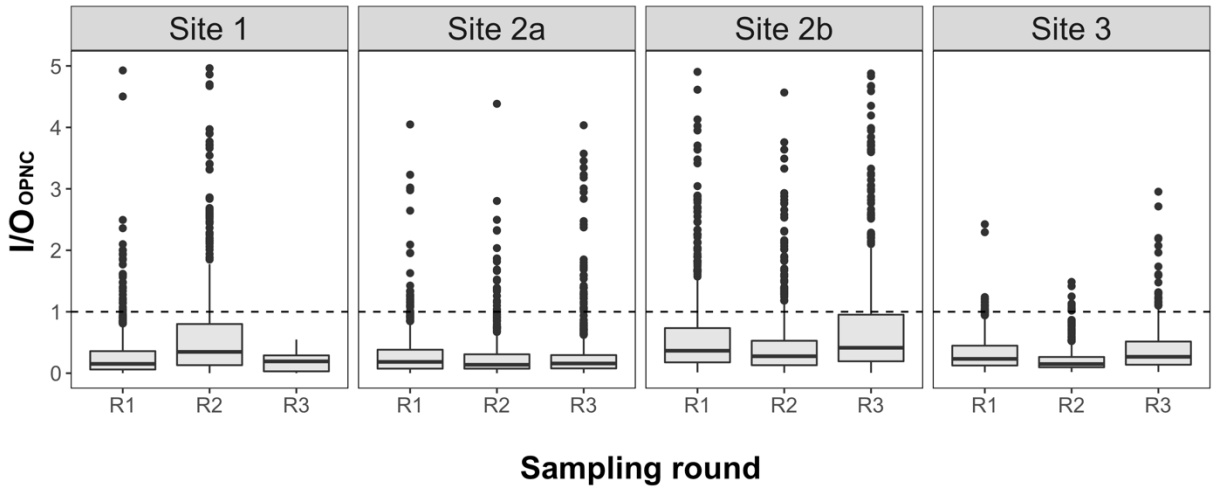

Fig. 4. Boxplot of the hourly averaged indoor/outdoor particle number concentration ratio (I/O_{OPNC}). Data points larger than 5 (0.8 % of the total observations across all sites and all sampling rounds) were excluded from plotting (max values are provided in **Table 3**).

Table 3. Summary of the hourly averaged indoor/outdoor total particle concentration ratio (I/O_{OPNC}) at three sites.

Site	Round	I/O_{OPNC}				N [a]
		Min	Median (IQR)	Mean (SD)	Max	
Site 1	R1	<0.01	0.15 (0.30)	0.29 (0.43)	4.93	653
	R2	<0.01	0.37 (0.72)	0.79 (1.43)	19.45	623
	R3	<0.01	0.19 (0.26)	0.18 (0.15)	0.55	40
Site 2a	R1	<0.01	0.18 (0.31)	0.31 (0.42)	4.05	610
	R2	<0.01	0.14 (0.24)	0.28 (0.43)	8.10	652
	R3	<0.01	0.16 (0.23)	0.39 (1.11)	18.82	619
Site 2b	R1	0.01	0.37 (0.58)	0.71 (1.27)	16.50	635
	R2	0.01	0.28 (0.41)	0.49 (0.73)	8.10	659
	R3	0.01	0.42 (0.79)	0.84 (1.34)	18.98	660
Site 3	R1	0.01	0.23 (0.32)	0.33 (0.31)	2.42	329
	R2	0.02	0.15 (0.17)	0.23 (0.23)	1.49	330
	R3	0.02	0.27 (0.38)	0.46 (0.73)	8.52	330

[a] The number of complete hours with both indoor and outdoor measurements.

2.4.4 Relationship between PAC usage metrics and indoor/outdoor total OPNC ratio (I/O_{OPNC})

Table 4 presents the results of the LMER models. Models 1-3 assessed the relationship between the I/O_{OPNC} and the "percent time the PACs were on different fan speed levels," "percent time the PACs were on," and "hourly total energy consumption of all PACs" metrics, respectively, on different time averaging scales. The coefficient estimates show the effect of per 10% change in

PAC usage time on I/O_{OPNC} for model 1 and model 2, and the effect of per one-watt change in PAC energy consumption on I/O_{OPNC} in model 3. In model 1, the coefficient estimates for the hourly time PACs were on sleep mode (β1), fan speed level 1 (β2), level 2 (β3), level 3 (β4), and Turbo (β5) were negative, indicating that regardless of the fan speed level, using PACs result in lower I/O_{OPNC}. However, the reductions in these coefficient estimates were non-linear, indicating that running the PACs at higher fan speed did not result in lower I/O_{OPNC} than at lower fan speed.

In model 2, regardless of the time averaging scale, the regression coefficients were negative for the percent time PACs were on (β1), indicating that keeping PACs on resulted in significantly lower I/O_{OPNC}. Ten percent increase in the hourly, daily, and total time PACs were used significantly reduced I/O_{OPNC} by 0.034 [95% CI: 0.028, 0.040; $p< 0.001$], 0.051 [95% CI: 0.020, 0.078; $p< 0.001$], 0.252 [95% CI: 0.150, 0.328; $p< 0.001$], respectively. **Fig. 5** shows the predicted hourly I/O_{OPNC} under 50% to 100% of PACs operating time, based on model 2 with an hourly averaging scale. Overall, hourly PAC operating time ranging from 50% to 100% results in I/O_{OPNC} smaller than 1, and with the increasing amount of hourly PAC operating time, the I/O_{OPNC} becomes lower. Similarly, in model 3 with different time averaging scales, the regression coefficients of the total energy consumption of all PACs (β1) were insignificant and the values were close to zero or negative, meaning that higher total energy consumption of PACs did not significantly lower I/O_{OPNC}.

Table 4. Summary of the results for the linear mixed-effects regression (LMER) models. The estimate shows the effect of per 10% change in PAC usage time for model 1 and model 2, and the effect of per one-watt change in PAC energy consumption for model 3, respectively, on I/O_{OPNC}.

Model	Averaging Scale	Coefficient	Estimate	Standard error	95% CI [a]
Model 1	Hourly	β_0	0.597	0.036	0.530 to 0.666 ***
		β_1	-0.015	0.036	-0.034 to 0.005
		β_2	-0.035	0.010	-0.041 to -0.028 ***
		β_3	-0.036	0.003	-0.043 to -0.029 ***
		β_4	-0.036	0.004	-0.043 to -0.028 ***
		β_5	-0.032	0.004	-0.043 to -0.023 ***
	Daily	β_0	0.701	0.143	0.442 to 0.980 ***
		β_1	0.158	0.099	-0.036 to 0.345
		β_2	-0.060	0.016	-0.091 to -0.029 ***
		β_3	-0.052	0.025	-0.103 to -0.004 *
		β_4	-0.046	0.017	-0.079 to -0.002**
		β_5	-0.005	0.019	-0.045 to 0.030
	Round	β_0	3.115	0.410	2.393 to 3.898 ***
		β_1	-1.879	0.500	-2.556 to -1.197 *
		β_2	-0.125	0.050	-0.198 to -0.052 *
		β_3	-0.462	0.087	-0.590 to -0.333 **
		β_4	-0.297	0.030	-0.342 to -0.253 ***
		β_5	-0.405	0.050	-0.479 to -0.329 **
Model 2	Hourly	β_0	0.595	0.036	0.526 to 0.665 ***
		β_1	-0.034	0.003	-0.040 to -0.028 ***
	Daily	β_0	0.787	0.134	0.508 to 1.042***
		β_1	-0.051	0.014	-0.078 to -0.020 ***
	Round	β_0	2.575	0.396	1.689 to 3.337 ***
		β_1	-0.252	0.039	-0.328 to -0.150 ***
Model 3	Hourly	β_0	0.295	0.008	0.276 to 0.313 ***
		β_1	1.78e-04	1.17e-04	-4.48e-05 to 4.16e-04
	Daily	β_0	0.338	0.027	0.299 to 0.382 **
		β_1	4.41e-04	9.87e-04	-1.14e-03 to 2.57e-03
	Round	β_0	0.486	0.090	0.320 to 0.651 *
		β_1	-0.004	0.004	-0.012 to 0.006

[a] Level of significance: * $p < 0.05$, ** $p < 0.01$, *** $p < 0.001$.

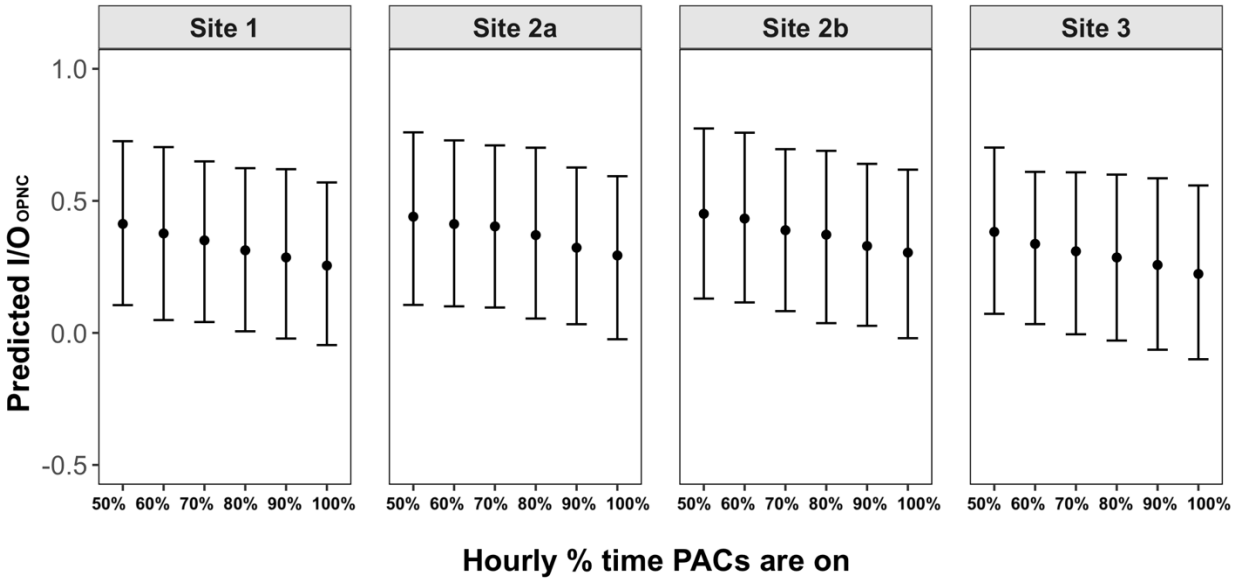

Fig. 5. Prediction of hourly I/O_{OPNC} under 50% to 100% of hourly PACs usage time at each site. The middle point represents the mean, and the top and bottom bars represent the upper and lower 95% confidence interval, respectively.

3.4.5 Survey results

A total of 10 clients and 12 staff from three sites participated in the post-hoc survey. Most respondents reported that cooking fumes (17, 77.3%) and cigarette smoke outdoors (17, 77.3%) were the main indoor sources of air pollution. Body and bathroom odors (2, 9.1%), vehicle exhaust (2, 9.1%), and indoor vaping (1, 4.5%) were also reported as indoor sources of air pollution. Of 22 respondents, 16 (72.7%) felt air quality was better with PACs. Among the respondents who did not feel air quality was better with PACs (4, 18.2%, 2 missing), three respondents were clients. These clients reported their ability to smell air fresheners, cigarette smoke, cooking fumes, and vehicle exhaust as the reasons they didn't feel the air quality was better. The only staff reported that air quality was not better with the PACs indicated it was due to continued smells of cooking fumes. Regarding the maintenance and operations of PACs, half

(11, 50%) of the respondents reported they hardly noticed staff cleaning PACs. Nearly 42% (5) of the staff responded that keeping the PACs running and the noise were the two primary concerns of operating the PACs. Among nine clients who responded to this question, over half (6, 66.7%) responded that they slept better with the PACs on and when the air quality was better.

2.5 DISCUSSION

To our knowledge, this study is the first to examine the use of portable HEPA air cleaners and their impacts on indoor total particle concentration in homeless shelters. The results of this study suggest that using HEPA PACs (with the number of units estimated according to the ANSI/AHAM recommendation) and increasing the amount of time they are turned on, can significantly reduce indoor total OPNC compared to the outdoors, in real-world operating fan speeds of the air cleaners at homeless shelters.

A congregate living setting, by definition, is a facility or housing where people reside and share at least one common room, such as a sleeping room, bathroom, or kitchen. In homeless shelters where supportive services such as meals and housekeeping are provided, various sources of particles could have existed, such as cooking fumes, the use of vacuums, and air freshener. In this study, though PACs were found to reduce indoor total OPNC, elevated peaks (> 250 #/cm^3) were still observed at each site. This highlighted the importance of source control. For example, staff and clients from site 1 and site 3 reported cooking fumes as the major indoor air pollution source, and clients from site 3 specifically mentioned that cigarette smoke from outdoors could be smelled in the sleeping dorm. This could explain the indoor total OPNC peaks observed at these two sites (**Table 2**). At site 1 where the highest outdoor total OPNC was observed (20,298

#/cm^3), the staff reported smoking activities happened right next to the location of outdoor particle sensors during round 2 sampling (**Table 2**). In addition to these common indoor particle sources, wildfire smoke is a concern generally for our region, and outdoor regional particle concentrations can reach high concentrations in the late summer-fall season. Wildfire smoke may not have been reported because of the timing of our survey which was conducted in the spring season.

Our study results show that with the use of PACs, the empirical median indoor total OPNC level was reduced by up to 84% compared to the outdoor levels. The LMER results of models 1 and 2 also supported that using PACs would result in lower indoor/outdoor total OPNC ratios. However, we did not observe significantly lower indoor/outdoor total OPNC ratios when the PACs operated under higher fan speed levels compared to low, according to the results of model 1. To further investigate this, we fit a separate LMER model to assess the effect of PACs operating at Turbo versus low fan speed level (sleep mode and speed level 1 to level 3) on indoor/outdoor total OPNC ratios (the results are presented in **Table A5**). Similarly, the results show that operating PACs under Turbo level did not result in significantly lower indoor/outdoor total OPNC ratios compared to low fan speed. This is consistent with a previous study that investigated the combined use of window A/C fans and HEPA PACs in classrooms located in a non-urban setting where the background particle concentration is low [92]. It was reported that using HEPA PACs alone at a high fan speed did not result in significantly lower $PM_{2.5}$ concentration compared to a lower fan speed. The authors suggested it was possible that the retention time of the particles was relatively short when the PAC fan speed/CADR is high, thus, resulting in lower particle filtration efficiency. Nevertheless, further studies are required to

investigate the flow dynamics, particle filtration efficiency, and CADR of the PACs under different fan speed levels.

In model 3, the trend of regression coefficients (β1) of model 3 was negative or close to zero, meaning that higher PACs energy consumption did not result in significant changes in indoor/outdoor total OPNC ratios. These coefficients were not statistically significant, which might be due to the noise in the data, or the variations in the energy consumption of the PACs operating at different fan speed levels were too small for the regression model to pin down the relationship between PAC energy consumption and indoor/outdoor total OPNC ratio. The energy consumption of the PACs operating at lower fan speed levels, including sleep mode, fan speed levels 1, 2, and 3 ranges from 2.8 – 10.4 and 8.7 – 21.9 wattages for the two models used in this study (**Table A1**). Nevertheless, the results of model 1 and model 2 concluded that the amount of time using the PACs was associated with lower indoor/outdoor total OPNC ratios.

Care should be taken when choosing which PACs for use in homeless shelters. Consistent with the existing guidance [12, 81, 93-96], this study suggested selecting HEPA PACs based on the CADR ratings and recommended working room size. While the existing guidance is formulated based on the CADR and room size at the highest fan speed settings (provided by manufacturers), the results of this study suggested that keeping HEPA PACs on all the time could significantly reduce indoor particle levels, regardless of what fan speed they are on. According to the survey results, the main challenge of operating the PACs on site reported by the shelter staff was to keep them on and running. For example, staff from the participating sites reported that PACs were unplugged from the electrical outlets to plug in other or personal electronic devices. In light of

this, electrical outlets should be secured to prevent PACs from being unplugged. The use of labels or signage to explain the purpose of the PACs and communicating with staff and clients to keep them plugged in or turned on would also help address this challenge. Other recommendations in the existing guidance include selecting HEPA PACs with third-party verification (e.g., CARB and AHAM) to avoid devices that could emit harmful gas (e.g., ozone) emissions. In the current study, noise was another concern that staff voiced regarding PAC use at shelter sites. There is growing evidence suggesting that noise is a major factor that affects behavior or attitude toward using PACs [97, 98]. Therefore, noise level should also be considered when selecting PACs to use. Using lower settings can reduce the noise levels, so additional PACs can be helpful to provide more air changes per hour if used in a setting where the highest fan speed setting is not practical.

In addition to the challenges operating the PACs in the shelters, the survey results also suggested that odors, including cigarette smoke, bathroom smells, air fresheners, and vehicle exhaust, were perceived as the major contributors to poor indoor air quality by the shelter staff and clients. This echoes previous studies investigating perceived indoor air quality among public facilities, which reported that sensory responses (e.g., olfactory, visual, and thermal comfort) are the primary ways that humans rely on to assess air quality in indoor environments such as home [99] and sports facilities [100].

The existing guidance rarely discussed the costs of running and maintaining PACs. Based on the energy consumption data this study collected, the average monthly energy consumption per PAC ranges from ~3.4 kWh to ~17.4 kWh depending on the PAC model used and the percent time

PAC operating under different fan speed levels. Other considerations include the cost and frequency of filter replacement, the need to designate staff that can clean and maintain PACs, and the design and ease of using the PACs. In this study, the PACs were brand new at the beginning of the field deployment. According to the manufacturer, the recommended HEPA lifespan of the PACs used in this study, which refers to the time of use when the CADR drops by 50%, is 12 months. Our study lasted for approximately 2.5 months, which was within the manufacturer's recommended HEPA filter lifespan. Zuraimi et al. tested the impact of artificial dust loading on the performance of a HEPA-based PAC in a controlled laboratory environment. They reported that the PAC airflow rate decreased by 49% of its initial value after 150 grams of ISO 12103-1 A1 ultrafine test dust (with particle diameter between 0.97 to 22.0 μm) was loaded on the PAC's filters [101]. Shaughnessy et al. reported that after 800 hours of intermittent operation in residential bedrooms, the airflow rate and CADR of HEPA-based PACs reduced by 26.5% and 25.0%, respectively [102]. As neither of these studies was based on multi-zone congregational living facilities, future studies on assessing the impacts of dust loading on PACs particle filtration efficiency are warranted.

This study has several limitations. First, the present study was not conducted during the wildfire season when the indoor particle concentrations would likely be higher. There may have been seasonal effects depending on the air pollution experienced at different times of the year. Therefore, the effectiveness of PACs in lowering indoor particle concentration in wildfire seasons might be different. Second, detailed time-activity information was not collected in this study, which limits our ability to characterize the impacts of sources (e.g., cooking, cleaning, window opening, etc.) on indoor particle levels. Third, compared to previous studies that relied

on cross-over design, this study was observational because the air cleaners were deployed not for the study but for COVID-19 control; it would have been unethical to randomize air cleaner use or sham filtration in this situation. Fourth, the applicability of the study results might be limited. Homeless shelters are not the sole type of congregate living setting. Some other common congregate living settings include nursing homes and correctional facilities. These settings could have different characteristics such as building conditions, the density of persons, the amount of time that people share a common space, and the sources of air pollution exposures. For facilities that open overnight, the concern about using PACs might be different (e.g., noise from PACs could be an issue in a sleeping dorm). Lastly, this study did not measure air exchange rates directly, which could impact the infiltration of particles of outdoor origins [6, 103]. This may lead to a biased comparison between the indoor and outdoor particle concentrations and the calculation of indoor/outdoor particle concentration ratios. In addition, we estimated the number of PACs deployed at each site according to the AHAM recommendations [88, 104], which were developed based on residential ventilation and particle deposition rates. In congregate living settings, the ventilation rate and particle deposition rate could have been different from residential environments. As previously mentioned, air filtration with PACs is recommended as a supplement to ventilation by various agencies, and there has been a growing interest in comparing the combined effectiveness of various ventilation and air filtration strategies. The objective of this study was not to answer such questions. Instead, our goal was to investigate the real-world effectiveness of HEPA PACs in reducing indoor particle concentration and provide qualitative insights on what factors impact the use of HEPA PACs in congregate living settings. Future studies building upon the current research and examining the effectiveness of HEPA PACs during different exposure scenarios (e.g., wildfire season) are warranted to formulate more

comprehensive guidance for reducing indoor exposures. However, as discussed, our study findings suggest that short-term use of HEPA PACs is effective in reducing indoor particle levels in community congregate settings.

2.6 CONCLUSIONS

This study shows that portable HEPA air cleaners are an effective short-term strategy to reduce indoor particle levels in community congregate settings during non-wildfire seasons, though the overall effectiveness depended on the length of time that the portable HEPA air cleaners were used. Keeping portable HEPA air cleaners on and running was the main challenge when operating them in shelters. These findings suggested the need for formulating practical guidance for using portable HEPA air cleaners in community congregate settings.

2.7 SUPPLEMENTARY MATERIALS

Table A1. Specifications of the HEPA PACs used in this study.

Model	**Winix C535**	**Winix Tower XQ**
CADR (dust/pollen/smoke) [a]	243/236/242	360/405/419
Energy consumption (watt) [b]		
Speed sleep mode	2.8	8.7
Speed level 1	5.4	15.6
Speed level 2	7.3	18.9
Speed level 3	10.4	21.9
Speed Turbo	50.6	76.8

[a] Manufacturer provided information.
[b] Measured.

Table A2. Calibration coefficients [a] of the optical particle counters (PurpleAir PA-II-SD).

Monitor ID	Slope	R^2	RMSE [b]
Monitor #1	0.43	0.99	272.61
Monitor #2	1.11	0.99	461.40
Monitor #3	1.24	0.99	248.83
Monitor #4	1.15	0.99	197.85
Monitor #5	1.58	0.97	896.25
Monitor #6	1.27	0.99	486.15
Monitor #7	1.32	0.99	192.03
Monitor #8	1.21	0.99	486.16
Monitor #9	1.32	0.99	456.67
Monitor #10	0.45	0.99	450.60
Monitor #11	1.25	0.99	607.67

[a] The calibration model for each monitor was fitted in the form of $C_{TSI\ 3330} = \beta_0 + \beta_1 \cdot C_{PA} + \varepsilon$, where $C_{TSI\ 3330}$ is the particle count with the diameter ranging from 0.3 – 10 μm (#/cm^3) measured by the reference instrument (TSI optical particle sizer model 3330, TSI Inc.); C_{PA} is the raw particle count measured by the continuous optical particle counters (PurpleAir PA-II-SD; PurpleAir) in size bin >0.3 μm (#/cm^3); β_0 is the intercept; β_1 is the slope; ε is the residual. β_0 was set to zero for fitting.

[b] RMSE: root mean square error. The RMSE of the post-calibrated optical particle counters were calculated using the equation $\text{RMSE} = \sqrt{\frac{\sum_{i=1}^{N}(C_{TSI\ 3330} - C_{PA_{cal}})^2}{N}}$ where N is the number of observations; $C_{TSI\ 3330}$ is the particle count with the diameter ranging from 0.3 – 10 μm (#/cm^3) measured by the reference instrument (TSI optical particle sizer model 3330, TSI Inc.); $C_{PA_{cal}}$ is the post-calibrated particle count measured by the continuous optical particle counters (PurpleAir PA-II-SD; PurpleAir) in size bin >0.3 μm (#/cm^3).

Table A3. Summary of the zero $PM_{2.5}$ measurements (0 µg/m^3) and zero total OPNC measurement (0 #/cm^3) based on the PurpleAir monitors' raw data by location and site.

Site	Location	Number of zero measurement (n)	Total number of measurements	% of zero measurement
$PM_{2.5}$				
Site 1	Indoor	9344	24791	37.7 %
	Outdoor	2689	18920	14.2%
Site 2a	Indoor	21867	24707	88.5 %
	Outdoor	6701	23881	28.1%
Site 2b	Indoor	27494	38091	72.2%
	Outdoor	6701	23881	28.1%
Site 3	Indoor	13505	21860	61.8%
	Outdoor	5248	21752	24.1%
Total OPNC (>0.3 µm)				
Site 1	Indoor	0	24791	0.00%
	Outdoor	0	18920	0.00%
Site 2a	Indoor	0	24707	0.00%
	Outdoor	0	23881	0.00%
Site 2b	Indoor	0	38091	0.00%
	Outdoor	0	23881	0.00%
Site 3	Indoor	0	21860	0.00%
	Outdoor	0	21752	0.00%

Table A4. Summary of the total PAC working minutes monitored at each site.

Site	Round	Number of PAC deployed	Total PAC working minutes monitored	Missing (%)
Site 1	R1	13	256613	0.003
Site 1	R2	13	255824	0.31
Site 1	R3	13	256619	0.0004
Site 2a	R1	10	197400	0
Site 2a	R2	10	197400	0
Site 2a	R3	10	197400	0
Site 2b	R1	11	217140	0
Site 2b	R2	11	217140	0
Site 2b	R3	11	217140	0
Site 3	R1	3	59220	0
Site 3	R2	3	47979	18.9
Site 3	R3	3	59220	0

Table A5. Summary of the LMER model [a] assessing the effect of PACs operating at Turbo fan speed versus low fan speed (sleep mode and level 1 to level 3) on I/O_{OPNC}. The estimate shows the effect of per 10% change in PAC usage time on I/O_{OPNC}.

Averaging scale	Coefficient	Estimate	Standard error	95% CI [a]
Hourly	β_0	0.593	0.035	0.526 to 0.661 ***
	β_1	-0.035	0.003	-0.041 to -0.028 ***
	β_2	-0.032	0.004	-0.039 to -0.024 ***
Daily	β_0	0.759	0.131	0.508 to 1.007 ***
	β_1	-0.055	0.014	-0.082 to -0.027 ***
	β_2	-0.019	0.017	-0.052 to 0.013
Round	β_0	2.585	0.415	1.700 to 3.361 ***
	β_1	-0.252	0.041	-0.328 to -0.152 ***
	β_2	-0.260	0.048	-0.349 to -0.138 ***

[a] The form of the LMER model is $I/O_{OPNC_{it}} = \beta_0 + \beta_1 T_{PAC-low_{it}} + \beta_2 T_{PAC-Turbo_{it}} + W_i + \varepsilon_{it}$; where $\beta_0 - \beta_2$ are the coefficients of the LMER models; $T_{PAC-low_{it}}$ is the percent time that the PACs were on lower fan speeds, including sleep mode, speed level 1 to level 3; $T_{PAC-Turbo_{it}}$ is the percent time that the PACs were on Turbo fan speed; W_i is the random effect factor, and ε_{it} is the residual.

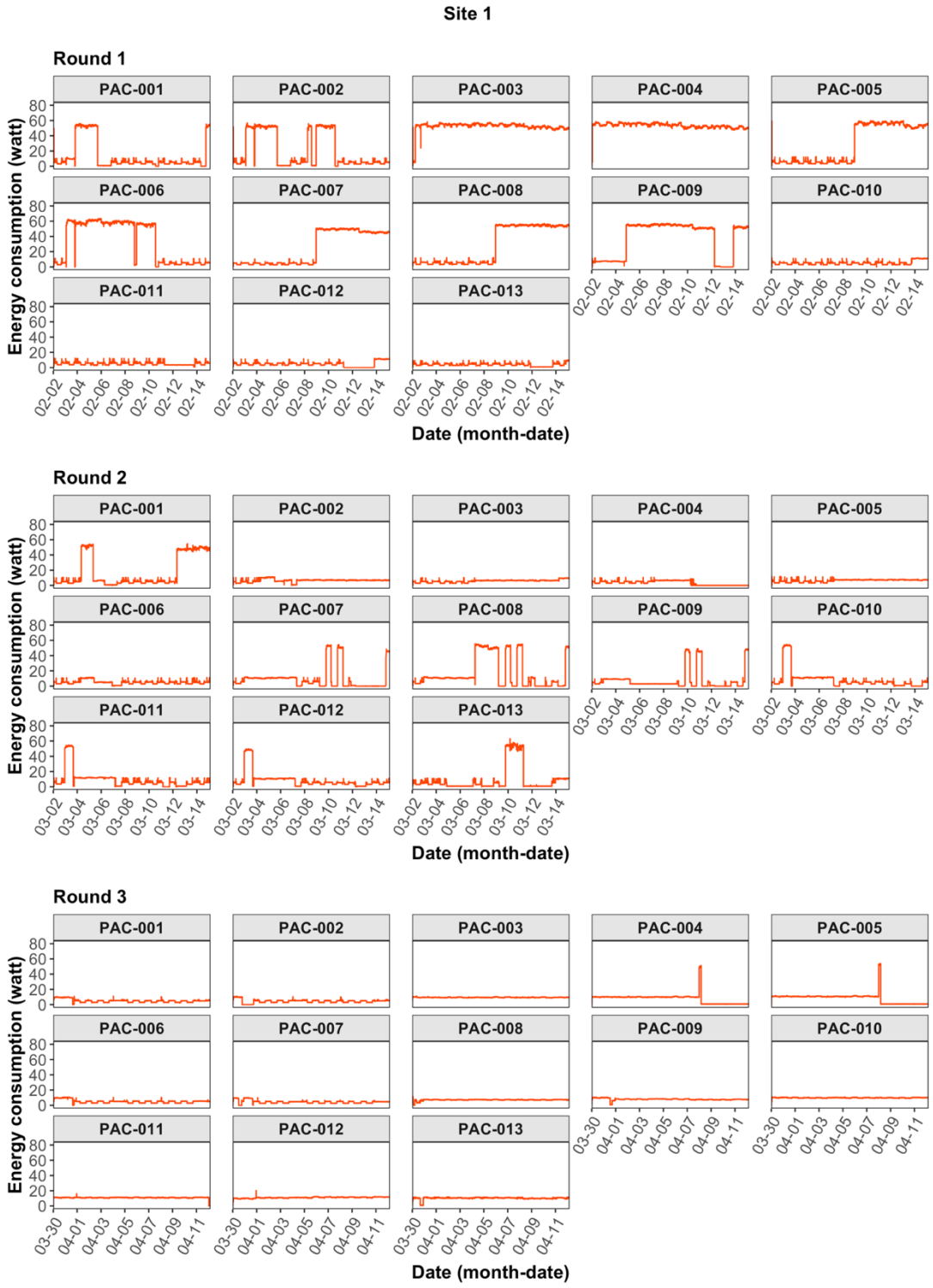

Fig. A1. Time series of the energy consumption of the PACs deployed at site 1 during three sampling rounds.

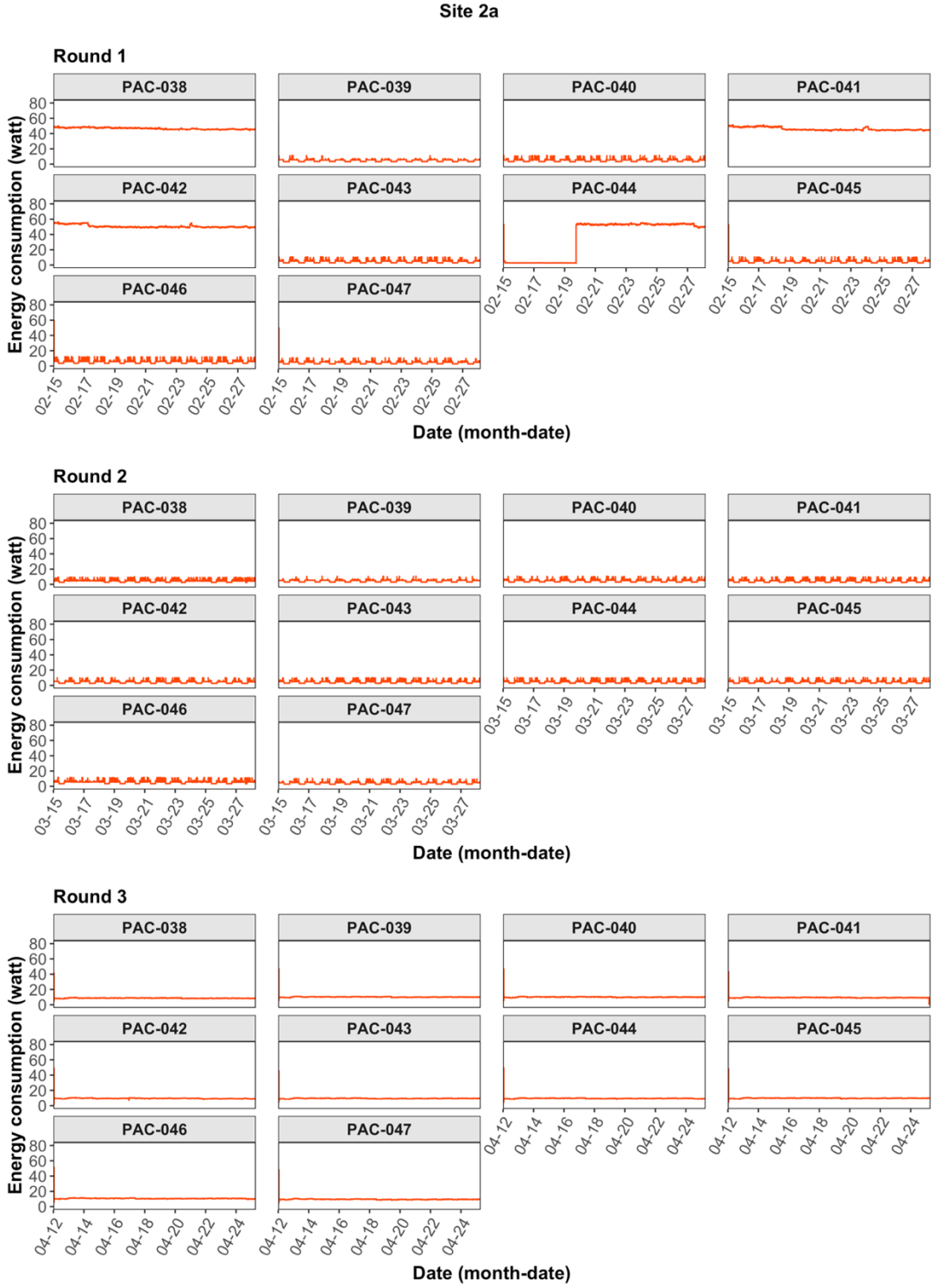

Fig. A2. Time series of the energy consumption of the PACs deployed at site 2a during three sampling rounds.

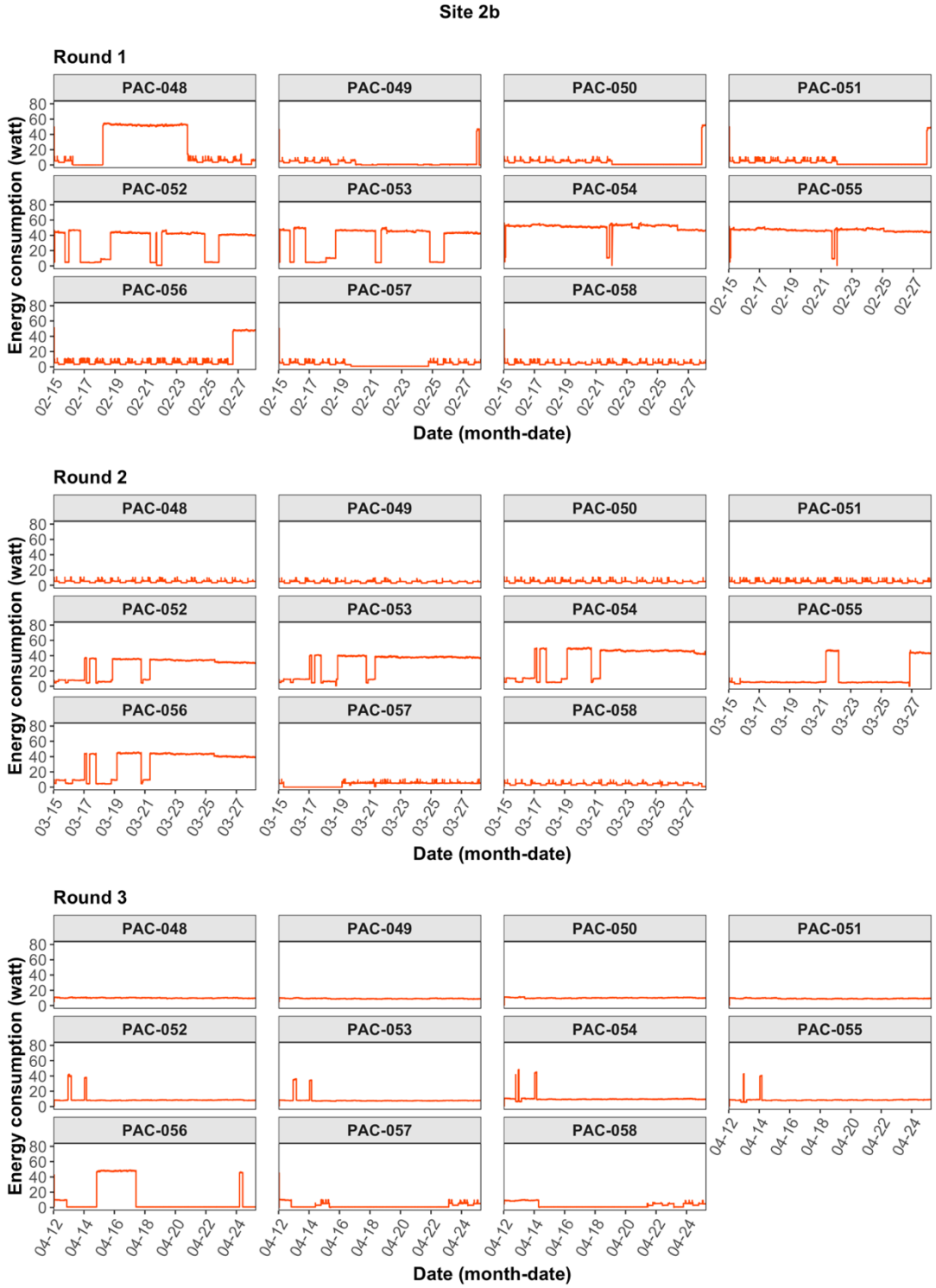

Fig. A3. Time series of the energy consumption of the PACs deployed at site 2b during three sampling rounds.

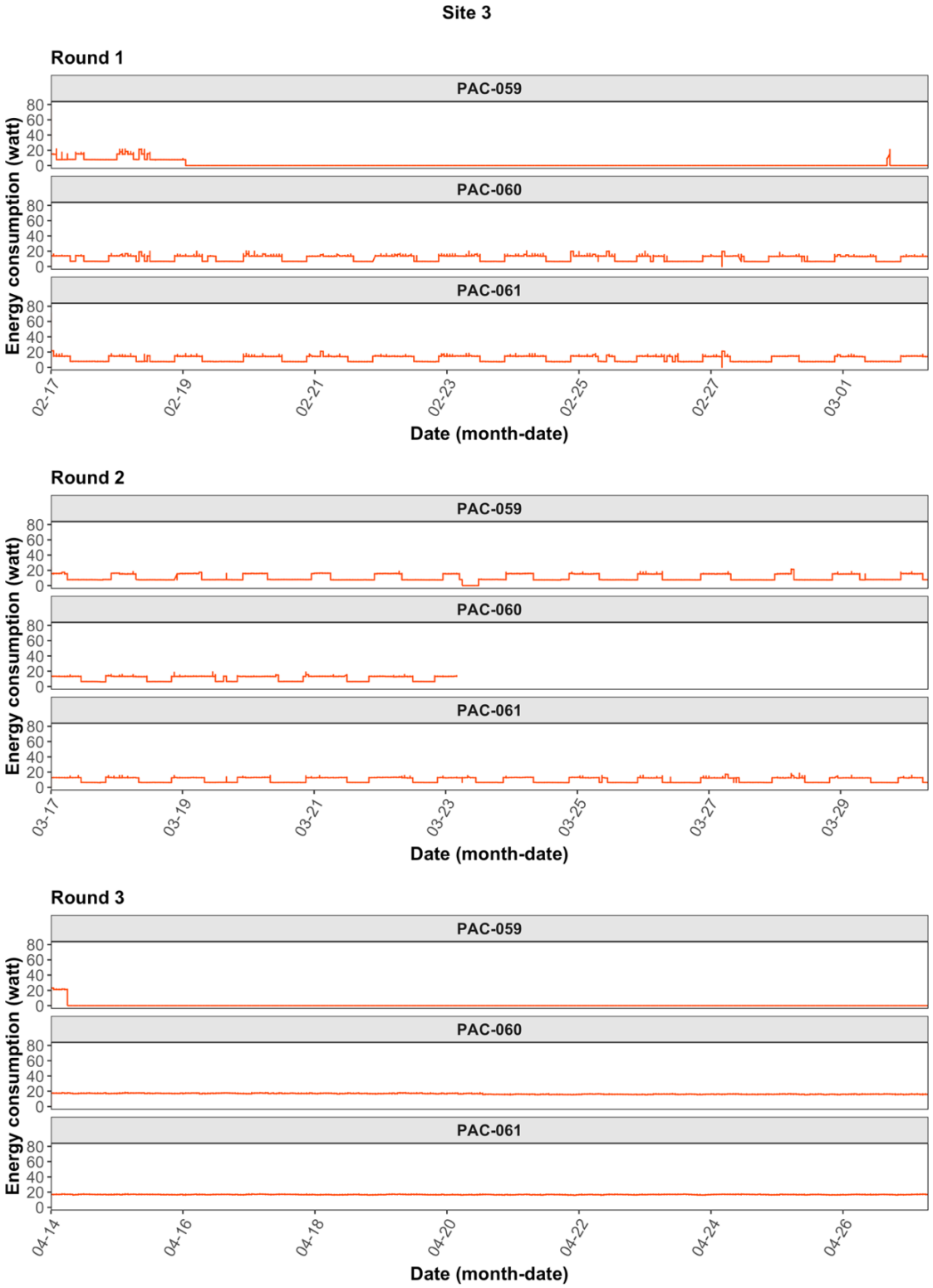

Fig. A4. Time series of the energy consumption of the PACs deployed at site 3 during three sampling rounds.

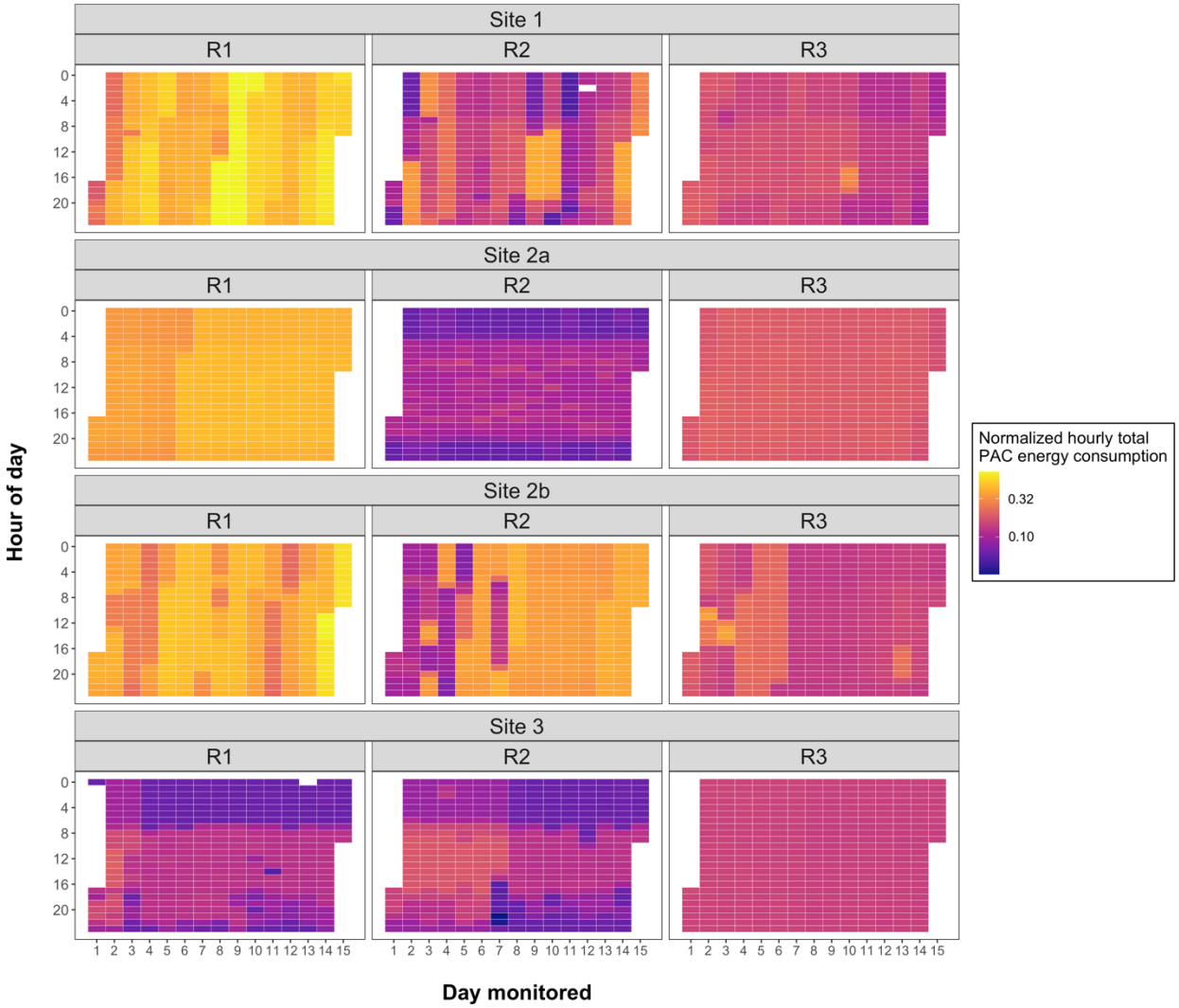

Fig A5. Heatmap of the normalized hourly total energy consumption of the PACs deployed at each site during three sampling rounds. The normalized hourly total energy consumption at each site was calculated using the equation $\frac{\sum_j^n \sum_i^t H_{ij}}{N \times H_{max} \times t}$, where H_{ij} is the energy consumption (watt) of the jth PAC at time i (minute) at each site; N is the total number of PAC deployed at each site; H_{max} is the maximum possible PAC energy consumption (watt) (i.e., the energy consumption when the PAC operated at Turbo fan speed); t is the time (minute). The normalized total energy consumption was aggregated hourly.

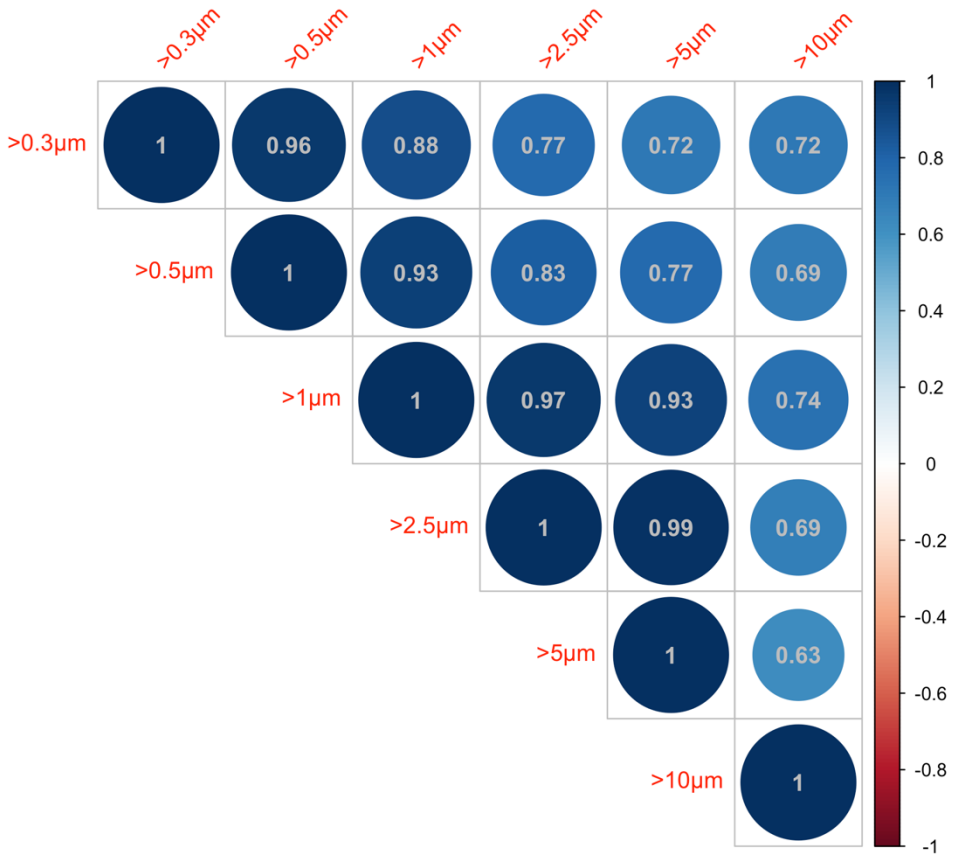

Fig A6. Pearson correlation between each pair of the raw PurpleAir size bins (all sites pooled together).

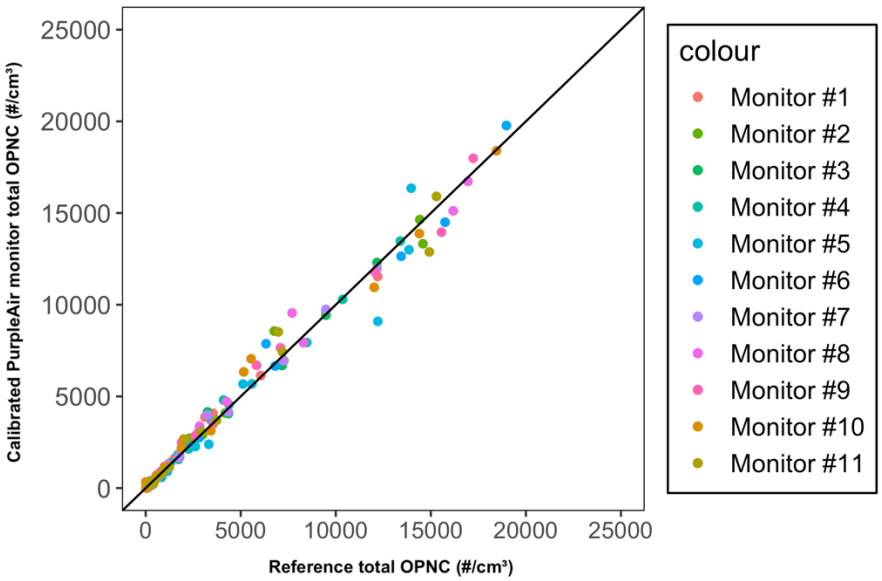

Fig A7. Parity plot of the reference total OPNC and the calibrated optical particle counter (PurpleAir PA-II-SD) total OPNC. The color represents the data from each PurpleAir monitor. The diagonal line represents the 1:1 relationship between the reference measurement and the calibrated PurpleAir monitor measurement.

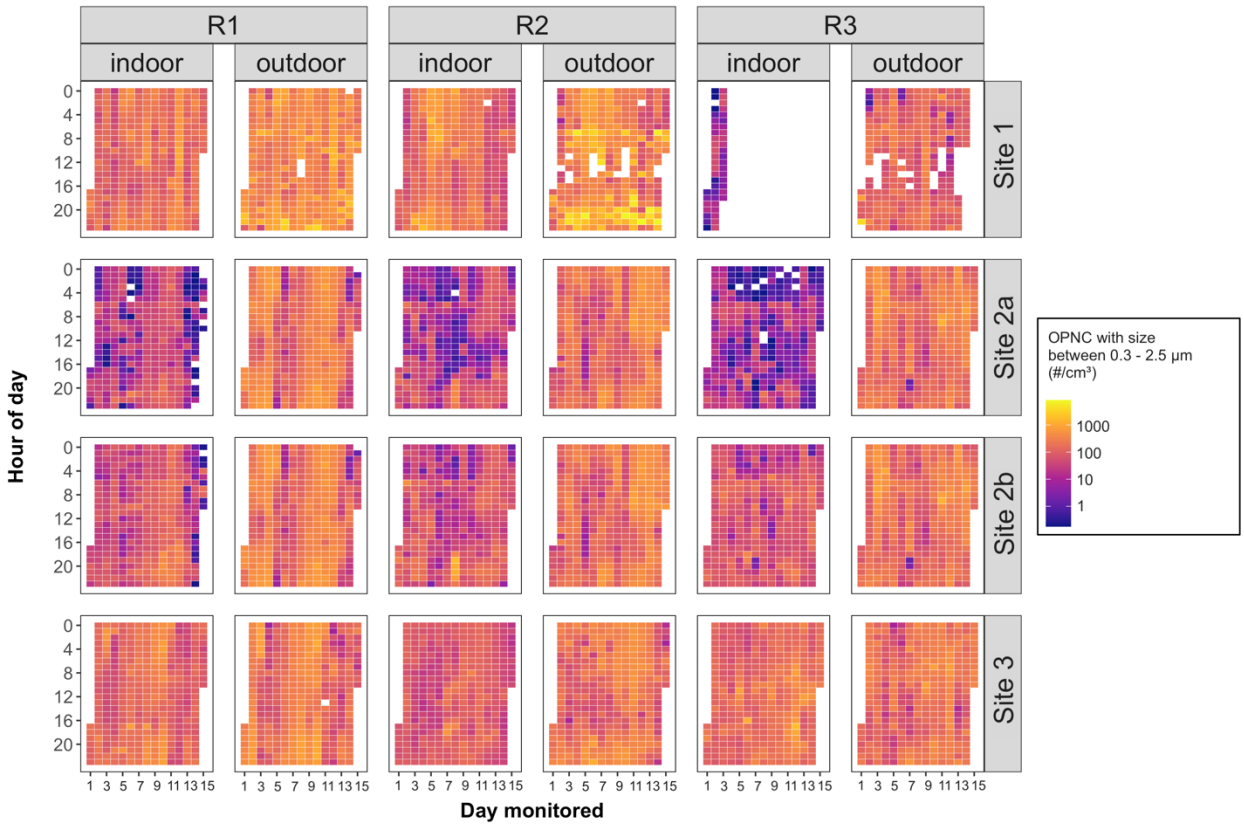

Fig A8. Heatmap of the indoor and outdoor OPNC with size between 0.3 – 2.5 µm at each site. For sites with multiple indoor monitors (site 1, site 2a, and site 2b), the average concentrations were plotted.

Funding sources

This project was supported by cooperative agreement EH20-2005 funded by the Centers for Disease Control and Prevention.

Author contribution: Ching-Hsuan Huang: Conceptualization, Data curation, Formal analy- sis, Investigation, Methodology, Visualization, Roles/Writing – original draft; Thu Bui: Investigation, Project administration, Writing – review & editing; Daniel Hwang: Investigation, Project administration, Writing – review & editing; Jeffry Shirai: Investigation, Methodology, Project ad- ministration, Resources, Writing – review & editing; Elena Austin: Methodology, Formal analysis, Writing – review & editing; Martin Cohen: Methodology, Writing – review & editing; Timothy Gould: Methodology, Resources, Writing – review & editing; Timothy Larson: Methodology, Writing – review & editing; Igor Novosselov: Methodology, Writing – review & editing; Shirlee Tan: Conceptualization, Funding acquisition, Methodology, Project administration, Resources, Supervision, Writing – review & editing; Julie Fox: Funding acquisition, Resources, Writing – re- view & editing; Edmund Seto: Conceptualization, Methodology, Formal analysis, Resources, Supervision, Writing – review & editing.

Acknowledgment: The authors wish to express special thanks to King County Health Engagement Action Resource Team (HEART Team) for mobilizing rapid HEPA air cleaner deployment and facilitating connection with study sites, and PHSKC Environmental Health Services COVID Recovery Program on Indoor Air for assisting with logistics and resources.

Declaration of competing interest: The authors declare that they have no known competing financial interests or personal relationships that could have appeared to influence the work reported in this paper.

CHAPTER 3. EFFECTS OF DUST LOADING ON THE LONG-TERM PERFORMANCE OF PORTABLE HEPA AIR CLEANER TO WOODSMOKE – A LABORATORY INVESTIGATION

This chapter is a manuscript in preparation. The authors of the manuscript are:

Ching-Hsuan Huang [1], Ningrui Liu [1, *], Jeff Shirai [1], Martin Cohen [1], Elena Austin [1], Edmund Seto [1]

[1] Department of Environmental and Occupational Health Sciences, University of Washington, WA 98195, USA

*Corresponding Author

3.1 ABSTRACT

Portable air cleaners (PACs) with high-efficiency particulate air (HEPA) filters are recommended by public health authorities to reduce indoor particles from wildfire smoke. While existing evaluations of HEPA PACs primarily focus on initial performance, long-term efficacy is unclear, especially in scenarios with elevated PM levels leading to significant dust accumulation on filters. Therefore, we aimed to investigate the impact of filter dust loading on the long-term efficacy of HEPA PAC in reducing indoor particles from woodsmoke. Using a custom designed blower system, we pre-loaded commercially available filter combinations of prefilter, charcoal filter, and HEPA filter with varying amounts of ASHRAE ISO 12103-1 A2 fine test dust. We then generated fresh woodsmoke in an exposure chamber to experimentally characterize the impact of filter loading on PAC particle filtration performance. Loadings were varied from 6.3 g to 46.0 g to represent 1– 11 months of continuous usage under the Turbo fan speed in typical US residential environment. We characterized the relationship between filter loading and airflow rate, pressure drop, power consumption, and clean air delivery rate (CADR). The CADR was calculated from the measured particle number concentrations. Results showed a non-linear decrease in CADR as the filter loading increases, though a non-monotonic relationship between filter dust loading, airflow rate and power consumption was found, indicating the influence of PAC's blower motor design and control mechanisms on airflow rate and energy performance characteristics. These findings support the use of PACs for up to 7 months under typical indoor concentrations without large decreases in performance.

Keywords: HEPA portable air cleaner (PAC), clean air delivery rate (CADR), woodsmoke, dust loading, particle

3.2 INTRODUCTION

Climate change has led to an increase in the prevalence and severity of wildfires in recent years, particularly in the Western United States (US) [105-110]. Originating from the burning of vegetation, wildfire smoke contains a complex mixture of particulate matter (PM), volatile organic compounds (VOCs), and hazardous air pollutants [111-113]. Numerous epidemiological studies have underscored the profound health effects of acute exposure to wildfire-related fine (< 2.5 μm, $PM_{2.5}$) and ultrafine (< 100 nm, UFP) particulate matter, linking it to elevated rates of cardiorespiratory morbidity, mortality, and hospital admissions [23, 112, 114, 115]. Moreover, wildfire smoke exacerbates pre-existing health conditions such as asthma and chronic obstructive pulmonary disease (COPD) [116, 117]. While public health authorities typically advise affected communities to seek refuge indoors and minimize outdoor activities during wildfire smoke events, studies reveal that indoor $PM_{2.5}$ concentrations can still reach hazardous levels, even with sealed windows [5, 6, 118].

In response to these challenges, various regulatory agencies have recommended the use of portable air cleaners (PACs) equipped with high-efficiency particulate air (HEPA) filters to mitigate indoor air pollutant exposure during wildfire episodes [12, 81]. When selecting a PAC, consumers are advised to consider factors such as filtration efficiency, clean air delivery rate (CADR), noise level, energy consumption, and filter lifespan [119]. The CADR, standardized by the Association of Home Appliance Manufacturer (AHAM), measures the effective volumetric airflow rate (in unit cubic per minute, ft^3/min or CFM) of particle-free air delivered by the PAC [88]. Based on three particle size categories, i.e., tobacco smoke (0.09 to 1 μm), dust (0.5 to 3 μm), and pollen (5 to 11 μm) representing fine, medium-sized, and coarse particles respectively,

the CADR accounts for both mixing characteristics of testing environment and PAC particle filtration efficiency [88, 104]. Consequently, the CADR is commonly employed by PAC manufacturers to characterize device performance over single-pass efficiency (SPE), which solely measures the percentage of particles removed in a single pass through the filter. Despite the recent addition of $PM_{2.5}$ CADR in AHAM guidelines [104, 120], size-resolved CADR is usually not tested or reported by the manufacturer. Particle deposition in the human respiratory tract is highly dependent on particle size [121]. Thus, size-resolved CADR by PAC, especially for ultrafine particle (<100 nm), is essential to be characterized.

The recent models of residential PACs typically incorporate three filter layers: a pre-filter for capturing larger particles such as dust, hair, and pollen, an activated carbon/charcoal filter for absorbing organic vapor, and a HEPA filter which theoretically removes at least 99.97% of particles with diameters of 0.3 μm. For the pre-filter, it is recommended to be cleaned, vacuumed, or washed periodically or when it is visibly dirty. The recommended lifespan for activated carbon filters and HEPA filters are typically three months and one year, respectively. While existing evaluations of HEPA PACs primarily focus on initial performance metrics [122-124], limited insights have been provided regarding their long-term effectiveness, especially in scenarios with elevated PM levels leading to significant dust accumulation on PAC filters over time.

Few studies have investigated the long-term effectiveness of HEPA PACs in terms of CADR, SPE, airflow rate, and power consumption, either in field or laboratory settings [101, 102, 125]. Zuraimi et al. explored the impact of artificial dust loading on the performance of a HEPA PAC

in a controlled laboratory environment, observing a 49% reduction in PAC airflow rate following the deposition of 150 g of ISO 12103-1 A1 ultrafine test dust (particle diameter: 0.97 to 22.0 μm) [101]. Shaughnessy et al. reported a 25.0% reduction in smoke CADR following 800 hours of intermittent operation in residential bedrooms [102]. Other countries, such as China, have provided guidelines for assessing PAC performance. The Cumulative Clean Mass (CMM) metric, which represents the dust loading amount when PAC's CADR is reduced to one half of its initial value, has been implemented to measure a PAC's long-term performance. Yet, there remains a gap in knowledge regarding the effects of long-term dust accumulation on PAC filtration efficiency, particularly concerning woodsmoke particles, which is critical for devising effective public health interventions during wildfire events.

To address this knowledge gap, we conducted a laboratory investigation utilizing a commercially available PAC. This study aims to elucidate the impact of filter dust loading on PAC performance, specifically examining airflow rate, pressure drop across filters, power consumption, and CADR concerning woodsmoke particles. Our objectives are to understand the long-term performance of PACs, provide insights into their performance under conditions of prolonged exposure to elevated levels of particulate matter, and offer guidance on maintaining PACs over the long run, including recommendations for filter replacement intervals to optimize performance.

3.3 METHODS

3.3.1 The tested HEPA PAC

A commercially available PAC (Winix C535, Winix America, Bannockburn, IL) was selected for evaluation in this study. This PAC contains 3 layers of filters, including a pre-filter, a charcoal filter and a HEPA filter. According to the manufacturer, the CADR of this model is 243, 246, and 232 ft^3/min for dust, pollen, and smoke, respectively. This PAC provides five fan speed level settings, including Sleep Mode, Level 1 to 3, and Turbo. This model was chosen because the same model of PAC was deployed in large numbers in a previous study which aimed to improve indoor air quality in homeless shelters in Seattle, Washington [126].

3.3.2 Experimental procedures

The experiment consisted of three phases, including filter dust loading (Phase A), characterization of airflow rate, pressure drop, and power consumption (Phase B), and chamber experiment for assessing PAC's woodsmoke particle filtration performance (Phase C).

Phase A: filter dust loading

During Phase A, PAC filters were loaded with different amount of the ASHRAE ISO 12103-1 A2 fine test dust [127] (Powder Technology, Inc, Arden Hills, MN) as a set, which contains a pre-filter, a charcoal filter, and a HEPA filter. The chemical composition and particle size distribution of the test dust are shown in **Table S1** and **Figure S1**. The mode and median particle size of the test dust are 346.41 nm and 368.61 nm, respectively.

The filter loading procedure was conducted in a plywood chamber (0.91 m (H) × 0.61 m (W) × 0.61 m (L), volume = 0.34 m^3) (**Figure 1 (a)**). The ASHRAE ISO 12103-1 A2 fine test dust was first dispersed into the chamber using a stainless-steel shaker bottle and resuspended with a blower and a mixing fan. During the loading process, the PAC with a brand-new set of filters installed was turned on and set to operate at the Turbo fan speed for loading. Before the procedure, each filter was weighed individually to determine its initial weight. Considering the dust loading amounts in previous studies, four dust amounts were targeted for the loading in this study, including 5, 20, 30, and 45 g. In addition to the 4 sets of filters with different loading amounts, we also assessed a blank filter set (with 0 g of test dust loaded), and a filter set that was used for 70 consecutive days in a congregate living setting/shelter (denoted as "shelter filter" hereafter), which had approximately 47.3 g of house dust loaded. This amount was estimated based on the average pre-weight of the blank filter sets. The average weights for the blank (with no dust loaded) pre-filter, charcoal, and HEPA filters are 127.7, 40.0, and 267.1 g, respectively [126].

Phase B: Characterization of airflow rate, pressure drop, and power consumption

The Phase B was to characterize PAC airflow rate, pressure drop across the filters, and power consumption at each fan speed level and filter loading. The face velocity and pressure drop were measured by a multi-function instrument equipped with a hot-wire anemometer and differential pressure sensor (TSI VelociCalc Multi-Function Ventilation Meter 9565, TSI Incorporated, Shoreview, MN). In order to reduce the outlet turbulence from the PAC to decrease the measurement errors, where the face velocity measurements were made, a cardboard extension was attached onto the outlet of PAC. The extension was shaped as an isosceles trapezoid with

bases of 0.37 m and 0.32 m, legs of 0.11 m, and a height of 0.02 m. The PAC outlet itself was also shaped as an isosceles trapezoid. The airflow face velocity measurements were taken at 3 locations in the PAC air outlet extension with 3 repeated measures respectively. The airflow rate was then calculated by multiplying the average measured face velocity by the area of the PAC air outlet extension face. To measure the pressure drop across the filters, a 3/8 inch hole was drilled in the PAC body to insert a tube from which to measure the pressure drop across the filter (**Figure 1 (b)**). Three replicate measurements were also taken to obtain the average. In addition, the power consumption was measured using a power data logger (HOBO® Plug Load Logger Model UX120-018, Onset Computer Corp, Bourne, MA).

(a) **(b)**

Figure 1. Photos of the (a) custom-built plywood chamber and (b) the location of the pressure sensing tube on the PAC body.

Phase C: Chamber experiment for assessing PAC woodsmoke particle filtration performance

The experiment for assessing PAC woodsmoke particle filtration performance was carried out in a horticultural grow tent/chamber lined with mylar (3.05 m (L) × 1.52 m (W) × 2.03 m (H), volume 9.44 m^3). Due to the size of the test chamber, the following experiment was conducted under the PAC fan speed Level 2 (measured airflow rate (SD) ranged from 101.54 (0.14) to 161.36 (1.22) ft^3/min, see **Table S2**) to prevent excessively rapid particle count reduction, which could exceed the detection capabilities of the instrumentation. To determine the baseline conditions for the chamber (i.e., without a PAC operating inside the tent), fresh woodsmoke was injected into the middle of the chamber at a height of 1 foot using a smoke gun (the Smoking Gun® Model BSM600SILUSC; Breville USA, Inc., Torrance, CA) and woodchips. The injection lasted approximately 15 s to achieve the target concentration, controlled within 100,000 #/cm^3 to prevent coincidence error from the air sampling instruments. All vents on the chamber were tightly sealed throughout the experiments, with a mixing fan placing inside to ensure the air was well-mixed. Total and size-resolved (10 – 10,000 nm) particle concentrations were measured 10 min after the particle dosing procedure to allow for adequate air mixing. Measurements were conducted using an optical particle counter (TSI Optical Particle Sizers Model 3300, TSI Incorporated, Shoreview, MN) and a scanning mobility particle sizer (NanoScan SMPS Nanoparticle Sizer 3910, TSI Incorporated, Shoreview, MN) at sampling rates of 1-second and 1-minute, respectively. The total and size-resolved natural decay constant of particles k_n (min^{-1}), accounting for air exchange and particle loss due to deposition onto the chamber inner surface, were then estimated.

To assess PAC woodsmoke particle filtration performance, the PAC was positioned in the chamber center with the above setup. Similarly, 10 min after the particle dosing procedure, the PAC installed with filters sets with different loadings was remotely activated and set to operate at fan speed Level 2. The total and size-resolved (10 – 10,000 nm) particle concentrations PAC measured until reaching baseline levels. The total and size-resolved particle decay rate (denoted as K_{PAC} (min^{-1})) due to air exchange, deposition on the chamber inner surface, and net removal of PAC were then estimated. Similarly, three replicates were taken for each measurement (k_n and K_{PAC} at different filter loadings). We assumed the particle loadings within the replicates are negligible.

3.3.3 Data analysis

One-minute averages of air samples were obtained for data analysis. The total and size-resolved natural decay constant of particles (k_n) were computed by fitting an exponential decay model to the particle concentration:

$$\ln(C_t) = \ln(C_R) - k_n t$$

where C_t is the total or size-resolved particle number concentration (#/cm^3) at time t; C_R is the total or size-resolved particle number concentration (#/cm^3) at the initial time (i.e., start of the decay period); k_n is the estimated natural decay constant (min^{-1}) of the total or size-resolved particle concentration in the chamber due to air exchange and particle deposition onto the chamber walls. The total or size-resolved particle decay constant due to air exchange, deposition

onto the chamber inner surface, and net removal of PAC (k_{PAC}) was calculated using the same approach by substituting k_n with k_{PAC}.

The total and size-resolved CADR (ft^3/min) was calculated using the following equation:

$$CADR = V \times (k_{PAC} - k_n)$$

where V (ft^3) is the volume of the test chamber; k_n is the estimated natural decay constant (min^{-1}) of the total or size-resolved particle concentration in the chamber, and k_{PAC} is the total or size-resolved particle decay constant (min^{-1}) when PAC is turned on.

For all statistical testing, $p \leq 0.05$ indicated statistical significance in this study. All analyses were conducted using R Version 4.2.3.

3.4 RESULTS

3.4.1 Filter loading in Phase A

The weight distribution of the loaded test dust by PAC filter layers during each experiment phase are shown in **Figure 2**. Final filter loadings were achieved at 6.3, 17.6, 30.3, and 46 g. For all filter loadings, the dusts were predominantly deposited onto the charcoal layer. During Phases A and B, the total dust weight changes for each loading category were found to be < 2% compared to the initial loading, thus deemed negligible (due to study limitations, no individual weighting were available for filters with 17.6 g loadings and the shelter filters). Filters loaded with ISO 12013-1 A2 fine test dust exhibited a lighter color compared to those collected from the shelter.

The shelter filters had visible accumulation of household dust primarily on the pre-filter, resulting in a darker appearance (**Figure 3**).

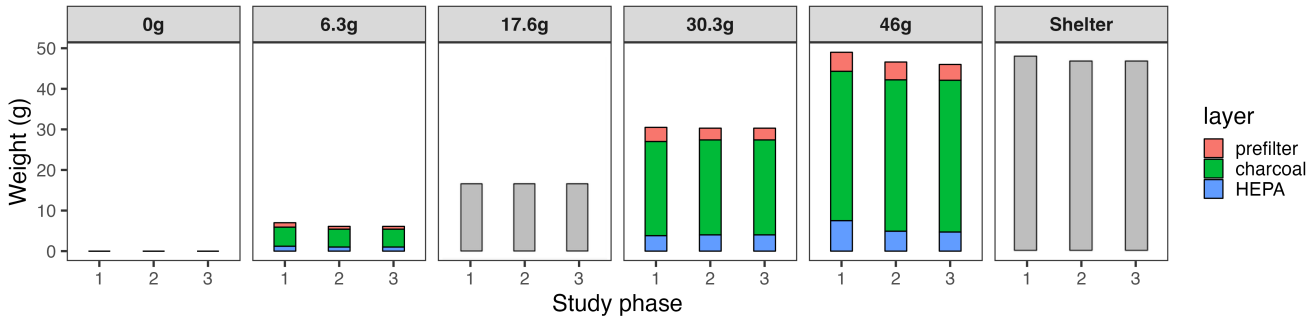

Figure 2. Weight distribution of the loaded dust by PAC filter layers for different loading categories and study phases. Due to study limitations, individual weights were not available for the filter sets with 17.6 g loadings and the shelter filters.

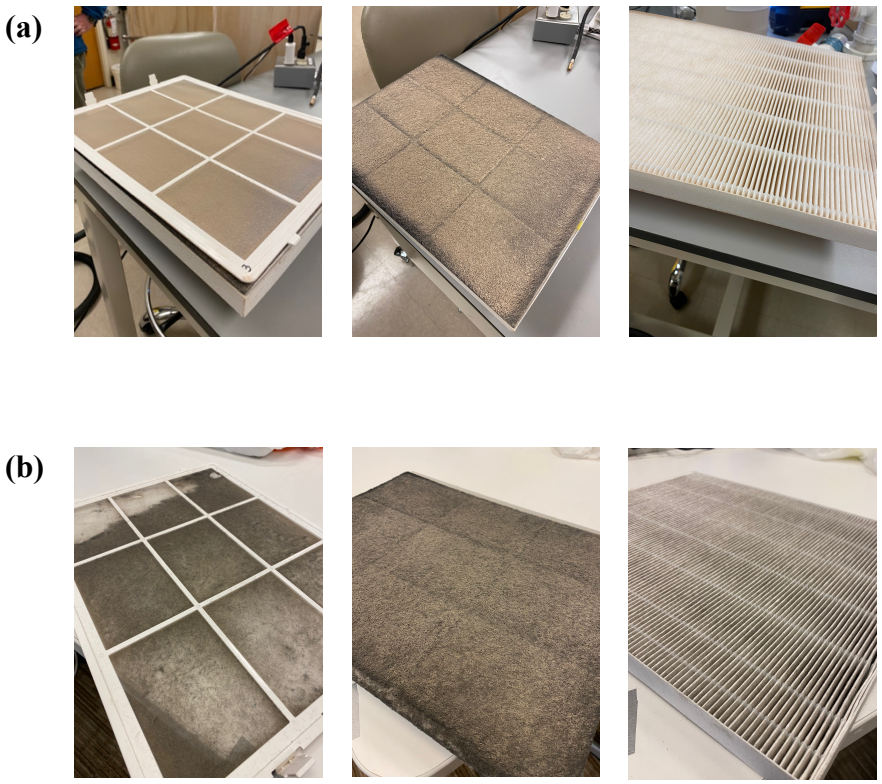

Figure 3. Photos of the (a) filters loaded with ASHRAE ISO 12103-1 A2 fine test dust (30.3 g), and (b) shelter filters collected from a congregate living setting. From left to right: pre-filter, charcoal filter, HEPA filter.

3.4.2 Characterization of airflow rate, pressure drop, and power consumption in Phase B

the PAC average airflow rate ranged from 74.26 to 373.56 ft^3/min while the pressure drop across all three filters ranged from 0.091 to 0.414 inch H_2O, depending on the fan speed level and filter loading (**Table S2**). Variations in air velocity were observed across different measurement points along the outlet vent, reflecting the influence of the PAC's design. Larger openings on the left and right area of the vent led to velocities in those regions, particularly at lower fan speeds. The linear model suggests an overall decreasing trend of airflow rate with the increasing filter loading (**Figure 4 (a)**), which is possibly due to the larger airflow resistance from the loaded filters.

However, a non-monotonic relationship was notably observed between the airflow rate and filter loading within each fan speed level. Airflow rate did not consistently decrease with increasing filter loading; instead, an increase was observed at each fan speed level at 30.3g of filter loading. Similarly, a non-monotonic relationship was found for pressure drop (**Figure 4(b)**), which did not consistently increase with filter loading, albeit minimal differences among various dust loadings were noted, particularly under lower fan speed (Level 1 to Level 3), which was possibly due to the instrument's limited precision. The figure showing the relationship between airflow rate and pressure drop is provided in the **Figure S2**. Similarly, no clear relationship was observed between airflow rate and pressure drop. The relationship between PAC power consumption and filter loadings was also non-monotonic. An increase in power consumption was found at 30.3g filter loading as well, corresponding to the trend between airflow rate and filter loading (**Figure 4 (c)**).

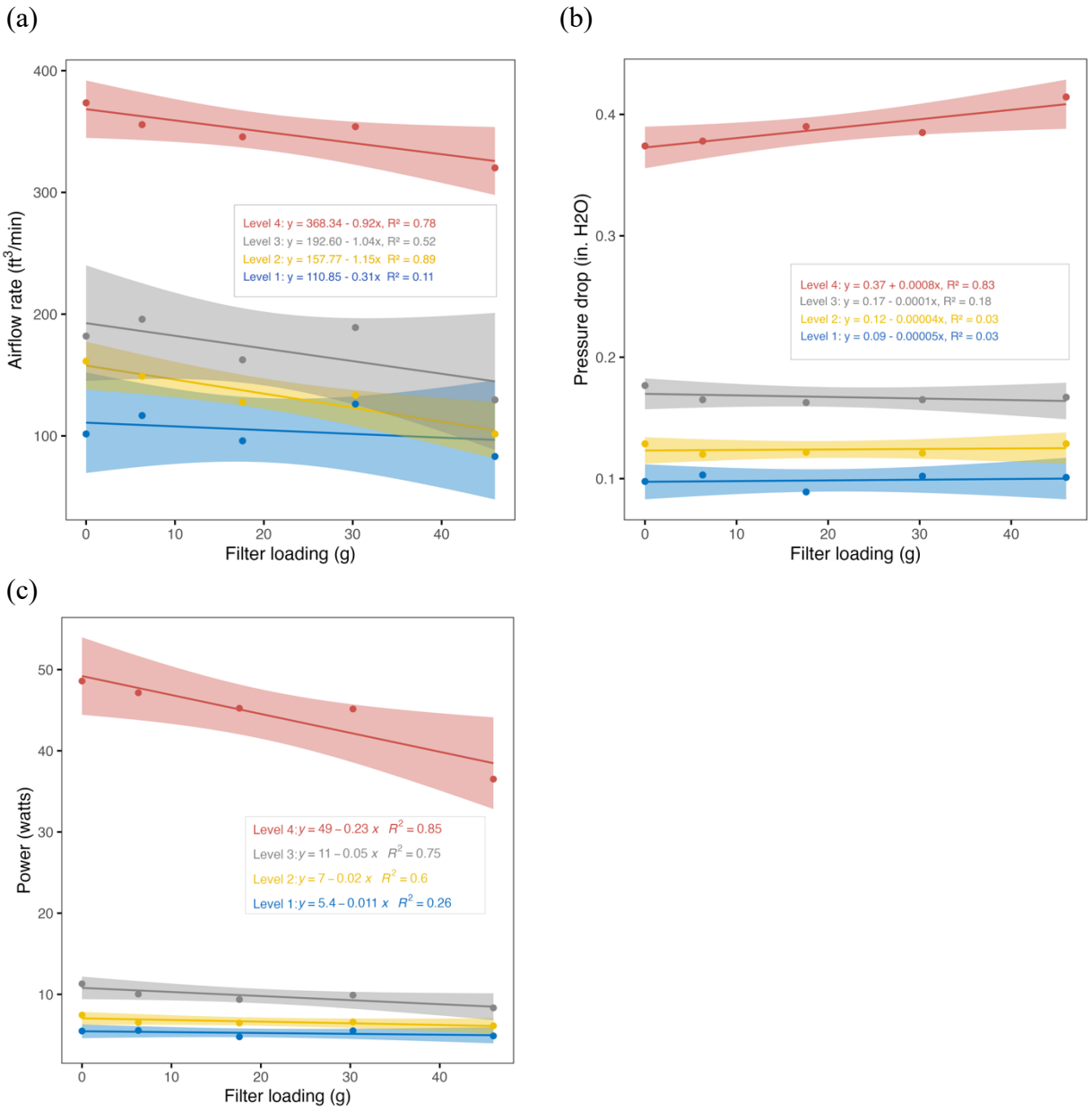

Figure 4. PAC's (a) airflow rate, (b) pressure drop, and (c) power consumption at different fan speeds and filter loadings. The corresponding linear models fitted for each fan speed level are shown in each panel.

3.4.3 Woodsmoke filtration performance in Phase C

The experiments for the PAC woodsmoke filtration efficiency were conducted on two separate days. The mean and standard deviation (SD) of temperature during the experiment day one and two was 9.6 ± 1.0 ℃ and 9.5 ± 1.0 ℃, respectively, whereas the mean relative humidity was 75.6 ± 4.1 % and 76.2 ± 4.5 %, respectively. The estimated natural total particle decay constants due to air exchange and particle deposition on the chamber wall were 1.8 ± 0.03 $h^{-1}$and 0.9 ± 0.01 h^{-1}, respectively, for each experiment day. The differences in experimental conditions between two days were likely influenced by variations in wind speed and gusts. The recorded average wind speed on the first day was 15 miles per hour (mph) with gusts up to 21 mph, while on the second day, it was 13 mph with no gusts.

Figure 5 illustrates the total particle CADR (10 – 10,000 nm) under different filter loadings and the shelter filter at fan speed Level 2. The total particle CADR of PAC with different filter loadings ranged from 95.46 to 114.93 ft^3/min, with the filter loadings of 30.3 g (114.93 ± 7.13 ft^3/min) having the highest CADR, followed by 0 g (109.69 ± 4.21 ft^3/min), 17.6 g (104.02 ± 10.55 ft^3/min), 6.3 g (100.19 ± 3.94 ft^3/min), and 46.0 g (80.31 ± 9.97 ft^3/min) loading. The total particle CADR of the shelter filter, with approximate 47.3 g dust loadings, was estimated to be 95.46 ± 3.59 ft^3/min. A non-monotonic relationship between CADR and filter loadings was observed before reaching 30.3 g, which is similar to the relationship between airflow rate and power consumption with filter loadings. The peak CADR observed at 30.3 g filter loadings was attributed to the highest airflow rate at this loading level. Furthermore, though the shelter filter had slightly higher loading compared to the highest laboratory test dust loading (47.3 g vs. 46.0 g), its woodsmoke CADR at fan speed Level 2 did not appear to be lower. Statistical analysis

using the Kruskal-Wallis test revealed significant differences in the total particle CADR of PACs at different filter loadings ($p < 0.05$). Pairwise comparison with Dunn's test further indicated significant differences in the total particle CADR of PAC with 46.0 g filter loading compared to the one with 30.3 g filter loading.

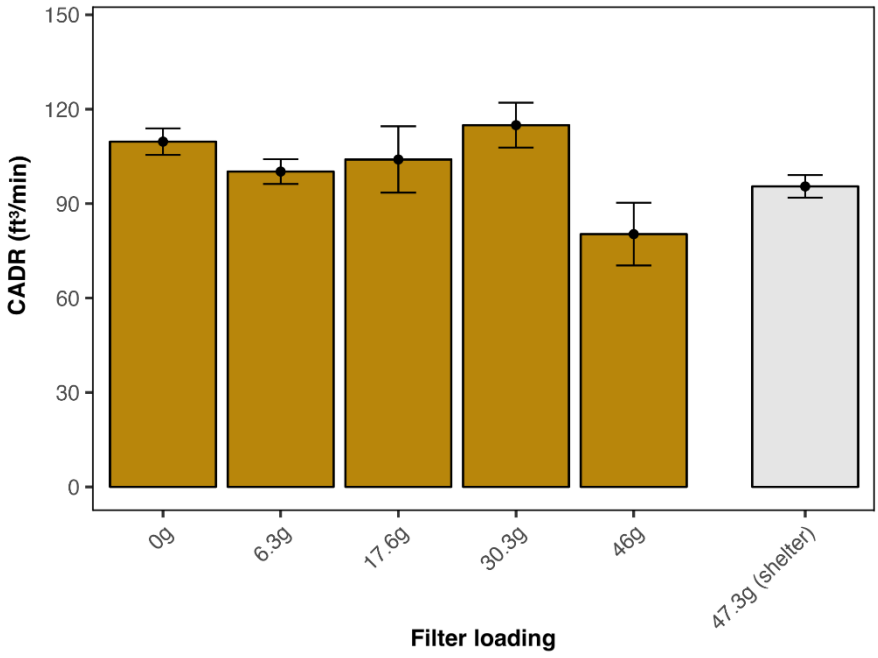

Figure 5. Total particle CADR for woodsmoke (size range: 10 – 10,000 nm) of the tested PAC at different filter loadings under fan speed Level 2.

Due to very low concentration (<10 #/cm^3) observed for particle size bins < 42.2 nm and > 700 nm in the generated woodsmoke, no particle decay was noted within those size bins. Thus, size-resolved CADR was calculated only for particles fall within the size bin range of 42.2 – 700 nm (**Figure 6**). The size-resolved CADR appeared to be higher for the larger particles (> 300 nm) across all filter loadings. Generally, the size-resolved CADR follows a consistent trend, with the filter loaded with 30.3 g test dust having the highest CADR for each size bin, followed by 0,

17.6, 6.3, and 46 g loadings, except for particles larger than 400 nm. Larger uncertainties were observed for particles that are at the extremes the size spectrum (i.e., for size bin 42.2 – 56.2 nm, 400 – 500 nm, and 550 – 700 nm). Based on the Kruskal-Wallis test, the PAC CADR of particles between 56.2 – 133.4 nm (size bin 56.2 – 75 nm, 75 – 100 nm, and 100 – 133.4 nm) were significantly different at varying filter loadings ($p < 0.05$). Pairwise comparison with Dunn's test indicated that the CADRs of these particle size bins with 46.3 g filter loading were significantly different from the one with 30.3g filter loading. The results suggest that the CADR does not show a significant drop until the dust loading increases over 30.3 g. Similar to the findings of total CADR, although the shelter filter had the highest filter loading, it did not appear to have the lowest size-resolved CADR among all, possibly because of the different characteristics of loaded dust.

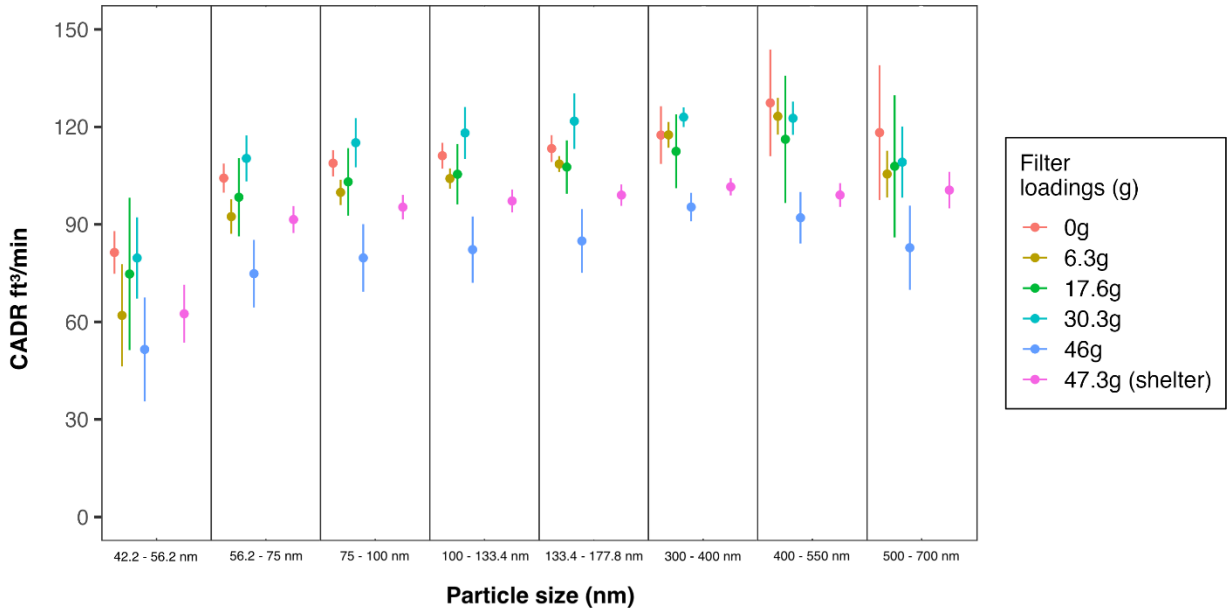

Figure 6. Size-resolved particle CADR (woodsmoke) of the tested PAC at different filter loadings under fan speed Level 2. The vertical bars represent the standard error of the estimates.

To simulate realistic environmental conditions, we estimated the tested PAC's filter loading and CADR over various usage durations under two fan speed levels, including Level 2 and the Turbo fan speed. We first determined the CADR of the Turbo fan speed by dividing the CADR at fan speed Level 2 by its corresponding airflow rate. This ratio was then multiplied by the CADR under fan speed Level 2 by the airflow rate of the Turbo fan speed to obtain the CADR for the Turbo setting. The resulting CADR of the Turbo fan speed level was calculated to be 253.94 ft^3/min. The simulation method is outlined in detail in the **Supplementary Materials**. These estimations were conducted considering different scenarios in residences located in Seattle, Washington, including environments with typical hourly indoor $PM_{2.5}$ concentrations (14.2 $\mu g/m^3$) [98], hourly indoor $PM_{2.5}$ concentrations with major PM sources (e.g., cooking) (23.8

μg/m^3) [98], and hourly indoor $PM_{2.5}$ concentrations during active wildfire events (47.4 μg/m^3) [6]. Constant indoor $PM_{2.5}$ concentrations and PAC airflow rates were assumed over time for each scenario, with continuous PAC usage (24 hours per day) under the Turbo fan speed.

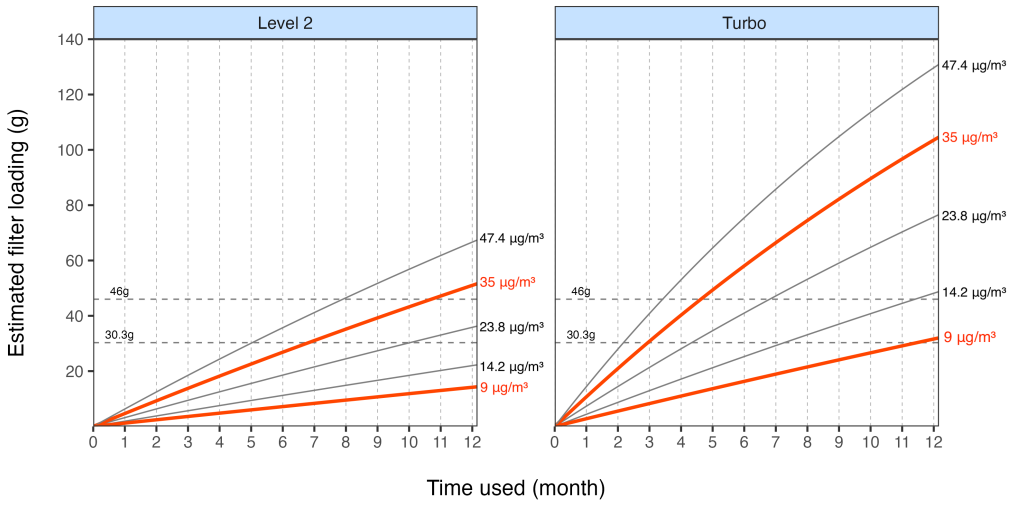

Figure 7. Estimated PAC filter loading as a function of time under Level 2 and Turbo fan speeds. The simulation assumes continuous operation (24 hours per day) for each fan speed setting. Note that the y-axes have different scales for each panel.

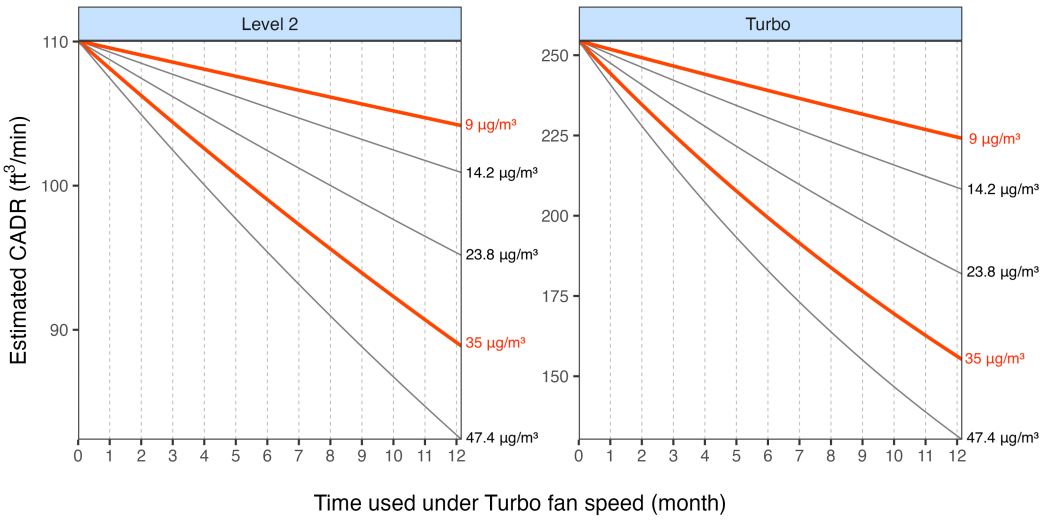

Figure 8. Estimated PAC CADR as a function of time under Level 2 and Turbo fan speeds. The simulation assumes continuous operation (24 hours per day) for each fan speed setting. Note that the y-axes have different scales for each panel.

The results indicate that under the typical US residence scenario (with an hourly indoor $PM_{2.5}$ concentration of 14.2 µg/m^3), the estimated filter loading reaches approximately 30 g after continuous PAC usage for 7.2 months with continuous Turbo fan speed usage (**Figure 7**). This timeframe was shorter than the suggested lifetime (12 months) for replacing the HEPA filter by the PAC manufacturer. Under the same scenario, the estimated filter loading reaches approximately 46 g (corresponding to the dust amount observed for significant CADR drop) after 11.4 months of continuous usage. In high pollution scenarios, such as households with cooking activities (with an hourly indoor $PM_{2.5}$ concentration of 23.8 µg/m^3) and during wildfire events (with an hourly indoor $PM_{2.5}$ concentration of 47.4 µg/m^3), the estimated filter loading reaches approximately 76.7 g and 131.0 g after 1-year use, respectively. These values exceed the estimated amounts when the CADR experiences a significant drop (from 30.3 to 46.0 g). Moreover, the total CADR decreased by 18% and 49% after 12 months of continuous PAC usage at the Turbo fan speed under typical US residence conditions and during wildfire events,

respectively (**Figure 8**). It is important to note that these estimations assume constant indoor $PM_{2.5}$ levels and continuous operation at Turbo fan speed. Therefore, the calculated filter loadings and CADR decrease may be overestimations, as we aimed to simulate the worst-case scenario.

3.5 DISCUSSION

Our study findings reveal that filter loading can significantly impact HEPA PAC performance metrics, including airflow rate, pressure drop, power consumption, and CADR. While a non-monotonic relationship was identified between filter loading and airflow rate, as well as between filter loading and power consumption, an overall decreasing trend was observed, which underscores the degradation of PAC's long-term performance over time and emphasizes the necessity of conducting regular filter replacements. However, the frequency of filter replacement should be tailored to specific operational parameters, such as fan speed level and operation time, as well as environmental conditions, including background particle concentration. Adjusting the replacement schedule based on these factors ensures optimal performance and longevity of the PAC in maintaining indoor air quality.

In our study, we observed a two-step reduction in PAC airflow rate and power consumption as the filter loading increased. The first reduction occurred when the filter loading increased from 0 g to 30.3 g, and the second-step reduction occurred when the filter loading increased from 30.3 to 46 g. Despite these non-monotonic relationships, overall negative trends were noted between PAC airflow rate, power consumption, and filter loading, with moderate linearities found (R^2 value = 0.89 for airflow rate and filter loading; R^2 value = 0.60 for power consumption and filter

loading; **Figure 4(a)** and **(c),** fan speed level 2). Our findings align with those of Zuraimi et al.[101], who reported a similar non-monotonic decrease in power consumption and airflow rate with increasing filter loading, while overall linear decreasing trends were observed, albeit with stronger linearities (R^2 value = 0.97 for airflow rate and filter loading; R^2 value = 0.95 for power consumption and filter loading) compared to our results.

To further investigate this phenomenon, we conducted an examination of how filter blockage with solid material affects the PAC's blower motor temperature and power consumption. The detailed experiment protocol is provided in the **Supplementary Materials.** Briefly, two thermocouples were taped to the tested PAC's blower motor to monitor its temperature during operation, while power consumption was simultaneously measured with 100%, 67%, 33%, and 0% of the pre-filter area blocked. First, as shown in **Figure S3**, we observed the fan speed did not remain constant as the % filter blocked area increased. This corresponds to the natural behavior of a centrifugal fan, wherein increased system resistance leads to decreased airflow and power consumption. Second, as depicted in **Figure S4**, we noted a two-step, non-monotonic decrease in PAC power consumption and motor temperature with increasing filter blockage. This could possibly be explained by the fan motor's proprietary control algorithm, in which as the system resistance increases to a certain threshold, the fan speed is adjusted to enhance airflow, resulting in higher power consumption. The observed non-constant fan speed levels and two-step reduction in airflow rate and power consumption as filter loading increased underscore both the operating principle of centrifugal fans and the presence of the manufacturer's proprietary motor control algorithm in optimizing PAC fan operation. Indeed, our tested PAC utilizes a centrifugal fan design with a brushless direct current (BLDC) motor, also known as an electronically

commutated motor (ECM), which offers variable fan speed operation based on feedback sensor data and the manufacturer's proprietary motor control algorithm [128]. Typically, ECM blowers respond to system resistance by increasing fan speed, which consequently results in higher power consumption [129]. These findings highlight the close relationship between PAC energy performance characteristics and its design, such as fan and blower motor used, and the proprietary fan speed control mechanisms.

In our analysis of total CADR, a notable reduction was observed at a filter loading of 46.0 g compared to the previous loading amount of 30.3 g, indicating a potential decline in total CADR once the filter loading surpasses 30.3 g. The size-resolved CADR analysis revealed differential filtration efficiency across particle size bins. For particle filtration with fibrous filter such as HEPA filter, three main physical mechanisms contribute to its effectiveness for capturing particles, including interception, inertial impaction, and diffusion. While ultrafine particles (<0.1 μm or 100 nm) primarily undergo diffusion filtration, larger particles mainly filtered by inertial impaction and interception. For particles ranging between 0.1 – 0.4 μm in size, neither diffusion nor interception mechanism is optimally efficient for filtration. This characteristic renders them as the most penetrable particle size (MPPS) and contributes to their relatively lower filtration efficiency compared to particles of other sizes. In our results, the smallest CADR were found for particles < 56.2 nm at each filter loading, which is different from the theoretical MPPS of HEPA filter, possibly due to the tested PAC uses multiple layers of filters and the effects of filter loadings affecting the filter solidity, causing the MPPS to shift towards smaller size. Previous research on aircraft cabin HEPA filters highlighted the influence of filter fiber solidity on the MPPS, with increased solidity enhancing particle collection via inertial impaction. However,

diffusion-related collection remained largely unaffected, leading to a decreased MPPS that reflects the combined effects of impaction and diffusion [130]. Furthermore, in our study, the majority of the test dusts were loaded on the charcoal layer rather than the HEPA filter, which could potentially shift the MPPS. Despite these variations, a consistent trend of highest total CADR at 30.3 g and a subsequent decline at 46 g filter loading was observed across all particle size bins. In our simulation of filter loading and CADR degradation under various usage condition, time, and scenarios, the estimated CADR of the Turbo fan speed level was 253.94 ft^3/min, exceeding the CADR of cigarette smoke provided by the manufacturer (232 ft^3/min). This discrepancy may be attributed to differences in particle size distribution between fresh woodsmoke particles (with mode and median particle size of 90.71 nm and 79.41 nm, respectively, as measured in our study) and the standard cigarette smoke particle (0.1 – 1 μm) used according to the AHAM AC-1 standard. Generally, the CADR tends to increase as the particle size decreases [131].

Our filter loading, varied from 6.3 g to 46 g, represented approximately 1 – 11 months of continuous PAC usage under the Turbo fan speed under in a typical US household environment without major particle source (**Figure 7**). The filter loading and CADR degradation were projected to be increase and decrease non-linearly, respectively, under this scenario. Our results support the use of PACs for up to 7.2 months under typical indoor concentrations without observing a significant drop in CADR. However, in a US residential environment with a major particle source, such as cooking, the PAC filter loading could reach 30.3 g in approximately 4.3 months, leading to a significant drop in CADR. Therefore, based on our findings, it is

recommend replacing the filter more frequently than the manufacturer's suggested time when using PACs under polluted environments.

One major challenge with filter replacement in HEPA PACs extends beyond merely maintaining filtration efficacy. It encompasses various factors, including cost, labor, waste generation and sustainability, which contribute to the overall trade-off and cost-effectiveness that users might consider. For instance, the replacement filter for the HEPA PAC evaluated in this study cost approximately $80 USD for a one-year supply (as recommended by the PAC manufacturer), including one HEPA filter and three charcoal filters. This expense represents a recurring cost for users, which may be a higher cost for users in environments with high particle concentration that require more frequent filter replacements. Furthermore, the effort required for regular maintenance can be considerable, involving both time and labor. The disposal of used filters raises environmental concerns from a sustainability perspective. Therefore, while regular filter replacement is crucial for ensuring optimal HEPA PAC performance and maintaining indoor air quality, it is essential to balance these practical and environmental trade-offs, conserving both immediate benefits and long-term implications.

The study is limited by its laboratory-based approach, which may not fully capture real-world variability in environmental conditions. First, the use of ASHRAE ISO 12103-1 A2 fine test dust for filter loading may not entirely replicate real-world dust accumulation scenarios, as household dust composition differs from standardized test dust and typically contains larger particles. This limitation is evident in our results, where the Shelter filter, loaded with approximately the same weight of house dust (47.3 g) as our highest laboratory loading (46 g), did not exhibit the same

performance in terms of CADR. Second, our estimation of PAC CADR and filter loadings over time relied on assumptions, including continuous operation under Turbo fan speed and steady indoor $PM_{2.5}$ concentration and airflow rate, which may not align with real-world conditions. These assumptions were made to simulate extreme use cases, aiming to help consumers anticipate potential worst-case scenarios and providing a conservative estimation. Third, our study focused solely on one PAC model, limiting its generalizability to other models with different design features and filtration technologies, such as PACs powered by different types of blower motors. Fourth, while our evaluation primarily targeted the filtration of woodsmoke particles, woodsmoke contains various gaseous compounds that may affect indoor air quality. Although the PAC tested in our study included an activated carbon filter, we did not specifically assess its performance in removing gaseous pollutants, such as VOCs. Future studies concentrating on the filtration of gas pollutants could provide valuable insights on this.

3.6 CONCLUSIONS

While existing evaluations of HEPA PACs primarily focus on initial performance, long-term efficacy is unclear, especially in scenarios with elevated PM levels leading to significant dust accumulation on filters. In this study, we investigated the impact of filter dust loading with ASHRAE ISO 12103-1 A2 fine test dust on the efficacy of HEPA PAC in reducing indoor particles from woodsmoke and performance metrics including airflow rate and power consumption. Results show a non-monotonic relationship between filter loading and airflow rate, as well as between filter loading and power consumption. Despite this non-monotonic behavior, an overall decreasing trend was observed, which underscores the degradation of PAC's long-term performance over time and emphasizes the necessity of conducting regular filter

replacements. These findings support the use of PACs for up to 7 months under typical indoor concentrations without a significant decrease in performance. However, in environments with major pollution sources, it is advisable to replace the PAC filter more frequently than the manufacturer's recommended interval.

3.7 SUPPLEMENTARY MATERIALS

PAC motor temperature and power consumption with varying filter area blockage level

A laboratory experiment was conducted to examine how filter blockage with solid materials affects the tested PAC's blower motor temperature and power consumption. Two thermocouples were taped to the PAC's blower motor to measure its temperature during operation, while simultaneously measuring power consumption under varying degrees of pre-filter blockage, including 0%, 33%, 66.7%, and 100%. The pre-filter area was blocked using a plastic sheet. Two additional thermocouples were used to measure the ambient temperature simultaneously during the experiment. The power consumption of the air cleaner was measured using a power data logger (HOBO® Plug Load Logger Model UX120-018, Onset Computer Corp, Bourne, MA). The temperature and energy data were both logged at 1-sec intervals.

Filter loading and CADR estimation

To estimate PAC's filter loading and CADR over extended usage time under the Turbo fan speed level, we first derived the CADR of the Turbo fan speed by dividing the CADR at fan speed Level 2 by its corresponding airflow rate. This ratio was then multiplied by the airflow rate of the Turbo fan speed to obtain the CADR for the Turbo setting. Then, we fit a linear regression model using the estimated total CADR at each filter loading as the dependent variable, and filter loading as the independent variable.

The slope and the intercept were plugged into the following equation:

$$\mathrm{CADR(t)} = \mathrm{a} + \mathrm{b} \times \mathrm{dust\,(t)} \qquad \text{Eq.(1)}$$

$$\mathrm{dust(t)} = \mathrm{dust\,(t-1)} + \mathrm{CADR(t-1)} \times 1.7 \times (\mathrm{C_{in}}/\,10^{6}) \qquad \text{Eq.(2)}$$

where in eq. (1), $\mathrm{CADR\,(t)}$ is the CADR (ft^3/min) at time t, a and b are the intercept and slope of the linear regression model fitted for total CADR vs. filter loading, respectively.

In eq. (2), $\mathrm{dust(t)}$ is the filter loading (g) at time t; $\mathrm{dust\,(t-1)}$ and $\mathrm{CADR\,(t-1)}$ are the filter loading (g) and CADR (ft^3/min) at time $\mathrm{t-1}$, respectively; $\mathrm{C_{in}}$ is the assumed hourly indoor $PM_{2.5}$ concentration ($\mu g/m^3$) under each scenario, assumed to be steady over time. The factor of 1.7 is used to convert units from ft^3/min to m^3/h. This equation estimates the cumulative filter loading by adding the amount of dust collected from the air at time $\mathrm{t-1}$ to time t.

The PAC airflow rate under the Turbo fan speed was also assumed to remain steady over time.

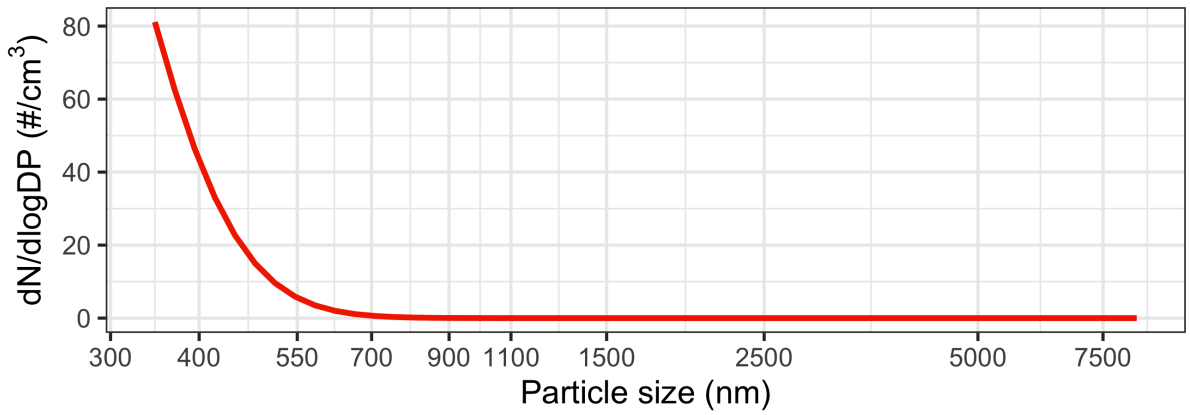

Figure S1. Particle size distribution of the ISO 12103-1 A2 fine test dust, measured by TSI OPS 3330.

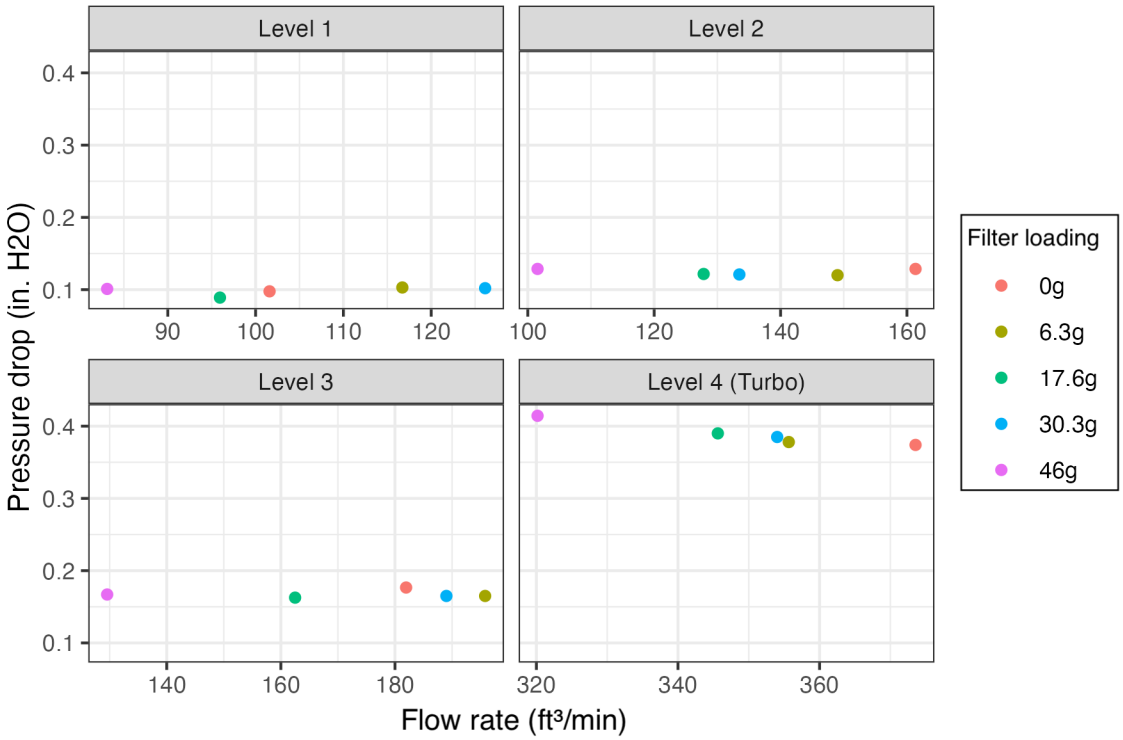

Figure S2. Relationship between PAC airflow rate and pressure drop across the filter set at different fan speed level and filter loadings

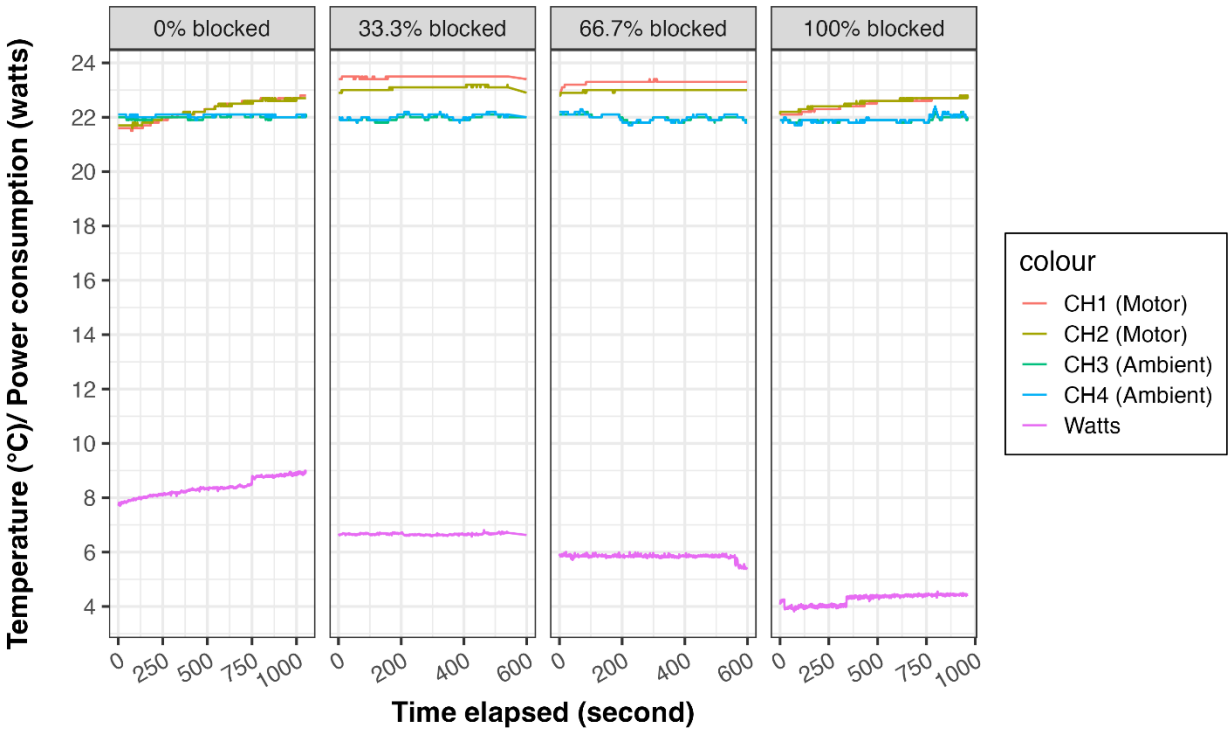

Figure S3. PAC motor temperature and power consumption with different percentage of filter area blocked by solid material. Measurements were taken and fan speed Level 2.

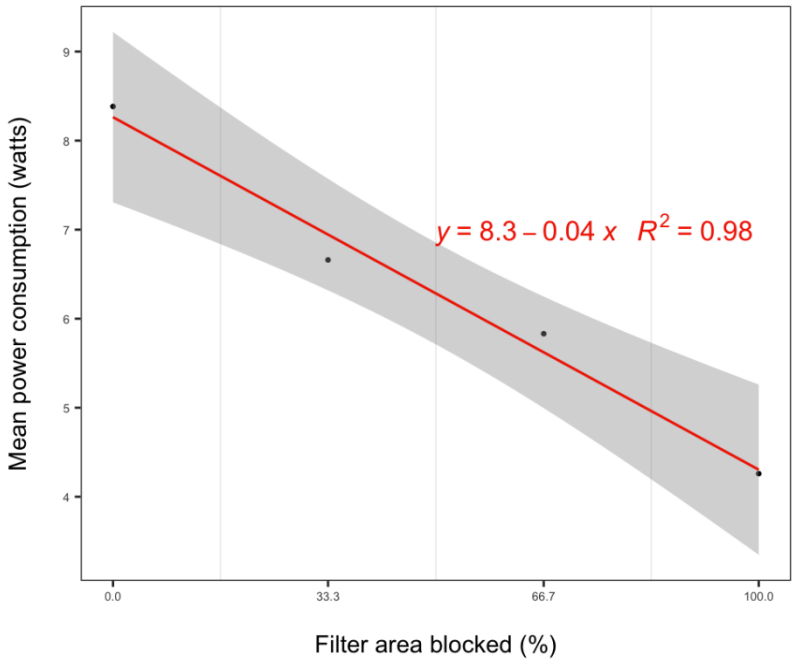

Figure S4. Relationship between the PAC mean power consumption and % filter area blocked.

Table S1. Chemical component of the ASHRAE ISO 12103-1 A2 fine test dust provided by the manufacturer.

Component	% of weight
SiO_2	69 – 77%
Al_2O_3	8 –14%
Fe_2O_3	4 – 7%
CaO	2.5 – 5.5%
K_2O	2 – 5 %
Na_2O	1 – 4 %
MgO	1 – 2%
TiO_2	0 – 1%

Table S2. Summary of the measured PAC face velocity and flow rate at different filter loadings and fan speed level.

Filter loading	Fan speed level	Face velocity (ft/min)								Averaged airflow rate (ft^3/min)	
		Left		Middle		Right		Average			
		Mean	SD	Mean	SD	Mean	SD	Mean	SD	Mean	SD
Blank	Lv4	921.33	6.81	828.33	10.69	983.67	0.58	911.11	5.70	373.56	2.34
	Lv3	550.00	9.85	343.33	4.51	438.00	2.00	443.78	5.42	181.95	2.22
	Lv2	528.00	2.65	289.33	4.16	363.33	6.81	393.56	2.99	161.36	1.22
	Lv1	324.33	12.50	161.00	8.72	258.00	9.54	247.78	9.38	101.59	3.85
6.3g	Lv4	938.67	41.30	740.67	23.71	923.00	5.57	867.44	16.84	355.65	6.90
	Lv3	550.00	3.61	348.00	18.33	534.67	1.15	477.56	5.42	195.80	2.22
	Lv2	353.67	5.51	270.67	2.89	466.00	4.00	363.44	3.98	149.01	1.63
	Lv1	241.67	4.04	183.67	2.08	428.67	2.52	284.67	0.58	116.71	0.24
17.6g	Lv4	852.00	5.57	744.00	5.00	933.00	7.00	843.00	3.76	345.63	1.54
	Lv3	475.33	3.21	416.00	3.61	297.67	2.08	396.33	2.03	162.50	0.83
	Lv2	355.67	12.42	286.67	1.53	293.00	2.65	311.78	4.35	127.83	1.78
	Lv1	237.33	2.52	142.00	2.00	322.67	1.53	234.00	2.00	95.94	0.82
30.3g	Lv4	933.00	2.00	739.00	2.00	918.33	2.08	863.44	0.51	354.01	0.21
	Lv3	513.00	2.00	377.00	1.00	493.00	1.00	461.00	0.67	189.01	0.27
	Lv2	406.67	1.53	231.67	1.53	338.33	1.53	325.56	1.35	133.48	0.55
	Lv1	401.00	2.65	216.00	3.61	306.00	1.00	307.67	2.33	126.14	0.96
46g	Lv4	990.00	3.61	549.67	3.51	803.00	1.00	780.89	0.51	320.16	0.21
	Lv3	314.33	4.16	283.67	3.06	350.00	32.23	316.00	12.73	129.56	5.22
	Lv2	382.33	0.58	114.67	2.08	246.00	2.65	247.67	0.33	101.54	0.14
	Lv1	321.33	4.04	101.67	1.53	185.00	1.00	202.67	0.58	83.09	0.24
Shelter (47.3g)	Lv4	939.00	1.00	693.67	4.04	754.00	1.00	795.56	0.84	326.18	0.34
	Lv3	423.00	4.58	354.67	2.08	405.00	1.00	394.22	0.69	161.63	0.28
	Lv2	377.00	1.00	128.00	1.00	252.67	0.58	252.56	0.38	103.55	0.16
	Lv1	254.67	4.16	96.67	1.53	192.00	1.00	181.11	1.84	74.26	0.75

Table S3. Summary of the measured PAC pressure drop and power consumption at different filter loadings and fan speed level.

Filter loading	Fan speed level	Pressure drop (inch H_2O)		Power consumption (watt)	
		Mean	**SD**	**Mean**	**SD**
Blank	Lv4	0.374	0.000	48.593	1.594
	Lv3	0.177	0.001	11.297	0.015
	Lv2	0.129	0.001	7.443	0.006
	Lv1	0.098	0.002	5.480	0.035
6.4g	Lv4	0.378	0.000	47.147	0.102
	Lv3	0.165	0.000	10.033	0.025
	Lv2	0.120	0.000	6.537	0.006
	Lv1	0.103	0.000	5.550	0.046
17.6g	Lv4	0.390	0.000	45.240	0.026
	Lv3	0.163	0.001	9.367	0.015
	Lv2	0.122	0.001	6.470	0.000
	Lv1	0.089	0.000	4.767	0.012
30.5g	Lv4	0.385	0.001	45.153	0.021
	Lv3	0.165	0.000	9.900	0.010
	Lv2	0.121	0.000	6.600	0.078
	Lv1	0.102	0.000	5.513	0.031
46.8g	Lv4	0.414	0.002	36.510	0.020
	Lv3	0.167	0.000	8.333	0.015
	Lv2	0.129	0.001	6.123	0.012
	Lv1	0.101	0.000	4.877	0.025
Shelter (47.3g)	Lv4	0.410	0.000	39.343	0.015
	Lv3	0.178	0.000	9.343	0.006
	Lv2	0.134	0.000	6.537	0.006
	Lv1	0.091	0.001	4.593	0.012

CONCLUSIONS

Through evidence-based findings, this research addresses critical aspects related to the efficacy of portable air cleaners (PACs) in mitigating particle exposure in community congregate settings. Our findings characterize the performance of low-cost optical particle sensors, underscore the efficacy of HEPA portable air cleaners (PACs) in reducing indoor particle levels in community settings, and highlight the importance of filter maintenance for sustained performance. Moreover, this research contributes to ongoing efforts to improve public health outcomes and indoor air quality.

Chapter 1 focuses on improving the performance of low-cost PM sensors through statistical approaches. Through a standardized experimental protocol in an aerosol chamber, enhanced calibration algorithms are developed for both mass indices and size-resolved number concentration. By assessing sensor-to-sensor data reproducibility with polydisperse test aerosols, discrepancies between OEM-calibrated size distribution and reference measurements from single particle sizers are identified. The calibration models adjusted for particle CRI and density demonstrate improved accuracy, enabling more reliable data collection for air quality assessment.

Chapter 2 evaluates the real-world effectiveness of PACs equipped with high-efficiency particulate air (HEPA) filters, particularly in community congregate settings such as homeless shelters. This research, conducted in collaboration with Public Health – Seattle & King County, assesses the impact of over four thousand distributed HEPA PACs on reducing indoor particle levels. Using a low-cost optical particle sensor calibrated with algorithms developed in Chapter

1, the study examines user experience and factors influencing HEPA PAC usage, providing practical guidance for their utilization in shelter environments. The findings highlight the significant impact of PAC usage duration on reducing indoor particle levels, emphasizing the effectiveness of HEPA PACs as a short-term strategy for reducing indoor particle levels in community congregate living settings.

Chapter 3 investigates the long-term performance of portable HEPA air cleaners in filtering woodsmoke particles, particularly relevant to the challenges faced in the Pacific Northwest region during wildfire season and winter months. Through laboratory investigations, the study evaluates the effects of dust loading on HEPA air cleaner filtration efficiency, offering insights into their long-term effectiveness in mitigating woodsmoke pollution in indoor environments. The findings support continuous HEPA PAC usage under the max fan speed up to 7 months without observing significant reduction in its performance under typical US residential environment. However, in environments with major pollution sources, it is advisable to replace the PAC filter more frequently than the manufacturer's recommended interval.

While this research provides insights into the efficacy of HEPA PACs and the use of low-cost optical particle sensor for indoor air quality management, some limitations must be acknowledged. One major limitation is the generalizability of the findings. Chapter 1 focuses on a specific type of low-cost optical particle sensor, which may limit the applicability of the results to other sensor technologies. In Chapter 2 and 3, the evaluation of HEPA PAC filtration effectiveness was conducted in the Seattle area focused on homeless shelters. These homeless shelters might not be representative of other congregate environments such as educational and

recreational facilities, limiting the broader applicability of the findings. Building characteristics, such as age and design, might also impact the effectiveness of HEPA PAC in improving indoor air quality. Furthermore, the studies focused on a specific air cleaner model, which might not represent the performance of other models. Another limitation is the focus on particulate air pollution; other indoor air pollutants, such as volatile organic compounds (VOCs) and biological contaminants were not addressed. These pollutants could also pose significant public health risks and should be considered in future research to provide a more comprehensive assessment of indoor air quality. For Chapter 2, the study design did not include direct assessment of SARS-CoV-2 transmission, which was infeasible due to ethical and logistical constraints. However, our results suggest a potential for HEPA PAC in reducing airborne transmission of viruses, as measured indirectly by airborne particles.

These limitations emphasize the need for further research to explore the performance of different types of low-cost air quality sensors and portable air cleaning technologies in diverse settings, and against a broader spectrum of indoor air pollutants. Future studies investigating health outcomes associated with exposure to reduced particulate levels in congregate living setting through longitudinal studies correlating HEPA PAC usage with respiratory, cardiovascular, and mental health outcomes, including cognitive function, particularly in settings such as schools and recreational settings, could be explored. Also, our study in Chapter 2 highlighted varying levels of HEPA PAC usage in homeless shelters. Further investigation into user behavior, acceptance, and adherence to user guidelines could help formulate strategies on promoting HEPA PAC use, including the development of educational programs aimed at improving awareness and proper usage of HEPA PACs, particularly in community congregate settings with vulnerable

populations. In conclusion, this research highlights the importance of optimizing the efficacy of HEPA PACs in mitigating indoor particle exposures, addressing challenges such as continuous operation and practical guidance for utilization in shelter environments. By providing evidence-based strategies, this work contributes to the ongoing efforts to improve indoor air quality and public health outcomes.

REFERENCES

1. Brook, R.D., et al., *Particulate matter air pollution and cardiovascular disease.* Circulation, 2010. **121**: p. 2331-2378.

2. US Environmental Protection Agency, *Air Quality - National Summary.* 2023.

3. Klepeis, N.E., et al., *The National Human Activity Pattern Survey (NHAPS): a resource for assessing exposure to environmental pollutants.* J Expo Anal Environ Epidemiol, 2001. **11**: p. 231-252.

4. World Health Organization, *WHO global air quality guidelines: particulate matter (PM2.5 and PM10), ozone, nitrogen dioxide, sulfur dioxide and carbon monoxide.* 2021.

5. O'Dell, K., et al., *Outside in: the relationship between indoor and outdoor particulate air quality during wildfire smoke events in western US cities.* Environmental Research: Health, 2022. **1**(1): p. 015003.

6. Xiang, J., et al., *Field measurements of PM2.5 infiltration factor and portable air cleaner effectiveness during wildfire episodes in US residences.* Science of The Total Environment, 2021. **773**: p. 145642.

7. May, N.W., C. Dixon, and D.A. Jaffe, *Impact of Wildfire Smoke Events on Indoor Air Quality and Evaluation of a Low-cost Filtration Method.* Aerosol and Air Quality Research, 2021.

8. He, J., et al., *Network of low-cost air quality sensors for monitoring indoor, outdoor, and personal PM2.5 exposure in Seattle during the 2020 wildfire season.* Atmospheric Environment, 2022. **285**: p. 119244.

9. Jiao, W., et al., *Community Air Sensor Network (CAIRSENSE) project: evaluation of low-cost sensor performance in a suburban environment in the southeastern United States.* Atmospheric Measurement Techniques, 2016. **9**(11): p. 5281-5292.

10. Lu, T., et al. *Leveraging Citizen Science and Low-Cost Sensors to Characterize Air Pollution Exposure of Disadvantaged Communities in Southern California*. International Journal of Environmental Research and Public Health, 2022. **19**, DOI: 10.3390/ijerph19148777.

11. Carvlin, G.N., et al., *Development and field validation of a community-engaged particulate matter air quality monitoring network in Imperial, California, USA.* Journal of the Air & Waste Management Association, 2017. **67**(12): p. 1342-1352.

12. Centers for Disease Control and Prevention, *Ventilation in Buildings.* 2021.

13. US Environmental Protection Agency, *Clean Air in Buildings Challenge.* 2022.

14. Barn, P., et al., *Infiltration of forest fire and residential wood smoke: an evaluation of air cleaner effectiveness.* J Expo Sci Environ Epidemiol, 2008. **18**(5): p. 503-511.

15. Cai, J., et al., *Particle removal efficiency of a household portable air cleaner in real-world residences: A single-blind cross-over field study.* Energy and Buildings, 2019. **203**: p. 109464.

16. Cox, J., et al., *Effectiveness of a portable air cleaner in removing aerosol particles in homes close to highways.* Indoor Air, 2018. **28**(6): p. 818-827.

17. Beelen, R., et al., *Long-Term Effects of Traffic-Related Air Pollution on Mortality in a Dutch Cohort (NLCS-AIR Study).* Environmental Health Perspectives, 2008. **116**(2): p. 196-202.

18. Krewski, D., et al., *Overview of the reanalysis of the Harvard Six Cities Study and American Cancer Society Study of Particulate Air Pollution and Mortality.* J Toxicol Environ Health A, 2003. **66**(16-19): p. 1507-51.

19. Krewski, D., et al., *Extended follow-up and spatial analysis of the American Cancer Society study linking particulate air pollution and mortality.* Res Rep Health Eff Inst, 2009(140): p. 5-114; discussion 115-36.

20. Pope, C.A., 3rd, et al., *Lung cancer, cardiopulmonary mortality, and long-term exposure to fine particulate air pollution.* Jama, 2002. **287**(9): p. 1132-41.

21. Pope, C.A., 3rd, et al., *Particulate air pollution as a predictor of mortality in a prospective study of U.S. adults.* Am J Respir Crit Care Med, 1995. **151**(3 Pt 1): p. 669-74.

22. Samet, J.M., et al., *Fine particulate air pollution and mortality in 20 U.S. cities, 1987-1994.* N Engl J Med, 2000. **343**(24): p. 1742-9.

23. Pope, C.A., 3rd and D.W. Dockery, *Health effects of fine particulate air pollution: lines that connect.* J Air Waste Manag Assoc, 2006. **56**(6): p. 709-42.

24. Cohen, A.J., et al., *Urban air pollution.* Comparative quantification of health risks: global and regional burden of disease attributable to selected major risk factors, 2004. **2**: p. 1353-1433.

25. Brown, J.S., K.L. Zeman, and W.D. Bennett, *Ultrafine particle deposition and clearance in the healthy and obstructed lung.* Am J Respir Crit Care Med, 2002. **166**(9): p. 1240-7.

26. Schwartz, J. and L.M. Neas, *Fine Particles Are More Strongly Associated Than Coarse Particles with Acute Respiratory Health Effects in Schoolchildren.* Epidemiology, 2000. **11**(1): p. 6-10.

27. Elbayoumi, M., N.A. Ramli, and N.F.F. Md Yusof, *Spatial and temporal variations in particulate matter concentrations in twelve schools environment in urban and overpopulated camps landscape.* Building and Environment, 2015. **90**: p. 157-167.

28. Patel, M.M., et al., *Spatial and Temporal Variations in Traffic-related Particulate Matter at New York City High Schools.* Atmospheric environment (Oxford, England : 1994), 2009. **43**(32): p. 4975-4981.

29. European Parliament, *Directive 2008/50/EC of the European Parliament and of the Council of 21 May 2008 on ambient air quality and cleaner air for Europe*, in *152*, EU, Editor. 2008, Official J. p. 1-44.

30. EPA, *40 CFR Parts 50 - Reference Methods for the Determination of Fine Particulate Matter as PM2.5 in the Atmosphere (Appendix L)*, EPA, Editor. 1997a.

31. Seto, E., et al. *Use of low-cost particle monitors to calibrate traffic-related air pollutant models in urban areas*. in *International Environmental Modelling and Software Society*. 2014.

32. Liu, X., et al., *Low-cost sensors as an alternative for long-term air quality monitoring.* Environmental research, 2020. **185**: p. 109438.

33. Kuhn, T., et al., *Air quality during and after the Commonwealth Games 2018 in Australia: Multiple benefits of monitoring.* Journal of Aerosol Science, 2021. **152**: p. 105707.

34. Makhsous, S., et al., *Methodology for Addressing Infectious Aerosol Persistence in Real-Time Using Sensor Network.* 2021.

35. Hegde, S., et al., *Indoor household particulate matter measurements using a network of low-cost sensors.* Aerosol and Air Quality Research, 2020. **20**(2): p. 381-394.

36. Li, J., et al., *Spatiotemporal distribution of indoor particulate matter concentration with a low-cost sensor network.* Building and Environment, 2018. **127**: p. 138-147.

37. Duncan, G.E., et al., *Usability of a personal air pollution monitor: Design-feedback iterative cycle study.* JMIR mHealth and uHealth, 2018. **6**(12): p. e12023.

38. Cordero, J.M., R. Borge, and A. Narros, *Using statistical methods to carry out in field calibrations of low cost air quality sensors.* Sensors and Actuators B: Chemical, 2018. **267**: p. 245-254.

39. Feenstra, B., et al., *Performance evaluation of twelve low-cost PM2.5 sensors at an ambient air monitoring site.* Atmospheric Environment, 2019. **216**: p. 116946.

40. Kelly, K.E., et al., *Ambient and laboratory evaluation of a low-cost particulate matter sensor.* Environmental Pollution, 2017. **221**: p. 491-500.

41. Sayahi, T., A. Butterfield, and K.E. Kelly, *Long-term field evaluation of the Plantower PMS low-cost particulate matter sensors.* Environmental Pollution, 2019. **245**: p. 932-940.

42. Tryner, J., et al., *Laboratory evaluation of low-cost PurpleAir PM monitors and in-field correction using co-located portable filter samplers.* Atmospheric Environment, 2020. **220**: p. 117067.

43. Wang, Z., W. Delp, and B. Singer, *Performance of low-cost indoor air quality monitors for PM2.5 and PM10 from residential sources.* Building and Environment, 2020. **171**: p. 106654.

44. Zusman, M., et al., *Calibration of low-cost particulate matter sensors: Model development for a multi-city epidemiological study.* Environment International, 2020. **134**: p. 105329.

45. Austin, E., et al., *Laboratory Evaluation of the Shinyei PPD42NS Low-Cost Particulate Matter Sensor.* PLoS One, 2015. **10**(9): p. e0137789.

46. Phuleria, H.C., et al., *Air quality impacts of the October 2003 Southern California wildfires.* Journal of Geophysical Research: Atmospheres, 2005. **110**(D7).

47. Wallace, L.A., S.J. Emmerich, and C. Howard-Reed, *Source Strengths of Ultrafine and Fine Particles Due to Cooking with a Gas Stove.* Environ Sci Technol, 2004. **38**: p. 2304-2311.

48. Afshar-Mohajer, N., et al., *Characterization of particulate matters and total VOC emissions from a binder jetting 3D printer.* Building and Environment, 2015. **93**: p. 293-301.

49. Kinney, P.L., et al., *Traffic Impacts on PM(2.5) Air Quality in Nairobi, Kenya.* Environmental science & policy, 2011. **14**(4): p. 369-378.

50. Chen, J., et al., *A review of biomass burning: Emissions and impacts on air quality, health and climate in China.* Science of The Total Environment, 2017. **579**: p. 1000-1034.

51. Gall, E.T., et al., *Indoor air pollution in developing countries: research and implementation needs for improvements in global public health.* American journal of public health, 2013. **103**(4): p. e67-e72.

52. Sousan, S., et al., *Inter-comparison of low-cost sensors for measuring the mass concentration of occupational aerosols.* Aerosol Science and Technology, 2016. **50**(5): p. 462-473.

53. Wang, Y., et al., *Laboratory Evaluation and Calibration of Three Low-Cost Particle Sensors for Particulate Matter Measurement.* Aerosol Science and Technology, 2015. **49**(11): p. 1063-1077.

54. Renard, J.B., et al., *LOAC: a small aerosol optical counter/sizer for ground-based and balloon measurements of the size distribution and nature of atmospheric particles – Part*

1: Principle of measurements and instrument evaluation. Atmos. Meas. Tech., 2016. **9**(4): p. 1721-1742.

55. Nagy, A., et al., *Numerical and experimental study of the performance of the dual wavelength optical particle spectrometer (DWOPS).* Journal of Aerosol Science, 2007. **38**(4): p. 467-478.

56. Njalsson, T. and I. Novosselov, *Design and Optimization of a Compact Low-cost Optical Particle Sizer.* Journal of Aerosol Science, 2018.

57. Molenar, J.V. *Theoretical Analysis of PM 2.5 Mass Measurements by Nephelometry*. 2003.

58. Liu, H.-Y., et al., *Performance Assessment of a Low-Cost PM2.5 Sensor for a near Four-Month Period in Oslo, Norway.* Atmosphere, 2019. **10**: p. 41.

59. Jayaratne, R., et al., *The influence of humidity on the performance of a low-cost air particle mass sensor and the effect of atmospheric fog.* Atmos. Meas. Tech., 2018. **11**(8): p. 4883-4890.

60. Chakrabarti, B., et al., *Performance evaluation of the active-flow personal DataRAM PM2.5 mass monitor (Thermo Anderson pDR-1200) designed for continuous personal exposure measurements.* Atmospheric Environment, 2004. **38**(20): p. 3329-3340.

61. Sioutas, C., et al., *Field evaluation of a modified DataRAM MIE scattering monitor for real-time PM2.5 mass concentration measurements.* Atmospheric Environment, 2000. **34**(28): p. 4829-4838.

62. Malm, W., D. Day, and S. Kreidenweis, *Light scattering characteristics of aerosols as a function of relative humidity: Part I - A comparison of measured scattering and aerosol concentrations using the theoretical models.* Journal of the Air & Waste Management Association, 2000. **50**(5): p. 686-700.

63. Manikonda, A., et al., *Laboratory assessment of low-cost PM monitors.* Journal of Aerosol Science, 2016. **102**: p. 29-40.

64. Vaddi, R.S., Y. Guan, and I. Novosselov, *Behavior of ultrafine particles in electro-hydrodynamic flow induced by corona discharge.* Journal of Aerosol Science, 2020: p. 105587.

65. He, J.Y. and I.V. Novosselov, *Design and evaluation of an aerodynamic focusing micro-well aerosol collector.* Aerosol Science and Technology, 2017. **51**(9): p. 1016-1026.

66. Vaddi, R.S., Y. Guan, and I. Novosselov, *Particle Dynamics in Corona Induced Electro-hydrodynamic Flow.* arXiv:1902.02986, 2019.

67. Xiang, J., et al., *Using Vehicles' Rendezvous for In Situ Calibration of Instruments in Fleet Vehicle-Based Air Pollution Mobile Monitoring.* Environmental Science & Technology, 2020. **54**(7): p. 4286-4294.

68. Shefelbine, T., C. Forehand, and K. Rink, *3MTM Ceramic Microspheres in Architectural Paint.* 2015.

69. Henry, M., et al., *The 2019 Annual Homeless Assessment Report (AHAR) to Congress.* The U.S. Department of Housing and Urban Development, Office of Community Planning and Development, 2020.

70. Culhane, D., et al., *Estimated Emergency and Observational/Quarantine Capacity Need for the US Homeless Population Related to COVID-19 Exposure by County; Projected Hospitalizations, Intensive Care Units and Mortality.* UCLA: Campuswide Homelessness Initiative, 2020.

71. Perri, M., N. Dosani, and S.W. Hwang, *COVID-19 and people experiencing homelessness: challenges and mitigation strategies.* Canadian Medical Association Journal, 2020. **192**(26): p. E716.

72. Baggett, T.P., et al., *Prevalence of SARS-CoV-2 Infection in Residents of a Large Homeless Shelter in Boston.* JAMA, 2020. **323**(21): p. 2191-2192.

73. Imbert, E., et al., *Coronavirus Disease 2019 Outbreak in a San Francisco Homeless Shelter.* Clinical infectious diseases : an official publication of the Infectious Diseases Society of America, 2021. **73**(2): p. 324-327.

74. Mosites, E., et al., *Assessment of SARS-CoV-2 Infection Prevalence in Homeless Shelters — Four U.S. Cities, March 27–April 15, 2020.* MMWR Morb Mortal Wkly Rep, 2020. **69**: p. 521–522.

75. Tobolowsky, F.A., et al., *COVID-19 Outbreak Among Three Affiliated Homeless Service Sites — King County, Washington, 2020.* MMWR Morb Mortal Wkly Rep, 2020. **69**: p. 523-526.

76. King County Regional Homelessness Authority, *2022 Point in Time Count.* 2022.

77. Agarwal, N., et al., *Indoor air quality improvement in COVID-19 pandemic: Review.* Sustainable cities and society, 2021. **70**: p. 102942.

78. Piscitelli, P., et al., *The role of outdoor and indoor air quality in the spread of SARS-CoV-2: Overview and recommendations by the research group on COVID-19 and particulate matter (RESCOP commission).* Environmental research, 2022. **211**: p. 113038.

79. Seattle Human Services, *HSD prepares its wildfire smoke response to support people experiencing homelessness.* 2021.

80. Barn, P.K., et al., *Portable air cleaners should be at the forefront of the public health response to landscape fire smoke.* Environmental Health, 2016. **15**(1): p. 116.

81. U.S. Environmental Protection Agency, *Clean Air in Buildings Challenge.* 2022.

82. Henderson, D.E., J.B. Milford, and S.L. Miller, *Prescribed burns and wildfires in Colorado: impacts of mitigation measures on indoor air particulate matter.* J Air Waste Manag Assoc, 2005. **55**(10): p. 1516-26.

83. Allen, R.W., et al., *An air filter intervention study of endothelial function among healthy adults in a woodsmoke-impacted community.* Am J Respir Crit Care Med, 2011. **183**: p. 1222-1230.

84. Barn, P., et al., *Infiltration of forest fire and residential wood smoke: an evaluation of air cleaner effectiveness.* Journal Of Exposure Science And Environmental Epidemiology, 2007. **18**: p. 503.

85. Sultan, Z., et al., *Indoor Air Pollution of Outdoor Origin: Mitigation Using Portable Air Cleaners in Singapore Office Building.* Aerosol and Air Quality Research, 2022. **22**(10): p. 220204.

86. Carmona, N., et al. *Indoor Air Quality Intervention in Schools: Effectiveness of a Portable HEPA Filter Deployment in Five Schools Impacted by Roadway and Aircraft Pollution Sources*. Atmosphere, 2022. **13**, DOI: 10.3390/atmos13101623.

87. Barn, P., *Evidence review: Home and community clean air shelters to protect public health during wildfire smoke events.* BC Centre for Disease Control, 2014.

88. Association of Home Appliance Manufacturers, *Method for Measuring Performance of Portable Household Electric Room Air Cleaners, AHAM AC-1-2013.* 2013.

89. California Air Resources Board, *List of CARB-Certified Air Cleaning Devices.* 2023.

90. Wallace, L., *Intercomparison of PurpleAir Sensor Performance over Three Years Indoors and Outdoors at a Home: Bias, Precision, and Limit of Detection Using an Improved Algorithm for Calculating PM2.5.* Sensors, 2022. **22**(7).

91. Wallace, L., et al., *Secondhand exposure from vaping marijuana: Concentrations, emissions, and exposures determined using both research-grade and low-cost monitors.* Atmospheric Environment: X, 2020. **8**: p. 100093.

92. Azevedo, A., et al., *Effects of portable air cleaners and A/C unit fans on classroom concentrations of particulate matter in a non-urban elementary school.* PLOS ONE, 2022. **17**(12): p. e0278046.

93. Public Health - Seattle & King County, *Guidance on Improving Indoor Air Quality for building operators and business owners- Strategies to reduce the risk of COVID-19 indoors.* 2021.

94. The American Society of Heating, Refrigerating and Air-Conditioning Engineers (ASHRAE), *Guidance for Covid-19 Risk Reduction in Residential Buildings.* 2021.

95. Washington State Department of Health, *Ventilation and Air Quality for Reducing Transmission of Airborne Illnesses.* 2022.

96. Washington State Department of Health, *Recommendations for wildfire smoke and COVID-19.* 2022.

97. Brugge, D., et al., *In-home air filtration for improving cardiovascular health: lessons from a CBPR study in public housing.* Prog Community Health Partnersh, 2013. **7**(1): p. 49-56.

98. Huang, C.-H., et al., *Impacts of using auto-mode portable air cleaner on indoor PM2.5 levels: An intervention study.* Building and Environment, 2021. **188**: p. 107444.

99. Kim, S., J.A. Senick, and G. Mainelis, *Sensing the invisible: Understanding the perception of indoor air quality among children in low-income families.* International Journal of Child-Computer Interaction, 2019. **19**: p. 79-88.

100. Xie, R., et al., *Indoor air quality investigation of a badminton hall in humid season through objective and subjective approaches.* Science of The Total Environment, 2021. **771**: p. 145390.

101. Zuraimi, M.S., et al., *Impact of dust loading on long term portable air cleaner performance.* Building and Environment, 2017. **112**: p. 261-269.

102. Shaughnessy, R.J., et al., *Effectiveness of Portable Indoor Air Cleaners: Sensory Testing Results.* Indoor air, 1994. **4**(3): p. 179-188.

103. Zauli-Sajani, S., et al., *Higher health effects of ambient particles during the warm season: The role of infiltration factors.* Science of The Total Environment, 2018. **627**: p. 67-77.

104. Shaughnessy, R.J. and R.G. Sextro, *What Is an Effective Portable Air Cleaning Device? A Review.* Journal of Occupational and Environmental Hygiene, 2006. **3**(4): p. 169-181.

105. Westerling, A.L., *Increasing western US forest wildfire activity: sensitivity to changes in the timing of spring.* Philosophical Transactions of the Royal Society B: Biological Sciences, 2016. **371**(1696): p. 20150178.

106. Westerling, A.L., et al., *Warming and earlier spring increase western US forest wildfire activity.* science, 2006. **313**(5789): p. 940-943.

107. Marlon, J.R., et al., *Long-term perspective on wildfires in the western USA.* Proceedings of the National Academy of Sciences, 2012. **109**(9): p. E535-E543.

108. Abatzoglou, J.T., et al., *Compound Extremes Drive the Western Oregon Wildfires of September 2020.* Geophysical Research Letters, 2021. **48**(8): p. e2021GL092520.

109. Williams, A.P., et al., *Observed impacts of anthropogenic climate change on wildfire in California.* Earth's Future, 2019. **7**(8): p. 892-910.

110. Dennison, P.E., et al., *Large wildfire trends in the western United States, 1984–2011.* Geophysical Research Letters, 2014. **41**(8): p. 2928-2933.

111. Naeher, L.P., et al., *Woodsmoke health effects: a review.* Inhal Toxicol, 2007. **19**(1): p. 67-106.

112. Liu, J.C., et al., *A systematic review of the physical health impacts from non-occupational exposure to wildfire smoke.* Environ Res, 2015. **136**: p. 120-32.

113. Ciccioli, P., M. Centritto, and F. Loreto, *Biogenic volatile organic compound emissions from vegetation fires.* Plant Cell Environ, 2014. **37**(8): p. 1810-25.

114. Reid Colleen, E., et al., *Critical Review of Health Impacts of Wildfire Smoke Exposure.* Environmental Health Perspectives, 2016. **124**(9): p. 1334-1343.

115. Aguilera, R., et al., *Wildfire smoke impacts respiratory health more than fine particles from other sources: observational evidence from Southern California.* Nature Communications, 2021. **12**(1): p. 1493.

116. Reid, C.E., et al., *Critical Review of Health Impacts of Wildfire Smoke Exposure.* Environ Health Perspect, 2016. **124**(9): p. 1334-43.

117. Kiser, D., et al., *Particulate matter and emergency visits for asthma: a time-series study of their association in the presence and absence of wildfire smoke in Reno, Nevada, 2013–2018.* Environmental Health, 2020. **19**(1): p. 92.

118. Liang, Y., et al., *Wildfire smoke impacts on indoor air quality assessed using crowdsourced data in California.* Proceedings of the National Academy of Sciences, 2021. **118**(36): p. e2106478118.

119. U.S. EPA., *Guide to Air Cleaenrs in the Home.* 2018.

120. Association of Home Appliance Manufacturers, *Method for Measuring Performance of Portable Household Electric Room Air Cleaners, AHAM AC-1-2020.* 2020.

121. Thomas, R.J., *Particle size and pathogenicity in the respiratory tract.* Virulence, 2013. **4**(8): p. 847-58.

122. Ardkapan, S.R., et al., *Evaluation of air cleaning technologies existing in the Danish market: Experiments in a duct and in a test room.* Indoor and Built Environment, 2013. **23**(8): p. 1177-1186.

123. Ciuzas, D., *Indoor Air Quality Management by Combined Ventilation and Air Cleaning: An Experimental Study.* Aerosol and Air Quality Research, 2016. **16**(10): p. 2550-2559.

124. Peck, R.L., et al., *Efficiency of portable HEPA air purifiers against traffic related combustion particles.* Building and Environment, 2016. **98**: p. 21-29.

125. Batterman, S., C. Godwin, and C. Jia, *Long Duration Tests of Room Air Filters in Cigarette Smokers' Homes.* Environmental Science & Technology, 2005. **39**(18): p. 7260-7268.

126. Huang, C.-H., et al., *Assessing the effectiveness of portable HEPA air cleaners for reducing particulate matter exposure in King County, Washington homeless shelters: Implications for community congregate settings.* Science of The Total Environment, 2023. **891**: p. 164402.

127. Powder Technology Inc, *ISO 12103-1, A2 fine test dust.* 2023.

128. Yedamale, P., *Brushless DC (BLDC) motor fundamentals.* Microchip Technology Inc, 2003. **20**(1): p. 3-15.

129. Alavy, M., T. Li, and J.A. Siegel, *Energy use in residential buildings: Analyses of high-efficiency filters and HVAC fans.* Energy and Buildings, 2020. **209**: p. 109697.

130. Xu, B., et al., *Investigation of the Performance of Airliner Cabin Air Filters throughout Lifetime Usage.* Aerosol and Air Quality Research, 2013. **13**(5): p. 1544-1551.

131. Noh, K.-C. and M.-D. Oh, *Variation of clean air delivery rate and effective air cleaning ratio of room air cleaning devices.* Building and Environment, 2015. **84**: p. 44-49.